Structural characterization of f-ALS associated SOD1 mutant aggregates using conformation-specific antibodies

by

Gyana Gourab Mishra

A thesis
presented to the University of Waterloo
in fulfilment of the
thesis requirement for the degree of
Master of Science
in
Chemistry

Waterloo, Ontario, Canada, 2020

Author’s declaration

I hereby declare that I am the sole author of this thesis. This is a true copy of the thesis, including any required final revisions, as accepted by my examiners.

I understand that my thesis may be made electronically available to the public.

Abstract

Superoxide dismutase 1 (SOD1) is a metalloenzyme ubiquitously expressed in all cells and acts as an antioxidant enzyme by catalyzing the dismutation of superoxide radicals. Several mutations in the gene encoding SOD1 are linked to the fatal neurodegenerative disease, Amyotrophic lateral sclerosis (ALS). Despite this connection, there is no clear relationship between any quantifiable properties of SOD1 and ALS disease characteristics. One of the key hallmarks of ALS is the formation of SOD1 aggregates in motor neurons. The unfolded SOD1 goes though several post-translational modification steps *in vivo*, that includes metal binding, disulfide bond formation, and dimerization, to reach its final maturation form which is a stable homodimer. While the mature SOD1 is highly stable, the immature state of SOD1 (E,E $SOD1^{SH}$) is prone to misfold and aggregate, thereby potentially play a critical role in the disease pathology.

Here, we have developed a quantitative dot blot technique to characterise the aggregate structures of several immature SOD1 mutants using four conformation-specific antibodies. These antibodies can only bind to misfolded conformations of SOD1 upon exposure of their binding epitope regions which stays typically buried in the native structure of the protein. The aggregates were prepared in the form of inclusion bodies using the *E. coli* expression system grown in minimal media. Our results show that different SOD1 mutants exhibit a variable extent of binding to the conformation-specific antibodies, suggesting that SOD1 is displaying mutation-dependent conformational prion-strain behaviour by aggregating into distinct conformations. Hence, the developed quantitative dot blot protocol has provided valuable information on the mechanism of SOD1 aggregation and could potentially be expanded to study aggregate structures of other forms of SOD1 as well as several other proteins that are linked to other neurodegenerative diseases.

Acknowledgements

I would like to express my deepest gratitude to my supervisor, Dr Elizabeth Meiering, for her constant guidance throughout the project. I would also like to thank members of the Meiering lab, past and present, for their loving support. I would specifically like to thank Dalia Naser for her generous help in the experiments and making some of the figures for this thesis.

Table of Contents

List of Figures

List of Tables

List of Abbreviations

ALS ..... Amyotrophic Lateral Sclerosis
CCS ..... Copper chaperone for superoxide dismutase
E,E-SOD1^{SH} ..... metal free, disulfide reduced superoxide dismutase
E,Zn-SOD1^{SH} ..... Zinc bound, disulfide reduced superoxide dismutase
Cu,Zn-SOD1^{SS} ..... Copper and zinc bound, oxidised superoxide dismutase
GnHCl ..... Guanidine hydrochloride
fALS ..... familial amyotrophic lateral sclerosis
SDS ..... Sodium dodecyl sulfate
NC ..... Nitrocellulose membrane
IB ..... Inclusion body
IA ..... Iodoacetamide
n-OG ..... n-Octylglucoside
NP-40 ..... Nonidet P-40
IPTG ..... isopropyl β-d-1-thiogalactopyranoside
SDS-PAGE ..... Sodium dodecyl sulfate polyacrylamide gel electrophoresis
TEN ..... Tris(hydroxymethyl)aminomethane, Ethylenediaminetetraacetic acid, NaCl
Tris ..... Tris(hydroxymethyl)aminomethane
CMC ..... Critical micelle concentration
DSC ..... Differential Scanning Calorimetry
SOD1 ..... Superoxide dismutase 1
MQ ..... Milli-Q

1 Introduction:

1.1 Protein folding, misfolding and aggregation

1.1.1 Protein folding

Proteins are large organic macromolecules that are found in all forms of life on Earth. They are synthesized as a linear chain composed of individual amino acids that are covalently linked through peptide bonds. This linear polypeptide sequence is called the primary structure of the protein. This linear chain may fold into a complex and specific three-dimensional native protein structure[1]. The process of protein folding from its initial unfolded chain to its native state is complicated and influenced by various factors[2]. Multiple hypotheses have been proposed to explain this complex and precise folding process[3]. While none of these theories has been able to explain the process entirely, they certainly provide us with a better understanding of the factors involved in protein folding and pave the way for more advanced models.

One of the pioneering theories of protein folding is known as the classical model. It states that the protein folds along a distinct pathway, forming clearly defined intermediate structures before it ultimately achieves its final native fold[3]. This model is based on Levinthal's paradox that states that there is no undirected folding process for proteins, as the time it would take a protein to randomly sample every potential conformation before finding its native structure is longer than the current age of the universe[4]. This theory was also supported by the parallel work of Anfinsen who observed during his research work on ribonuclease that protein folding was a quick process[5]. It led to the idea that the primary sequence of the protein ultimately determines its three-dimensional native structure and folds through predetermined intermediates, rather than

randomly sampling available conformations; this idea is known as Anfinsen's dogma or the thermodynamic hypothesis.

As per Anfinsen's dogma, the formation of native protein structure requires three conditions to be fulfilled: 1) a unique structure at a global free energy minimum; 2) a stable structure that is unaffected by minute changes in the surrounding system, and 3) a structure obtainable through a kinetic pathway[3,5]. Building on this model, several new models on protein folding began to develop. One of the most accepted models is called the energy landscape model[6], according to which an unfolded protein has multiple folding pathways and potential intermediates early in the folding process, but as the protein acquires a more native-like state, there are fewer intermediates available to sample (Figure 1.1 B). The initial unfolded structure contains a certain degree of information to start the folding process, which often involves hydrophobic collapse. Early specific side-chain interaction in the secondary structure, as well as physiological conditions can provide more sampling limitation in this folding process, essentially making it more defined and efficient.

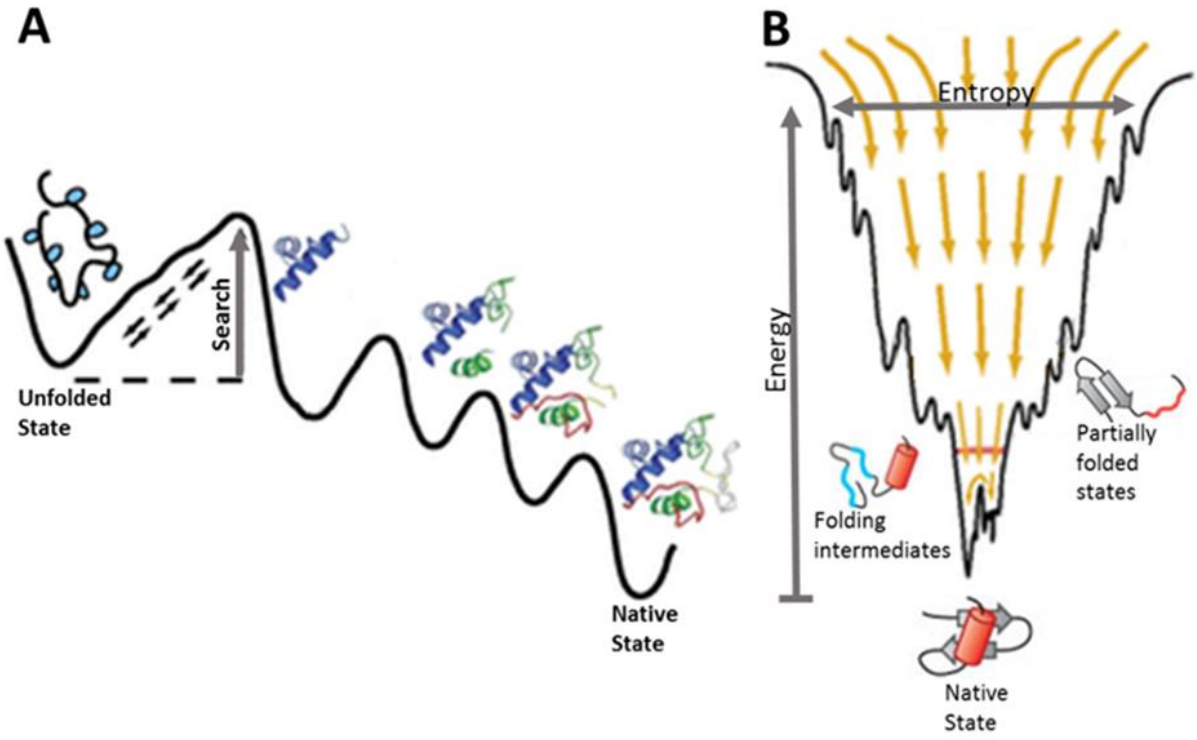

Figure 1.1: Protein folding models. (A) The classical view of a defined folding pathway. (B) the new view of multiple routes through a funneled energy landscape model. Image adapted from Englander *et al.*[3].

1.1.2 Protein misfolding and aggregation

The complex and intricate process of protein folding is strongly influenced by the cellular environment and proceeds under the influence of other partner proteins in oligomeric assemblies and of molecular chaperones and folding catalysts[7,8]. However, error during this folding process leads the protein to misfold. Protein misfolding generally includes misfolded or long-lived partly folded states that form during conformation sampling and/or as a result of genetic mutation[3,9]. There are several structural and cellular factors known to increase the probability of a protein to misfold. Some of these factors include the folding intermediate stabilized through non-native

long-range interactions[10], the partially folded regions of protein interacting with other cellular molecules during translation[11,12], failure of protein quality control system such as the ubiquitin-proteasome complex and molecular chaperones[13,14,15]. Variation in several environmental factors like temperature, pH, oxidative stress, abnormal presence of metal ions is also known to promote protein misfolding[16–19]. Misfolded or partially folded proteins often contain solvent-exposed hydrophobic residues which is in contrast with natively folded structures where these residues are more buried inside the protein structure[20]. Surface hydrophobic interaction between these misfolded species generally leads to higher-order non-native structures, also known as protein aggregates[21].

The formation of protein aggregates can be considered as a series of sequential and parallel events. Usually, aggregation starts with the protein molecule adopting an alternate conformation as mentioned before that may allow partial exposure of aggregation-prone sequence(s). Such aggregation-prone monomers are highly vulnerable to non-native protein-protein interactions at some level, leading to the initial formation of a non-native dimer or oligomer, subsequent aggregate growth or polymerisation, and eventually the formation of visible as well as subvisible particles due to limited solubility and/or sedimentation[22–25]. The non-native interactions that lead to the formation of higher-order structures could be through covalent bonds such as disulfide bonds between free cysteines and/or non-covalent interactions such as van der Waals contacts and hydrophobic interactions[9,26]. As the non-native protein conformation is considered as the initiator, the formation of aggregates is generally correlated with the stability and flexibility of the native protein structure[27,28]. Formation of oligomeric structures from these misfolded conformations is generally a concentration-dependent process[29–31], and the size of these oligomers range from dimers to multimers (e.g decamers)[32]. These

oligomers are thought to be the nucleation site for starting the aggregation process by recruiting other misfolded as well as natively folded protein molecules or interacting with other oligomers or a combination of both[33,34]. This can be modelled onto the energy landscape model, as illustrated in Figure 1.2. The aggregates show high variation in their stability and their structures vary from highly disorganized amorphous oligomers to highly organized amyloid fibrils with well-ordered straight fibrillar structure, composed of protofilaments[6,11,35]. Many studies on mouse models as well as patient samples have found the presence of protein aggregates in neurodegenerative diseases[36], the ageing process[37,38], and enhanced cytotoxicity[39]. Aggregates can be formed in the neuronal cells and propagate trans-cellularly[40] which is associated with the progression of neurodegenerative disorders such as Alzheimer's and Huntington's diseases and Amyotrophic Lateral Sclerosis (ALS)[41–43], the last being the disease of focus for this thesis. Due to the association of aggregate structures with these fatal diseases, it is imperative to have a detailed structural characterization of these aggregates. Such findings will not only help us advance our understanding of the fundamental principles that govern protein aggregation but also contribute to developing therapeutic strategies to prevent the associated diseases.

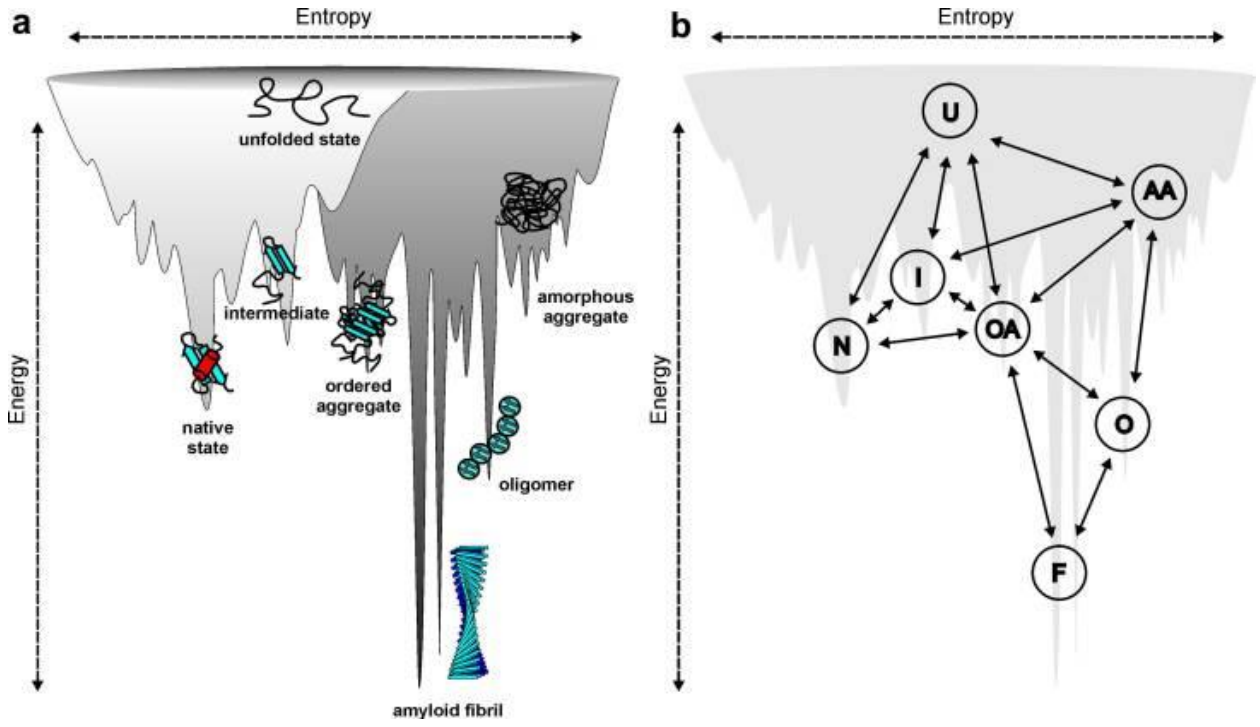

Figure 1.2: **Aggregation mechanism modelled to energy landscape model**. The diagram illustrates various pathways a misfolded protein could take to form higher order oligomeric and aggregate structures. These pathways are mapped onto the energy landscape model of protein folding. Image adapted from Jahn *et al*.[44].

1.2 Neurodegenerative disease and protein aggregation

Neurodegenerative diseases have been a significant focus in the scientific and medical community, considering the growing age of the world population. These diseases are generally characterised by the selective and progressive loss of neurons, leading to the development of neurological dysfunction, which can include memory, behavioural, and movement deficits[45]. A classic hallmark of neurodegenerative diseases is the formation of aggregates of one or multiple proteins which are formed in the intracellular space or extracellularly, with transmission to other neuron cells[46]. Factors like mutation as well as chemical modification such as the addition of

poly-glutamine repeat expansion in the protein sequences are generally linked with the progressive formation of these aggregates[47,48]. However, it is widely thought that the formation of aggregates is the end-point result with the soluble oligomers and misfolded protein species being crucial cytotoxic agents in these diseases[49,50]. Still, the mechanism of aggregate formation and their role in the disease pathogenesis is not clearly understood yet. There is also growing evidence of these aggregates exhibiting prion-like conformation and transcellular propagation which is described in detail in Section 1.2.5.

1.2.1 Amyotrophic Lateral Sclerosis

Amyotrophic lateral sclerosis (ALS) is a fatal degenerative motor neuron disease typically with an adult-onset. It has been characterized by the loss of motor neurons in the brainstem, spinal cord and motor cortex[51–53]. This leads to the loss of vital muscle control, often resulting in death due to respiratory failure[54]. While typical disease duration is 3-5 years, the onset and disease duration is highly variable, indicating multiple factors being involved in its pathogenesis.

ALS cases may be grouped into sporadic (sALS) which accounts for 90% of all cases and have no known cause and familial (fALS) which is known to have a genetic basis[51,52]. Approximately 15-20% of all fALS cases are linked to mutations in a protein called Cu, Zn superoxide dismutase 1 (SOD1)[51]. Currently, over 180 mutations in SOD1 are known to be associated with fALS (http://alsod.iop.kcl.ac.uk). These mutations are spread throughout the structure of the protein, and each mutation is associated with different average disease duration. There is nevertheless large heterogeneity in the disease duration even for a given mutation[55]. Despite very extensive investigations, a clear relationship between the biophysical properties of SOD1 mutants and ALS disease characteristics has not been found[51]. Mutation in SOD1 is

generally thought to promote misfolding of the protein and subsequence aggregation. Hence, characterization of the aggregate structures formed by these different mutants is critical to advance our understanding of the aggregation mechanisms and their role in disease pathogenesis.

1.2.2 Cu, Zn Superoxide dismutase 1 (SOD1)

In order to understand the pathology of SOD1-mediated ALS, it is critical to understand the structure and function of the protein. SOD1 is generally located in the cytoplasm and the mitochondria of the cell[56–58], but under stress, it is also found in the nucleus. The mature form of the protein forms a 32 kDa homodimer with each subunit comprised of 153 amino acids[59,60] (Figure 1.3). Each monomer is formed of eight antiparallel β-stands that create a Greek key β-barrel containing an intra-subunit disulfide bond between Cys57 and Cys146, one Zn and one Cu ion. SOD1 also contains two functional loops per monomer, the electrostatic loop and the Zn binding loop. The electrostatic loop is responsible for guiding the superoxide to the active site where the catalytic copper is present and coordinated by His46, His48, His63 and His120 residues. The zinc-binding loop contains His63, His71, His80 and Asp83 residues which are responsible for coordinating with the zinc ion that is known to provide structural stability[61].

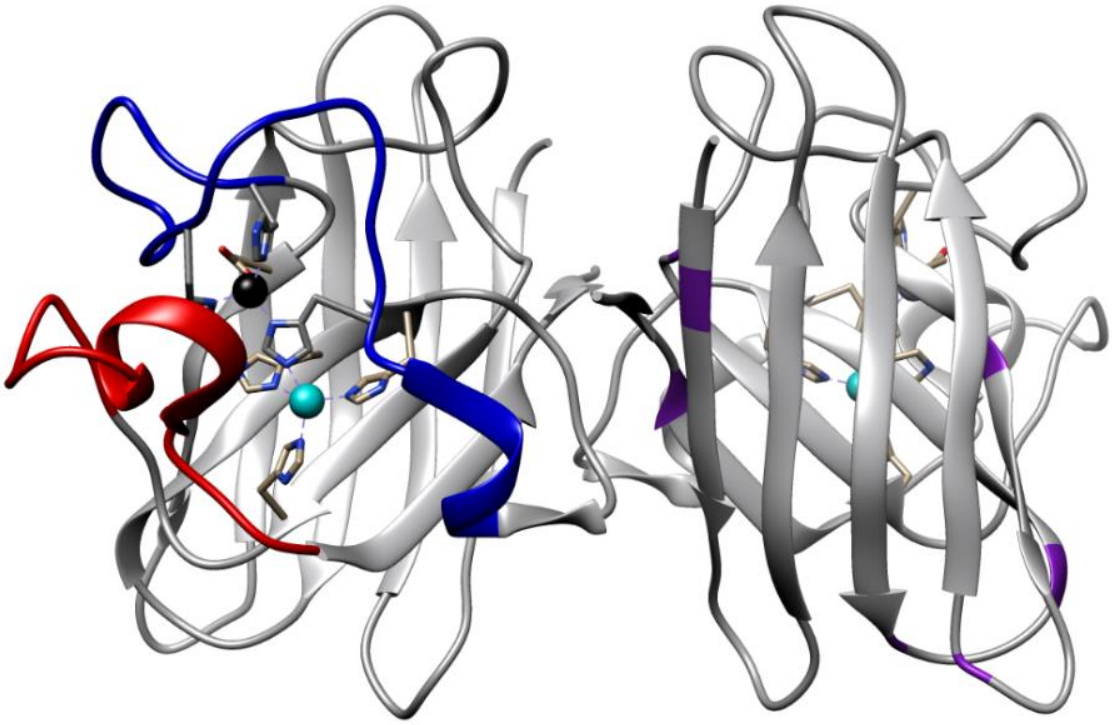

Figure 1.3: Ribbon structure of holo SOD1. Both monomers are shown in ribbon form. Zn (Black) and Cu (Cyan) are shown on the monomer on the left along with its coordinating residues. The Zinc-binding loop (blue) and electrostatic loop (red) are shown. Image is generated in Chimera (version 1.14) protein visualisation software using PDB ID: 1HL5.

SOD1 acts as an antioxidant enzyme by scavenging the toxic superoxide (O_2^-) radical that is formed as a natural by-product of many cellular processes[51,58]. SOD1 converts this free radical into molecular oxygen and hydrogen peroxide through a two-step ping-pong mechanism[62] (Figure 1.4). In the first step, Cu^{2+} is reduced by a superoxide molecule, generating dioxygen (O_2) and Cu^{1+}. The Cu^{1+} is then re-oxidised by a second equivalent of superoxide, that results in the regeneration of Cu^{2+} and formation of hydrogen peroxide.

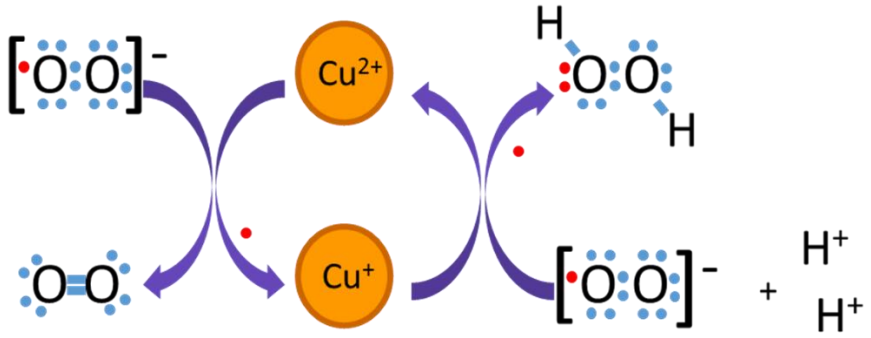

Figure 1.4: Ping pong mechanism of SOD1 activity. SOD1 utilizes a 'Ping-Pong' type reaction to catalyze the conversion of one equivalent of superoxide into molecular oxygen by reducing Cu(II) to Cu(I) ion and the second equivalent of superoxide into hydrogen peroxide by oxidising Cu(I) to Cu (II) ion. Image has been adapted from Rakhit *et al.*[63]

1.2.3 SOD1 and ALS

The role of mutation in the SOD1 gene was linked to ALS by Rosen et al. [64] in 1993. Since then, over 180 mutations dispersed throughout the structure of the protein were linked with the disease, as mentioned above. Initially, it was thought disease resulted from the loss of protective function in SOD1 mutants[65, 66]. But later it was shown that several fALS associated SOD1 mutants retain WT like activity but still promote disease progression[67–69]. Further, SOD1 knockout mice do not develop ALS symptoms[70], but upon expression of a mutant SOD1 protein, mice develop disease phenotype. This suggests a gain of toxic function rather than loss of native activity by SOD1 mutants[70,71]. However, the mechanism mediating the gain of toxic function is not well understood yet. The mutants have shown to induce their toxicity by endoplasmic reticulum stress[72,73], mitochondrial dysfunction[74], and glutamate toxicity[75].

Given the fact that protein aggregation has been reported to play a crucial role in the onset and progression of various neurodegenerative diseases, it is tempting to formulate that ALS follows a similar mechanism. Studies showed the presence of SOD1 aggregates in ALS patients and mouse models further support this idea[76,77], and the formation of these intracellular aggregates is the prominent hypothesis for SOD1-linked fALS onset and progression[78]. However, reports on the cytotoxic effect of soluble oligomers as well as prefibrillar structures have indicated their dominant role in causing the disease and suggested that aggregates might be the final stage of the disease progression[79]. It is also hypothesized that aggregates are formed as a protective cellular response, actively carried out by various cellular machinery[80]. Interestingly, the stability of the mutant protein or its propensity to form an aggregate is not strongly correlated with the disease duration[55]. A prime example of this is the V148I mutant, which has a short disease duration of ~1.7 years but is more stable than WT SOD1 with similar aggregation propensity[81]. Despite various biophysical studies on these aggregates, there has been no quantifiable property(s) which is directly correlated with the disease duration. Further, the aggregates found in ALS models are also reported to be composed of immature forms of SOD1 which indicates that the protein has the propensity to misfold during its maturation process and form non-native interactions with other molecules[82]. Hence, a structural investigation of these higher-order oligomer and aggregate structures formed by various states of mutant SOD1 protein molecules is imperative. It would help shed more light on the role of SOD1 in the disease and potential development of effective therapeutic methods which are currently very limited[83].

1.2.4 SOD1 maturation

SOD1 undergoes multiple post-translational maturation steps to reach its fully mature or holo form (Figure 1.5). The most immature state of the protein reduced apo SOD1 with empty(E) metal-binding sites (E, E $SOD1^{SH}$) and lacking the internal disulfide linkage preferentially exists as a monomer. The reduced apo SOD1 is thought to bind the structure stabilizing Zn through an unknown mechanism and forms the intermediate Zn bound reduced apo species (E, Zn $SOD1^{SH}$). Further modifications include the addition of catalytic Cu and the formation of the internal disulfide bond between Cys57 and Cys146. Previous studies have shown that the maturation of SOD1 is a sequential event[84]. However, the exact order of events and their role in SOD1 stability are ambiguous. One of the well-studied processes is the addition of Copper which is mediated by the copper chaperone protein for superoxide dismutase 1 (CCS)[62,84]. CCS has also been reported to catalyze the formation of an internal disulfide bond[85] as well as promote Zn binding[86]. Though there are also studies on CCS-independent Cu addition[87], the chaperone-mediated mechanism is thought to occur in most of the cases. The final, mature holo state of SOD1 is denoted as Cu, Zn-$SOD1^{SS}$.

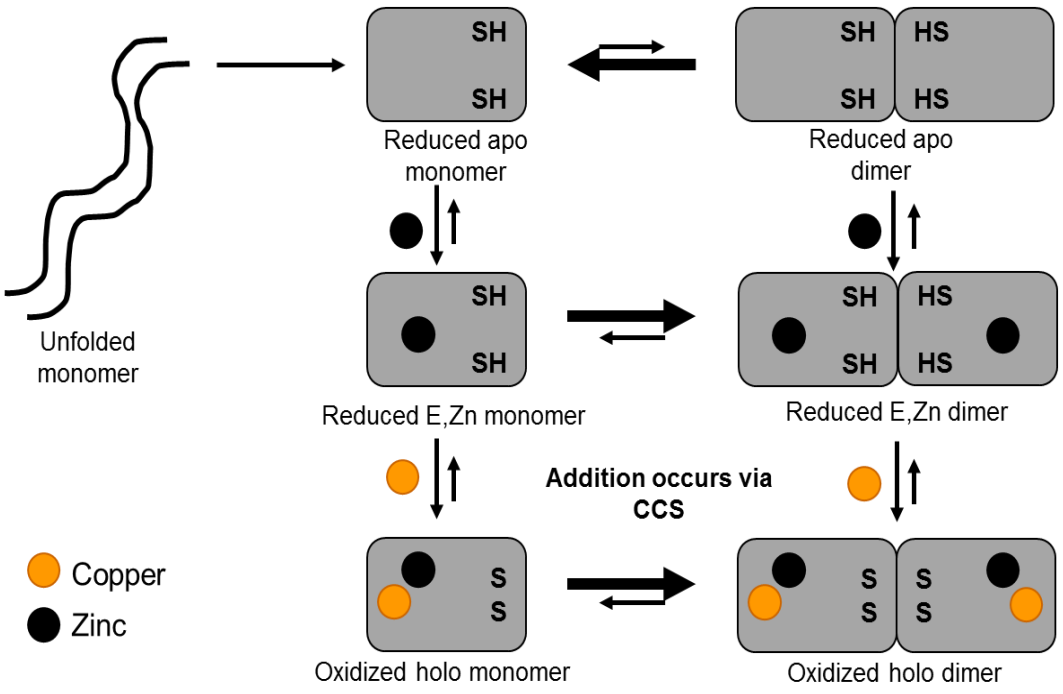

Figure 1.5: Maturation steps of SOD1. E,E-SOD1^{SH}, which is favored to exist as a monomer, obtains a stabilizing zinc ion cofactor to form E,Zn-SOD1^{SH}. This form then interacts with CCS to acquire a catalytic copper ion and to oxidize the disulfide bond between Cys57 and Cys146. This forms the mature protein, Cu, Zn-SOD1^{SS}.

The maturation process of SOD1 provides structural stability and confers enzymatic activity. DSC (Differential Scanning Calorimetry) studies have shown that the immature form of SOD1, E,E-SOD1^{SH}, is only marginally stable with a melting temperature, T_m, of 47.6 $^{\circ}$C, while the most mature form of the protein, Cu,ZnSOD1^{SS}, has a much higher T_m of 92.7°C. Recent studies by Harmeen Deol in the Meiering group have shown the monomeric E,Zn-SOD1^{SH} to have a T_m of about 57°C, indicating a more thermally stable structure than the metal-free variant, but less thermally stable than the mature form. The immature E,E-SOD1^{SH} is known to be highly aggregation-prone most probably because of its low stability leading to a conformational change. In particular, loop regions in SOD1 lose their restraint and become significantly disordered upon

dissociation of metal ions and reduction of the disulfide bond to form fibrillar aggregates which is the classic hallmark of ALS disease[88,89]. Other studies have reported that different mutants of this immature state of SOD1 have different aggregation propensities and tend to form aggregates of varying size[89]. Notably, these aggregates can also act as seeds and induce aggregation of natively folded and other misfolded forms of SOD1. Such propagation is believed to be carried out in a manner that resembles prion-like conformational strain behavior of these immature and/or misfolded SOD1 species[90].

1.2.5 Prion like conformational strain behavior in ALS

The classical understanding of the progression of infectious diseases mandated the presence of nucleic acid materials for continuous production of pathological protein molecules. This has since been challenged by the discovery of neurological disorders, also known as prion diseases, where the misfolded infectious protein molecule propagates its effect by transforming the natively folded proteins into the misfolded conformation and hence, does not require any nucleic acid to maintain its life cycle[91]. This model of propagation is currently implicated in various neurodegenerative disorders, providing a possible explanation of protein aggregation pathology and spatiotemporal distribution of these aggregates in the neuronal system observed in these diseases. The process is understood by the initial monomeric protein misfolding leading to the formation of larger oligomeric structures which act as seeds to recruit other misfolded proteins as well as transform natively folded proteins into misfolded conformation and recruit them to form higher-ordered amyloid-like aggregate structures. Interestingly, various *in vitro* studies have shown that ALS-related proteins FUS[92], TDP-43[93] and SOD1[94–96] can form amyloid-like aggregates. It is important to note that different conformations of prion agents may have significant differences in their cytotoxic effect, abilities to recruit native protein, modes of

propagation, ability to counter cellular degradation machinery and these characteristics are used to define different "strains" of the prion[97]. Further, it has been established that the prion strains that are capable of dividing into a greater number of seeds are most capable of propagating[98]. Hence, the high levels of protein aggregates in the neuronal system provide evidence that motor neurons may be an efficient environment for ALS-associated prion-like seeds to form and propagate[99].

The first evidence that SOD1 may act in a prion-like manner was reported for various *in vitro* assays, where WT SOD1 and fALS-associated mutant SOD1 were used for aggregation studies. These studies were performed by destabilizing the native protein by chelating the metal content and reducing the disulfide bond[94,96,100]. The fact that these studies saw destabilization-induced aggregate formation further supports the idea that the immature E,E-SOD1^{SH} is critical as a primary aggregation substrate. The first cellular study to illustrate prion-like behavior of misfolded SOD1 species was carried out by the addition of recombinant SOD1 aggregates to cultured cells overexpressing SOD1 variants[101]. Here the aggregates entered the cells via micropinocytosis and induced aggregation of cytosolic SOD1. Further, it was established that the endogenous WT SOD1 becomes misfolded when an ALS-linked SOD1 mutant is overexpressed in the cultured cells[102]. One recent study has shown that these aggregates exit from the infected cells via extracellular vesicles called exosomes to propagate to other cells[103]. Evidence of prion-like propagation was shortly followed by studies demonstrating different transmissible strains of SOD1. A 2016 study by Ayers *et al.*[104] used a G85R mouse model which exhibits ALS symptoms that do not present until roughly 20 months of age and injected it with the spinal homogenates from paralyzed mice that carry the G93A mutation of SOD1. They saw that ALS symptoms were developed within 3-months post-injection supporting the idea that different

LS related SOD1 mutants might possess different conformational strains which in turn results in different disease characteristics. Evidence of conformational strains was also shown by binary epitope mapping of insoluble materials from the spinal cord of transgenic mice expressing WT, G85R, D90A, or G93A SOD1 variants[105]. The study found the presence of two strains, denoted as strain A and strain B. WT, G85R and G93A samples were found to contain strain A aggregates whereas D90A samples were found to be either strain A or strain B. Additionally, strain B was correlated with rapid progression of the disease suggesting strain behaviour might be key to understand the heterogeneity in ALS pathology by various SOD1 mutants. In our current study, we investigated the structures of aggregates of SOD1 mutants formed in cells using *E coli* as the model system.

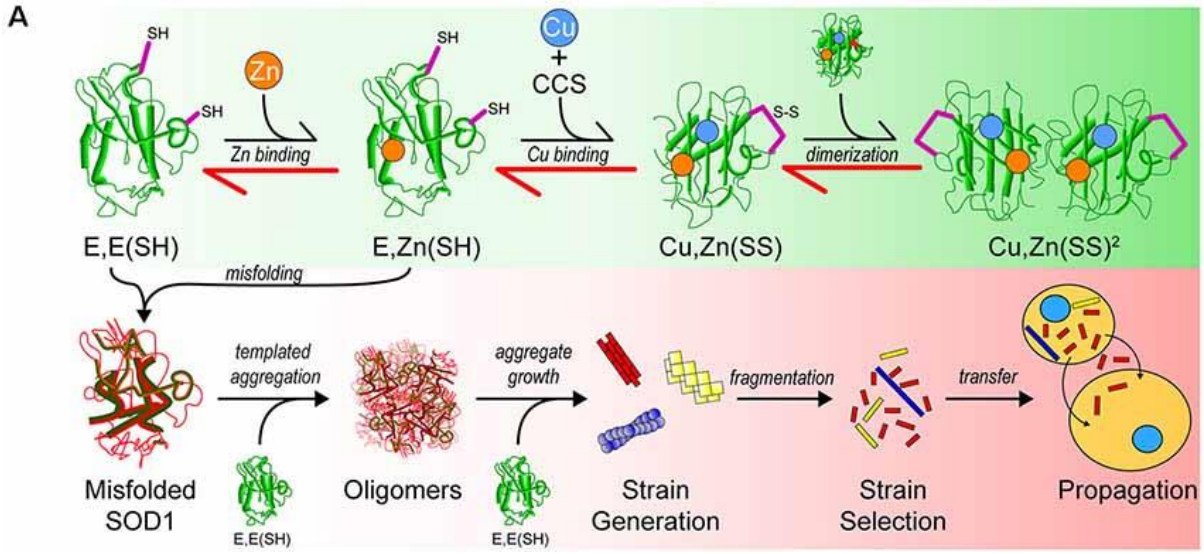

Figure 1.6: Prion like stain behaviour and strain propagation of SOD1. SOD1 can get misfolded at various points along its maturation process, leading to aggregation. The figure shows that this aggregation could propagate in a prion-like fashion. Figure adapted from McAlary *et al.*[90]

1.3 Structural characterization of fALS related SOD1 mutant aggregates

1.3.1 Inclusion bodies

Inclusion bodies (IBs) are large, dense aggregates located in the cytoplasm of the cell when a protein is overexpressed in a non-native host cell. Early on, it was considered as an obstacle in the heterologous expression technique when the protein of interest was accumulated in insoluble form leading to the formation of these inclusion bodies. However, in the last decade, various experiments showed functionally active or at least partially active polypeptides in bacterial inclusion bodies[106,107] (Figure 1.7). Since then, the idea of IBs has completely changed and revolutionized the field[108]. Because of the convenience in manufacturing, storing and transporting IBs, they have now attracted significant focus from biotechnology industries as a tool for mass production of active enzymes[109]. A recent study has also shown artificial IBs as an efficient means for targeted drug delivery by utilizing IBs as slow protein-releasing aggregates[110], making them a promising tool for biomedical applications.

Our current understanding is that IBs can contain a variety of different states of the protein, including native structures, non-native structures, and aggregated structures, as shown in Figure 1.7. IBs have been proposed as an attractive model to study protein aggregation and increasingly used to predict the aggregation propensity of proteins related to various neurodegenerative diseases[111,112]. A study in 2012 by Invernnizi *et al.* showed the presence of polyglutamine repeats in their IBs, which also occur in proteins that form aggregates in Huntington's Disease[113]. Another study reported that IBs that contain fungal prion proteins are dependent on the local cellular environment for aggregate propagation[114]. Previous work by

Dalia Naser and Susan Kelso in the Meiering lab has also used IBs to show different aggregation propensities of fALS mutant SOD1s both in the absence and presence of Zn. Hence, IBs provide a robust tractable model to study the structure and mechanism of protein aggregation, which may also provide valuable information on aggregation associated neurodegenerative diseases.

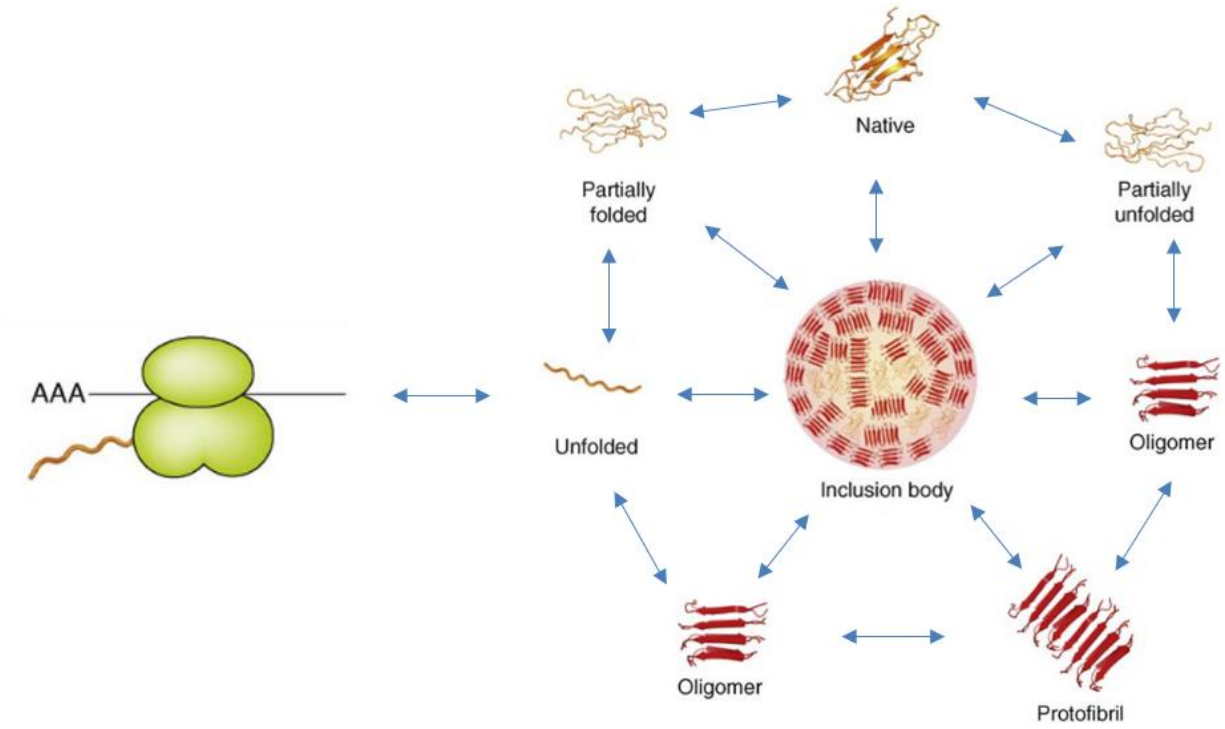

Figure 1.7: Inclusion body formation from different types of protein conformations. Inclusion bodies are formed as insoluble fraction due to protein misfolding. Several different conformations of the protein could be present in the inclusion body fraction. Image adapted from Groot *et al*.[111].

1.3.2 Conformation-specific antibodies to investigate fALS mutant SOD1 IBs

The mature holoSOD1 (Cu, ZnSOD1^{SS}) is a highly stable dimeric protein, and a lack of its proper maturation and/or mutation can promote the formation of a misfolded structure where regions that are usually buried become exposed. This phenomenon has led to the discovery of many conformation-specific antibodies against SOD1 misfolded structure[74,115,116]. As these antibodies are developed against epitopes in SOD1 that are generally buried in the folded native structure, they do not bind to the mature holoSOD1 but preferentially recognize those forms of SOD1 where the epitopes have increased exposure. Several monoclonal, as well as polyclonal antibodies, have now been developed against misfolded SOD1, and their corresponding epitopes span across the entire protein structure (Figure 1.8).

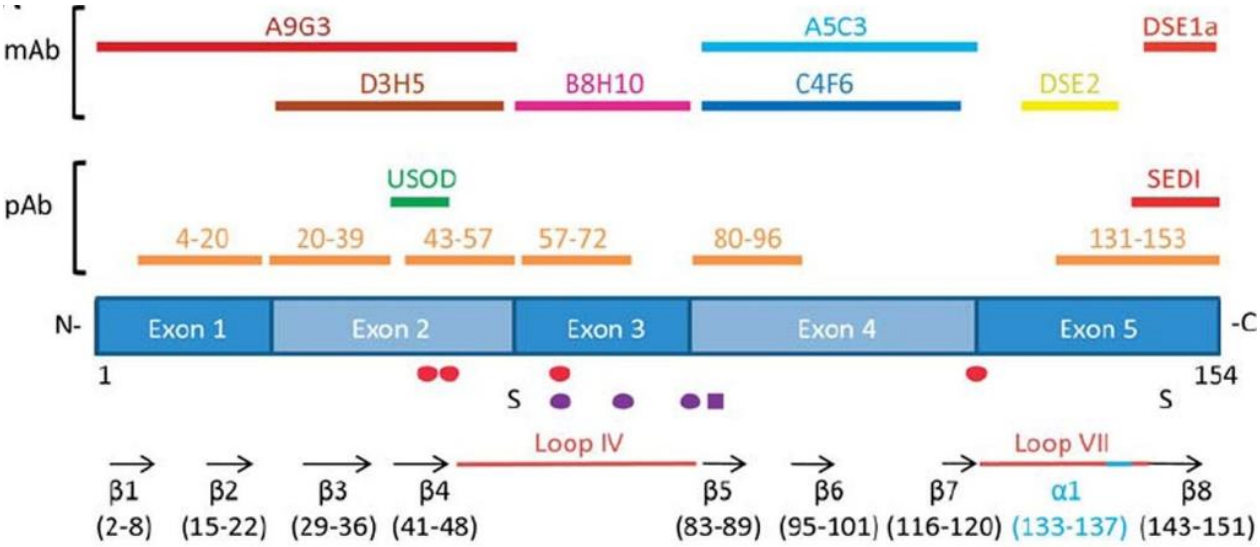

Figure 1.8: Epitopes of anti-SOD1 antibodies. Various monoclonal (mAb) and polyclonal (pAb) antibodies have been developed. Their binding to the exon regions as well as secondary structure in SOD1 is shown. Out of all these conformation specific antibodies, four antibodies have been used in this study (SEDI, USOD, AMF7 and B8H10). AMF7 is a high purity antibody version of DSE2 and binds to the same epitope region. Figure adapted from Pickles *et al.*[74]

Initially, these antibodies were developed for immunotherapy because of their specific interaction with misfolded SOD1 as well as their potential to become a safe drug that can cross the Blood-Brain Barrier and prevent neurotoxic misfolding and aggregation[117–119]. These studies showed that when misfolded SOD1s were targeted with some of these antibodies, it was effective in increasing mice life span as well as prevent cellular uptake of extracellular misfolded SOD1 species. The transgenic G93A mice were passively immunized with A5C3 and D3H5 antibodies, and while A5C3 did not show any significant increase in the survival rate, D3H5 extended the survival by 6-9 days[118]. A therapy based on adeno-associated virus-based delivery of D3H5 antibody also increased the life span of SOD1 G93A mice by up to 28%[120]. Recently, another group has reported the use of oligomer-specific antibody W20 that can target soluble misfolded G93A SOD1 and result in reduced SOD1 oligomer, increasing motor neuron survival[121]. Though these studies have shown antibody-based immunotherapy as a promising method, a comprehensive therapeutic is yet to be developed.

Apart from the biomedical application, conformation-specific antibodies have also been used to investigate the structure and cellular localization of misfolded SOD1 aggregates. A 2016 study by Pickles *et al.* found that misfolded SOD1 aggregates preferentially localize in the spinal cord mitochondria[122]. They showed that these aggregates exist in different conformations as some highly reacted with AMF7, some with B8H10 and others with both. These different aggregates were primarily composed of immature SOD1 and showed spatiotemporal variation in their spinal cord localization, supporting the idea that misfolded SOD1 operates in different mechanisms depending on the conformational strain. Binary epitope mapping using antibodies that recognize short peptides within SOD1 have shown the presence of different strains in SOD1 mutant mice model which was different from *in vitro* aggregates suggesting a key role of the

central nervous system in shaping the aggregation process[105]. A recent study has also used conformation-specific AMF7 and B8H10 antibodies to identify the interactomes that bind uniquely and commonly to different forms of SOD1 aggregates[123]. Other studies have used several antibodies to illustrate the prion-like propagation of SOD1 aggregates[124], nuclear export of misfolded SOD1[125] and recently, a role for misfolded SOD1 in sporadic ALS[126] providing further understanding of SOD1-mediated disease pathology. However, these observations also demand robust methods which can quantitatively assess the structures of mutant SOD1 aggregates in order to establish the strain behavior of the protein properly. In this thesis, I have developed a quantitative dot blot protocol to analyze the structures of immature SOD1 (E,E $SOD1^{SH}$) aggregates using four conformation-specific antibodies.

Immunoblotting techniques such as Western blot and dot blot are widely used and invaluable methods for quick and efficient detection of antibody binding to the desired sample. However, most of these studies are qualitative or semi-quantitative at best. Dot blot assays are one of the most straightforward methods for immunodetection. Samples are directly blotted onto either nitrocellulose or polyvinylidene difluoride (PVDF) membrane, which has high protein binding capacity. This is followed by incubation with primary and secondary antibodies and subsequent detection using either chemiluminescence or fluorescence. Studies have shown that SOD1 conformation-specific antibodies could be used to investigate the structural properties of different SOD1 states as well as aggregate structure. Using dot blot method, Pickles *et al.* have shown that the immature reduced apo E,E$SOD1^{SH}$ form of WT, A4V, G93A, G85R bind more strongly to the conformation-specific antibodies AMF7 and B8H10 than the oxidized apo E,E$SOD1^{SS}$ form and no significant signal is obtained for the mature holoSOD1[122], confirming that the immature forms of SOD1 exist in the misfolded state. Dot blot technique has also been

used to investigate the change in *in vitro* aggregate structure over time[127]. In this thesis, a quantitative dot blot protocol is developed to investigate the structures of inclusion bodies formed by 11 SOD1 mutants grown using *E. coli* expression system in metal-free minimal media. The results indicate that SOD1 IB structures could be quantitatively characterized using this method. This study is carried out in parallel with a high-resolution Quenched Hydrogen-Deuterium Amide Exchange NMR experiments by others in the Meiering group which are also developed to investigate these IB structures. Together, these methods provide valuable information on different aggregate strains of SOD1 mutants and potentially help explain strain-dependent aggregation mechanism, cytotoxicity, and disease pathology.

1.4 Thesis Objectives

Following the extensive research on SOD1 aggregates as described in the previous sections, this thesis aims to expand our knowledge on various immature SOD1 mutant aggregate structures. Inclusion bodies of 11 SOD1 mutants were prepared in *E. coli* cells grown in minimal media. The 11 mutants studied are WT, A4V, G37R, G41D, G41S, G85R, G93A, G93D, I113T, V148I and V148G. These mutants were chosen to account for the effect of mutation throughout the structure of the protein (Figure 1.9) and different mutations on the same residue of the protein.

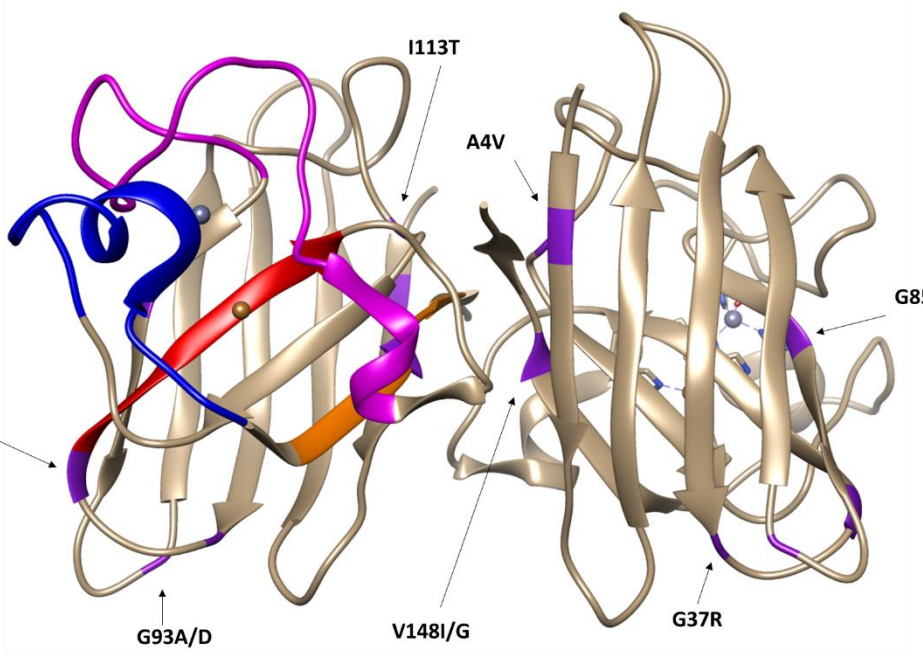

Figure 1.9: Ribbon diagram of SOD1 showing the sites of mutations and antibody binding regions. 11 mutants under investigation are highlighted in purple and shown with arrows. Epitope regions of the four conformation-specific antibodies are coloured in one of the monomers (SEDI – Orange, USOD – Red, AMF7 – Blue and B8H10 – Magenta). The image is made using Chimera (version 1.14) protein visualisation software with PDB ID: 1HL5.

The structure of the mutant aggregates was investigated using a quantitative dot blot technique that I developed to characterise mutant IBs binding with four conformation-specific antibodies SEDI, USOD, AMF7 and B8H10 which are known to recognize C-terminal dimer interface (aa 145-150), β-4 strand (aa 41-48), electrostatic loop (aa 125-142) and zinc-binding loop (aa 57-81), respectively (Figure 1.7). Some additional initial experiments to characterize various properties of the SOD1 inclusion bodies such as oxidation and homogeneity were also performed.

2 Materials and methods

2.1 Chemicals

TEN buffer was prepared by adding 2.42g Tris (20mM), 372mg EDTA (1mM), 5.85g NaCl (100mM) in 1 litre Milli-Q (MQ) and the pH was adjusted to 8. TEN-T buffer was prepared by adding Tween 20 to a final amount of 0.05% (v/v) to TEN buffer and mixed overnight. Chelexed MQ was obtained by running MQ through a chelex column. 1% (w/v) BSA (Heat Shock Isolation, Fraction V. Purity 98%, BioShop Inc.) was used in the blocking buffer. SEDI and USOD were purchased from Stressmarq Biosciences Inc. and AMF7, B8H10 were generously provided by our collaborators. Secondary fluorescent antibody Starbright 700 was purchased from BioRad Laboratories Inc and Alexa 488, 680 samples were generously provided by our collaborators.

2.2 Wild type (WT) and pseudo wild type (pWT) SOD1

Wild-type human SOD1 has four cysteine residues, Cys-6, Cys-57, Cys-111, and Cys-146. Cys-57 and Cys-146 form a conserved disulfide bond in the native structure. However, *in vitro* experiments showed that the free Cys-6 and Cys-111 could form aberrant disulfide bonds, resulting in irreversible thermal unfolding and precluding quantitative thermodynamic analysis[128]. Hence, a pseudo-WT (pWT) background was engineered for experiments with purified SOD1 mutants. pWT SOD1 has the free cysteine residues, Cys-6 and Cys-111, replaced with alanine and serine, respectively[129]. In this study, dot blot experiments that were carried out with purified SOD1 used this pWT background. However, all the studies with inclusion bodies were carried out using SOD1 mutants in the WT background to mimic the aggregation process of SOD1 in ALS.

2.3 SOD1 growth in rich media and protein purification

All SOD1 variants with pWT background were expressed using pHSOD1ASlacI1[130,131] in *E. coli* (QC779 strain). Plasmid containing SOD1 gene (pWT or mutant) that confers resistance to ampicillin was transformed into $SOD^{-/-}$ cells, which are resistant to chloramphenicol and kanamycin. The successfully transformed cells were inoculated in a small volume of LB media for overnight growth and the grown culture used as inoculum for 1L of 2TY media on the next day. Both the overnight LB media and 2TY media were supplemented with all three antibiotics. Cells were induced at an OD_{600} of 0.5-0.7 with 0.25mM final concentration of isopropyl β-D-1-thiogalactopyranoside (IPTG). While inducing with IPTG, $CuSO_4$ and $ZnSO_4$ were added to the media with a final concentration of 0.5mM and 0.01mM, respectively. The culture was grown for 8 hours post-induction.

Protein purification was carried out as mentioned in previous literature. Briefly, protein samples were initially subjected to copper charging and heat treatment to ensure proper metalation. Ammonium sulfate was added to the protein solution and passed through a hydrophobic column after filtering the protein solution through the nitrocellulose membrane. The protein eluted from the column was collected and dialysed against MilliQ for 8 hours (4 times). Finally, the sample was concentrated using amicon ultrafiltration membrane to obtain holoSOD1. The concentration of the protein sample was measured using UV-vis spectrophotometer at 280nm. To remove metals and obtain $apoSOD1^{SS}$, the sample was further dialysed against EDTA at pH 3.8, followed by dialysis against sodium acetate, NaCl at pH 3.8 and finally against 1mM HEPES at pH 7.8. Post dialysis the protein sample was reduced by denaturing using 2M guanidine hydrochloride (GnHCl) and 20mM HEPES (pH 7.8) followed by addition of reducing agent tris (2- carboxyethyl) phosphine hydrochloride (TCEP-HCl). The

sample was then incubated for 1 hour in an anaerobic condition and exchanged with buffer containing 1mM TCEP and 20mM HEPES to obtain purified E, E-SOD1^{SH}.

2.4 Inclusion body preparation

To obtain inclusion bodies, plasmids carrying genes of SOD1 mutants with WT background (no mutation at Cys-6 and Cys-111) were transformed into BL21 (DE3) *E. coli* strain. This strain of *E. coli* contains pLyS plasmid that confers resistance to chloramphenicol and a pET21 vector that confers resistance to ampicillin. The transformed cells were inoculated in 50mL of Luria broth (LB media) containing ampicillin (100μg/mL) and chloramphenicol (30μg/mL) and grown overnight at 37°C. Following overnight growth, 30mL of the culture was centrifuged (4,000 x g, 5 minutes, 4°C). 20mL of the supernatant is discarded, and the pellet was resuspended in the remaining 10mL of solution. The resuspended pellet sample was transferred to 1L of minimal media and grown until an optical density readings at 600nm (OD_{600}) of 0.5- 0.7 was reached. Composition of the minimal media is given in Table 2.1. As the culture reached suitable OD_{600}, it was induced with 0.1 mM final IPTG concentration and grown for an additional 4 hours. The cells were then pelleted by centrifugation (4,000g, 20 minutes, 4°C), flash-frozen, and stored at -80°C.

The frozen cell pellets were thawed and resuspended in 30mL of TEN buffer (20mM Tris, 1mM EDTA, 100mM NaCl, pH 8), then flash-frozen in liquid nitrogen, followed by thawing in a 40°C water bath (a freeze-thaw cycle). After this, the suspension was incubated with 3mg of DNase1 for 45 minutes at 4°C with occasional mixing by inverting. Post DNase I incubation, the sample was further subjected to three more freeze-thaw cycles, then centrifuged at 20,000x g for 20 minutes at 4°C to obtain insoluble inclusion body fraction. The inclusion bodies were resuspended in 8mL of TEN buffers thoroughly so that the entire solution becomes

homogeneous. The resuspended samples were further divided into smaller 15µL aliquots and frozen in -80C freezer. These smaller aliquots were used for dot blot and SDS-PAGE experiments. Initial IBs preparations were conducted on a smaller scale by me, where 1mL of the overnight culture was transferred into 50mL of minimal media. Samples were induced with same concentration of IPTG and IBs from the growth were prepared in a similar manner (freeze-thaw cycle along with DNase incubation). These samples were grown to optimise the quantitative dot blot protocol. Once optimised, the quantitative dot blot was used with large scale IB samples.

Components	**Stock Concentration**	**Final concentration**
M9 salts	10X	1X
Glucose	20%	0.4%
$CaCl_2$	100mM	100µM
$MgSO_4$	1M	2mM
NH_4Cl	100mg/mL	500µg/mL
Thiamine HCl	0.1%	0.0001%
Ampicillin	100mg/mL	100µg/mL
Chloramphenicol	30mg/mL	30µg/mL

Table 2.1: Composition of minimal media: SOD1 mutants were grown in the minimal media, and the inclusion bodies were obtained 4hrs post IPTG induction. 1X M9 salt contained a final concentration of 47.7mM Na_2HPO_4, 22mM KH_2PO_4, 8.3mM NaCl.

2.5 Quantitative dot blot assay

Quantitative dot blot was performed on the IBs of SOD1 mutants grown in minimal media without the addition of any metal. The nitrocellulose (NC) membrane (pore size: 0.45µm, Bio Rad Inc.) was prepared by immersing the membrane in 1mM EDTA, then chelexed MQ and finally TEN buffer for 5 minutes each. The membrane was then placed in a Bio-Dot microfiltration apparatus (BioRad). The membrane was again washed with 1mM EDTA, chelexed MQ and TEN buffer by adding the liquids to all the wells and then applying vacuum.

During the washing steps, one aliquot of each mutant was taken from -80^{0}C freezer and thawed at room temperature. The samples were mixed extensively by tapping the tube and drawing the solution up and down multiple times with a pipette to reduce the viscosity and maximize uniformity. 8µL of IB from each aliquot was taken and diluted in 112µL of TEN buffer (let this sample be denoted as Sample*). 8µL from Sample* was further diluted in 592µL of TEN buffer. 60µL from this was taken and mixed with 540µL of TEN buffer. The sample was then serially diluted 2-fold 4 times, each time by taking 200µL of sample and diluting in 200µL of TEN buffer. In this way, five serial dilutions of IB samples each with a 2-fold difference in protein amount were obtained, and 150µL from each was spotted onto the membrane and allowed to pass through without vacuum for 40-50 minutes. Once all the samples passed through the membrane, the membrane was washed four times with TEN-T buffer (20mM Tris, 1mM EDTA, 100mM NaCl, 0.05% Tween-20 pH 8). Here, 150µL of TEN-T buffer was loaded to each well and immediately drawn through using the vacuum. After washing, the membrane was removed from the apparatus. This was followed by blocking the membrane with 1% BSA prepared in TEN-T buffer for 1hr at room temperature. The blot was then incubated with the primary antibody that was diluted in blocking buffer for 2hr 30mins at room temperature (for

open container incubation experiments 1µL of primary antibody was diluted in 6mL of blocking buffer), washed with ~10ml of TEN-T (3 times for 5 minutes each) and finally incubated for 1hr with the secondary antibody that was also diluted with blocking buffer (generally, 2µL of secondary antibody was diluted in 10ml of blocking buffer). After the incubation, the blot was washed with ~10ml of TEN-T (5 times for 5 minutes each) and imaged in BioRad ChemiDoc MP imaging system. Densitometry from these blot images was calculated in BioRad Image Lab (Version 6.0.1) software volume tool (Figure 2.1A), and the background was subtracted using local background subtraction method[132].

In order to quantitatively measure the binding, two biological replicates were prepared by independently growing and preparing IB aliquots. Dot blot experiments on the samples from the first growth were performed in triplicate, i.e. using separate aliquots to perform three dot blots for each antibody (these replicates using aliquots from the same growth will be referred to as technical replicates). Similarly, dot blot experiments were performed in duplicate with the samples from the second growth (This is another set of technical replicates). The two sets of replicates from different growths are referred to as biological replicates. The signals from the dot blot experiments were normalised by quantifying the protein amount by SDS-PAGE. Briefly, for each dot blot experiment, 8µL from Sample* of each mutant was mixed with 22µL of loading buffer (0.125M Tris-Cl, pH 6.8, 4% (w/v) SDS, 20% (v/v) Glycerol, 10% (v/v) 2-mercaptoethanol, Bromophenol blue). Samples were prepared in duplicate for each mutant and boiled for 10-15 minutes in a PCR tube to minimize sample evaporation. After boiling, all samples were briefly vortexed. 15µL from each boiled sample was loaded onto SDS-PAGE, and duplicate samples of each mutant were run on different gels. Each gel also contained four different amounts of purified apo SOD1 (apo pWT) (0.625µg, 1.25µg, 2.5µg and 5µg) as the

protein standard. The gels were imaged in BioRad ChemiDoc MP imager, and band intensities were obtained using BioRad Image Lab 6.0.1 software. Background for each band densitometry peak was subtracted using the rolling ball method, as shown in Figure 2.1B. The radius of the rolling ball was kept constant (generally at 1mm) unless the background line entered the peak in which case the radius had to be increased for that measurement.

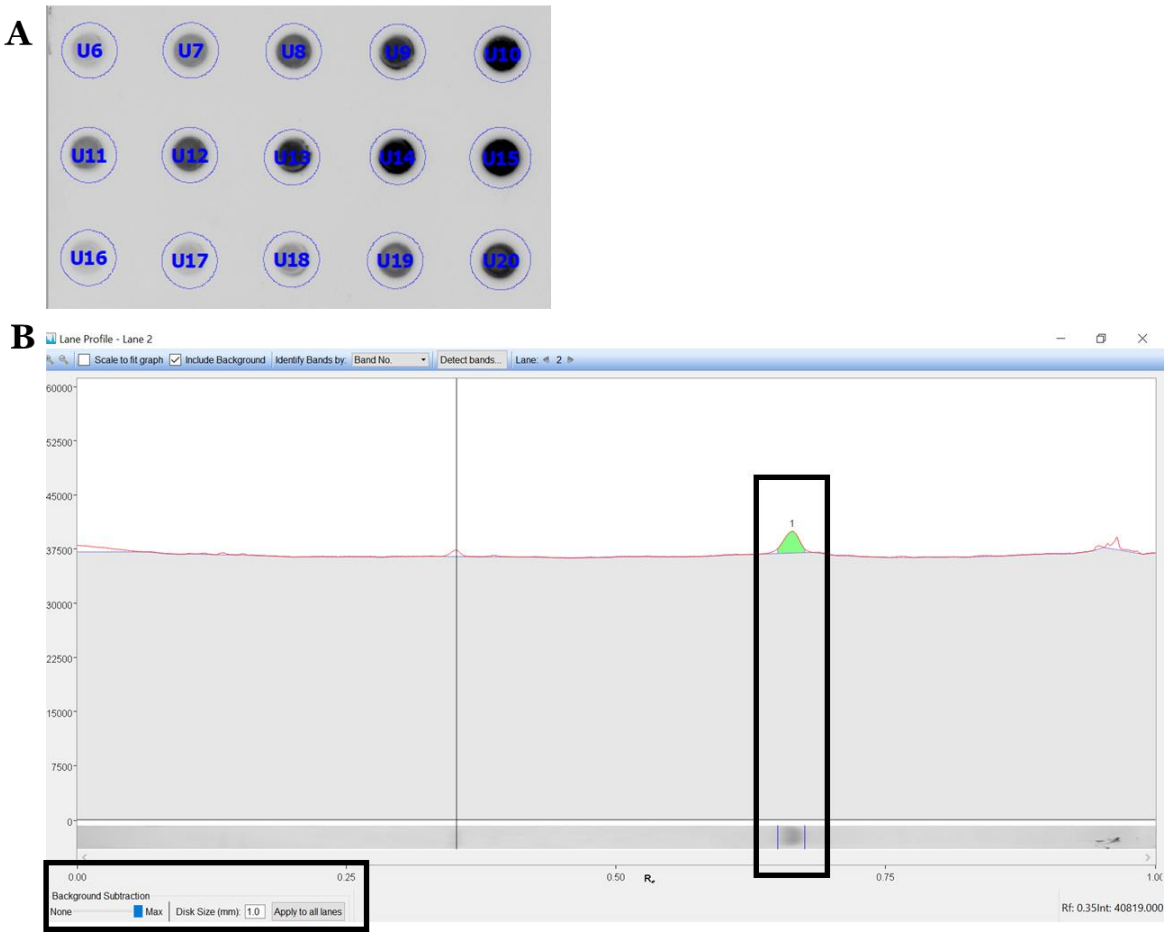

Figure 2.1: Background subtraction methods by Image Lab software. (A) The background signal intensities of the dot blots were subtracted using volume tool of Image lab software. Using this tool, a circle is drawn around the signal and the average value of all pixel intensities present in one-pixel region inside the circumference of the circle is considered as background. (B) Background signal subtractions for SDS-PAGE band intensities were carried out using rolling ball method. The radius of the rolling disc is chosen such that the background line touches both ends of the peak.

2.6 Washing IBs with mild detergents

Four mild detergents, Triton X-100, Tween 20, NP40 and n-Octylglucoside, were used to wash several SOD1 mutant IBs. Small aliquots of the IB samples that were in TEN buffer and frozen in -80 °C were thawed and centrifuged at 12000 RPM for 1 minute at room temperature. The supernatant was taken out and the pellet was resuspended in TEN buffer containing 1% (v/v) Triton X-100, 0.1% (v/v) Tween 20, 1% (v/v) n-Octylglucoside or 0.1% (v/v) NP40. After thoroughly resuspending the pellet, the sample was centrifuged at 12000 RPM for 1 minute. The supernatant was removed using 100µL pipette and kept in a separate tube, and the washed pellet was resuspended in TEN buffer. Both the supernatant and the washed pellet were run on a 12% SDS-PAGE along with the original inclusion body sample.

2.7 Iodoacetamide (IA) labelling of IBs

To assess the oxidation state of SOD1 in inclusion bodies, several variants were grown in minimal media as described in the previous section and labelled using iodoacetamide (IA), which reacts with free cysteine sulfhydryl groups. 1mL culture at 4-hrs growth post IPTG induction was centrifuged at 8000 RPM for 1 minute. The supernatant was removed using 1ml pipette and the cell pellet was resuspended in 30µL TEN buffer containing a final concentration of 0.5M IA. The resuspended pellet samples were then stored in -80^{0}C. The next part of the experiment has to be performed on the same day.

The samples were taken out of the freezer and subjected to flash-freeze in liquid nitrogen, followed by thawing in a 40°C water bath (a freeze-thaw cycle). After this, the suspension was incubated with 3mg of DNase1 for 45 minutes at 4°C with occasional mixing. Post DNase incubation, the sample was subjected to three more freeze-thaw cycles, then centrifuged at 8000

RPM for 1 minute to obtain the IB pellet fraction. The supernatant was removed, and the pellet was finally resuspended thoroughly in of 30μL TEN buffer containing 0.5M IA. SDS-PAGE samples were prepared for both the supernatant and the pellet fraction without adding any reducing agent and run on 15% SDS-PAGE.

3 Results

3.1 Optimization of the dot blot protocol

3.1.1 Choosing the optimum dot blot detection technique

In order to properly quantify dot blot signals, it is crucial that a proper secondary antibody be chosen, which provides a good dynamic range and a linear response in signal intensity for different sample concentrations. There are two types of detection methods used widely to measure immunoblot signals. One of these methods is called chemiluminescence where the secondary antibody is conjugated with an enzyme (generally horseradish peroxidase (HRP) or alkaline phosphatase (AP)) that catalyses the reaction of a suitable substrate (e.g. Luminol) generating a recordable signal in the form of light. Though chemiluminescence is highly sensitive, it generally has a small linear dynamic range, and the signal is highly dependent on the state of reaction between the enzyme and substrate as the signal is only generated when the reaction is ongoing. Both these factors made chemiluminescence an unsuitable detection technique for quantitative signal measurement of the dot blot experiments. The second method to detect immunoblot signal is through fluorescence where the secondary antibody is conjugated with a fluorophore that has specific excitation and emission wavelengths. Though it is known to be less sensitive than chemiluminescence, fluorescence detection provides a better dynamic linear range of detection as well as a more consistent signal over a period of time. Also, with the ongoing advancement in this field, there are many commercially available fluorescent secondary antibodies that provide highly robust signal and improved sensitivity making these antibodies attractive candidates for our quantitative measurements. I performed some initial experiments using chemiluminescence, but due to the advantages of stable, linear fluorescence detection, all the results described below were measured using fluorescence detection.

A 2016 study by Pickles *et al.*[122], used dot blot experiments with chemiluminescent detection to show that misfolded SOD1-specific AMF7 and B8H10 antibodies bind to apo and reduced apo form of various SOD1 mutants but very little to the holo form of SOD1. However, all three forms of SOD1 mutants showed signal when the proteins were denatured because of exposure of the antibody epitopes upon denaturation. The logical next step was to check whether denatured SOD1 samples could be used to normalize for varying SOD1 content of IB samples in our dot blot experiments. Ideally, this should mean that upon denaturation all SOD1 mutants show equal binding to conformation-specific antibodies so that any difference in antibody binding to various native SOD1 mutants as well as their aggregates could be quantitatively measured by effective normalisation with the denatured control. Hence, three secondary antibodies, Alexa 488, Alexa 680 and Starbright 700, were chosen to check which one(s) would provide the optimum signal for both native and denatured SOD1. All these antibodies have different excitation and emission wavelengths which are given in Table 3.1.

Secondary antibody	Excitation wavelength (nm)	Emission Wavelength (nm)
Alexa 488	488	520
Alexa 680	680	702
Starbright 700	470	700

Table 3.1: Excitation and emission wavelengths of fluorescent secondary antibodies: Three different secondary antibodies that were used for dot blot signal optimisation.

Purified recombinant apo I113T SOD1 was prepared in native and denatured forms and blotted onto three nitrocellulose membranes. All blots were incubated with AMF7 (primary antibody), and each blot was then incubated with one of the three secondary antibodies. The blots were imaged in two different instruments, 1) BioRad Pharos FX imager that uses lasers of set wavelengths for excitation together with filters to select the range of detection and 2) BioRad ChemiDoc MP imager that uses built-in UV transilluminator and white LEDs for epi (reflective) illumination as well as five additional LEDs for detection of a larger range of fluorophores. It is also equipped with a deeply cooled CCD detector[133]. Signals for both native and denatured protein showed a linear trend over ~10-fold and ~100-fold range of concentration, respectively (Figure 3.1). Starbright 700 showed the highest absolute signal intensity and signal to noise for native and denatured protein when the blots were imaged in BioRad ChemiDoc MP imager. So this secondary antibody and imager were used for signal detection in further experiments.

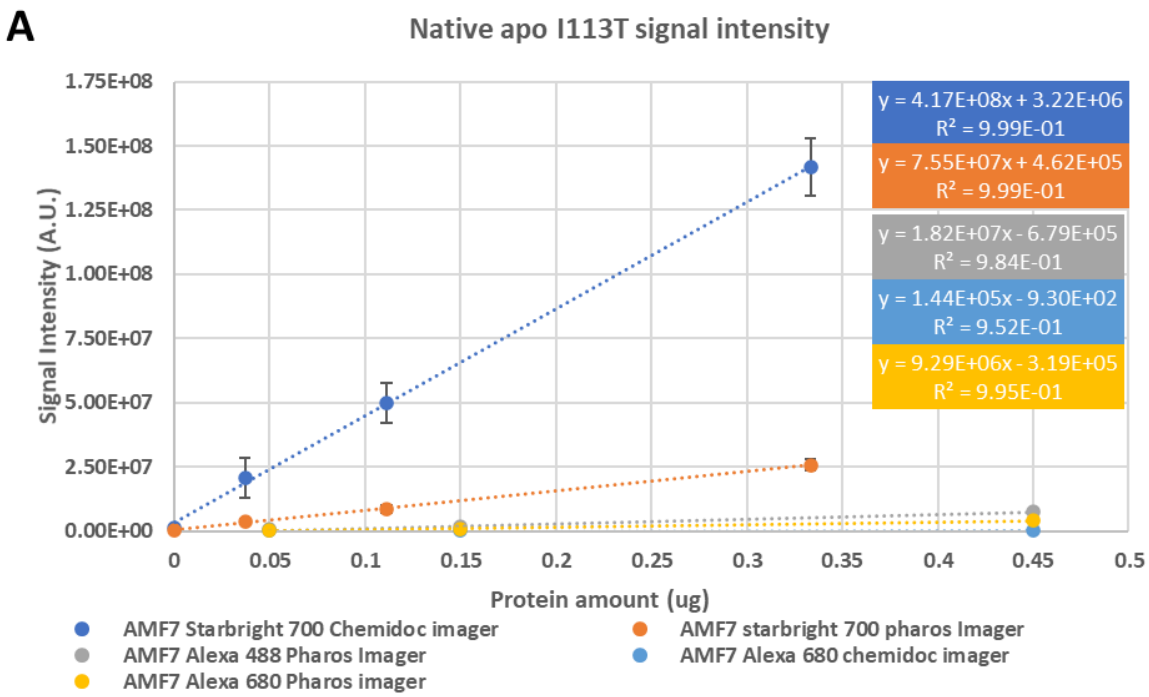

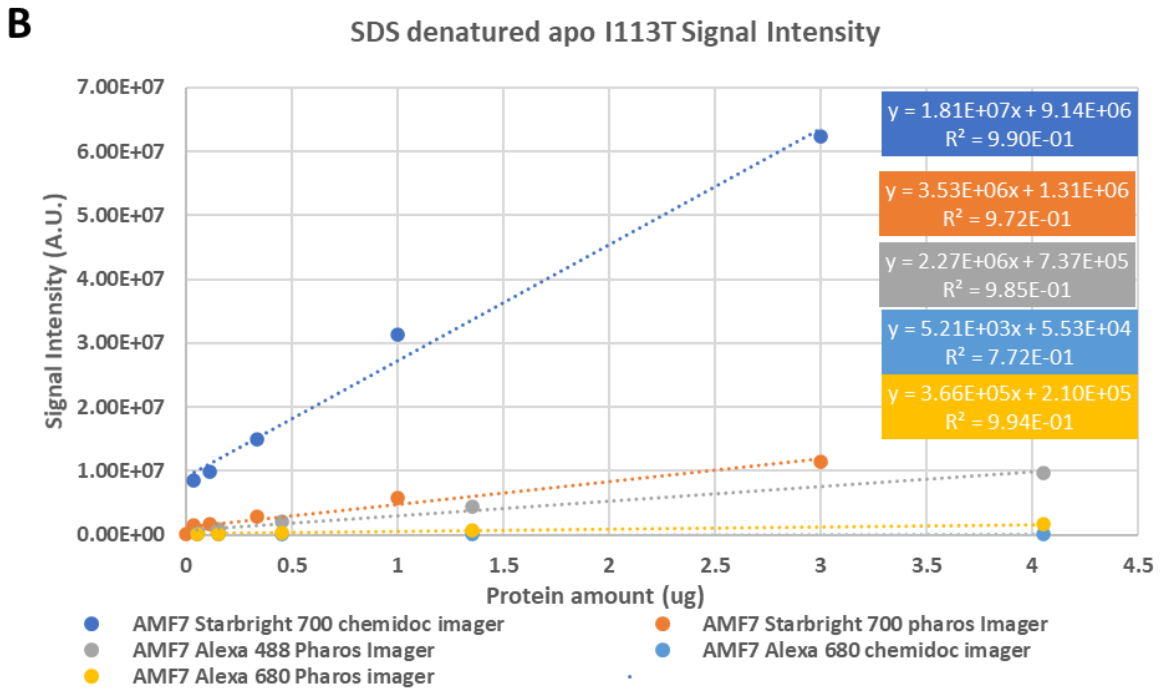

Figure 3.1: Optimisation of dot blot signal detection technique. Three different secondary antibodies, Starbright 700 (Dark Blue, Orange), Alexa 400 (Grey) and Alexa 680 (Blue and Yellow) were used to detect the signal of increasing concentrations of purified native and SDS-denatured apo I113T protein. Each antibody has different excitation and emission wavelengths. The blots were imaged in BioRad Pharos FX and/or BioRad Chemidoc MP imager. Starbright 700 seems to provide the highest signal for both native and denatured proteins.

3.1.2 Optimisation of primary antibody incubation

To obtain reliable data from the dot blot experiments, it was crucial that the primary antibody, as well as the secondary antibody, be uniformly distributed across the blot so that a sample with a given amount of protein gives consistent signal irrespective of its location on the blot. Our collaborators who originally developed the dot blot protocol to study conformation-specific antibody binding to various SOD1 mutants had suggested incubating the primary antibody in a sealed pouch to save on the amount of primary antibody used, which was limited. Incubating the blots with the primary antibody in a sealed pouch required a smaller volume of antibody solution (generally 1mL of blocking buffer was used with 1:1000 dilution of antibody). However, this method of primary antibody incubation showed high variability in signal when the same sample was blotted onto different regions of a blot, probably due to its inhomogeneous distribution of primary antibody across the blot area. To confirm this hypothesis, an experiment was conducted where three different amounts of A4V SOD1 IB were spotted onto the two NC membranes in various permutations of orientation and regions (Figure 3.2A). One of these membranes was incubated with the primary antibody in 1:1000 dilution in a sealed pouch. In contrast, the other blot was incubated with the primary antibody with 1:6000 dilution in an open container. Comparing the signals from both blots, the one incubated with the primary antibody in an open container showed less variability in signal for all three amounts of A4V IBs (Figure 3.2B). The absolute signal intensities obtained from both methods were also quite comparable, indicating that incubating the primary antibody in the open container with increased dilution from 1:1000 to 1:6000 does not affect its binding to the samples on the blot. Hence, all further quantitative dot blot experiments were carried out by incubating the NC blots with primary antibodies in open containers.

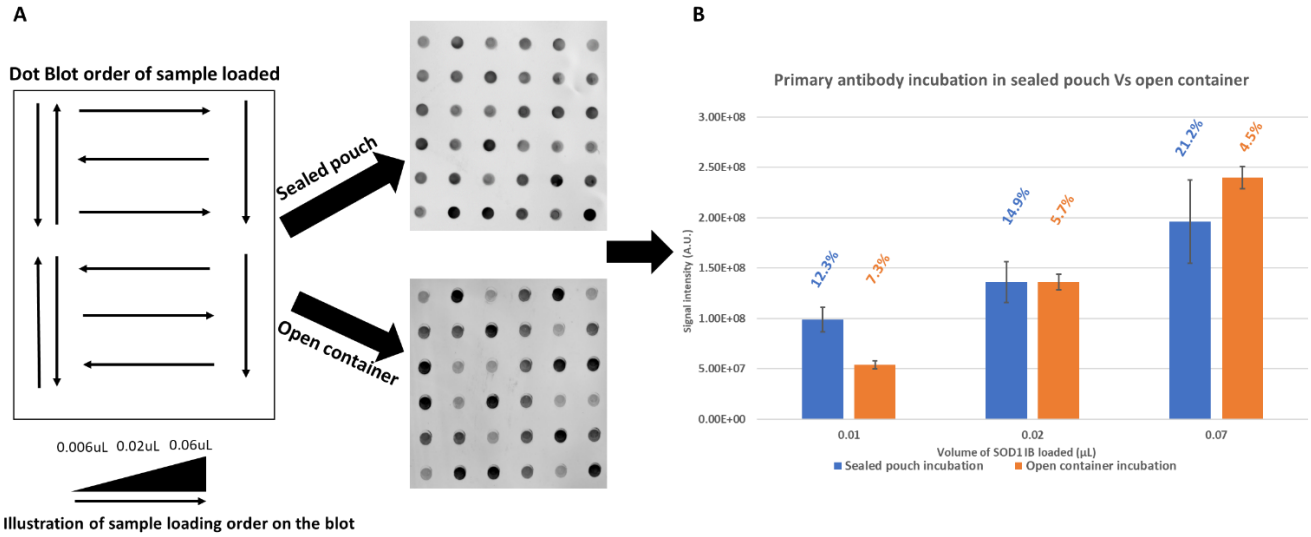

Figure 3.2: Variability of dot blot signals is lower using open container rather than sealed pouch for primary antibody incubation. (A)Three different amounts of A4V IB samples were loaded with a different permutation of orientation and regions on the membrane as indicated with arrows. The direction of the arrow indicates increasing IB amount. The samples were loaded in three different amounts with a 3-fold increase. (B) Signal intensities obtained from the blots incubated in primary antibody in a sealed pouch and an open container are compared. Amount of SOD1 IB refers to the volume of the undiluted original IB sample which is appropriately diluted in TEN buffer to obtain the highest volume of IB used (0.066µL), and this was then serially diluted 3-fold to obtain rest two amounts. % deviation given above the bars are calculated as 100 x (standard deviation of signals/average signal).

3.1.3 Finding the linear range of IB signal detection

With the protocol to obtain consistent signals across the dot blots now optimized, the next step was to check the linear range for IB signal detection. IBs can contain widely different amounts of SOD1 depending on the mutant and growth condition. Also, the quantity of inclusion body can vary from one growth to another for the same mutant. Some of the mutants that yield less amount of IB can bind strongly to conformation-specific antibodies because of high content of misfolded species in the aggregate while other mutants that express more IB can bind less to the antibodies. Hence, it was critical to find a robust range of IB amount that can be spotted onto the NC membrane and provide a linear signal for all SOD1 mutants.

To address the linearity problem, four different SOD1 mutants (WT, A4V, G37R and V148I) were chosen; two of these mutants (WT, V148I) express relatively low amounts of IB, while the other two mutants (A4V, G37R) generally express high amounts of IB (Figure 3.3B). All four of these mutant SOD1 IBs were spotted onto four different NC membranes in five different concentrations with 2-fold serial dilution. Each blot was incubated with one of the four conformation-specific antibodies (SEDI, USOD, AMF7, B8H10) and the experiments were performed in triplicate. The amounts of SOD1 in the mutant IBs were quantified using SDS-PAGE as described in the Methods (Section 2.4).

The results illustrated that the dot blot signals showed good linearity with the amount of protein for the three lowest concentration data points but started to plateau the two highest concentrations (Figure 3.3A). For all four confirmation-specific antibodies, highly linear fits were obtained when fitting the measured average signal for the blank wells together with the 3 lowest amounts of IB (corresponding to a 4-fold range in the amount of protein). These linear fits

were further used to assess the affinity of these antibodies towards all 11 SOD1 mutants under study.

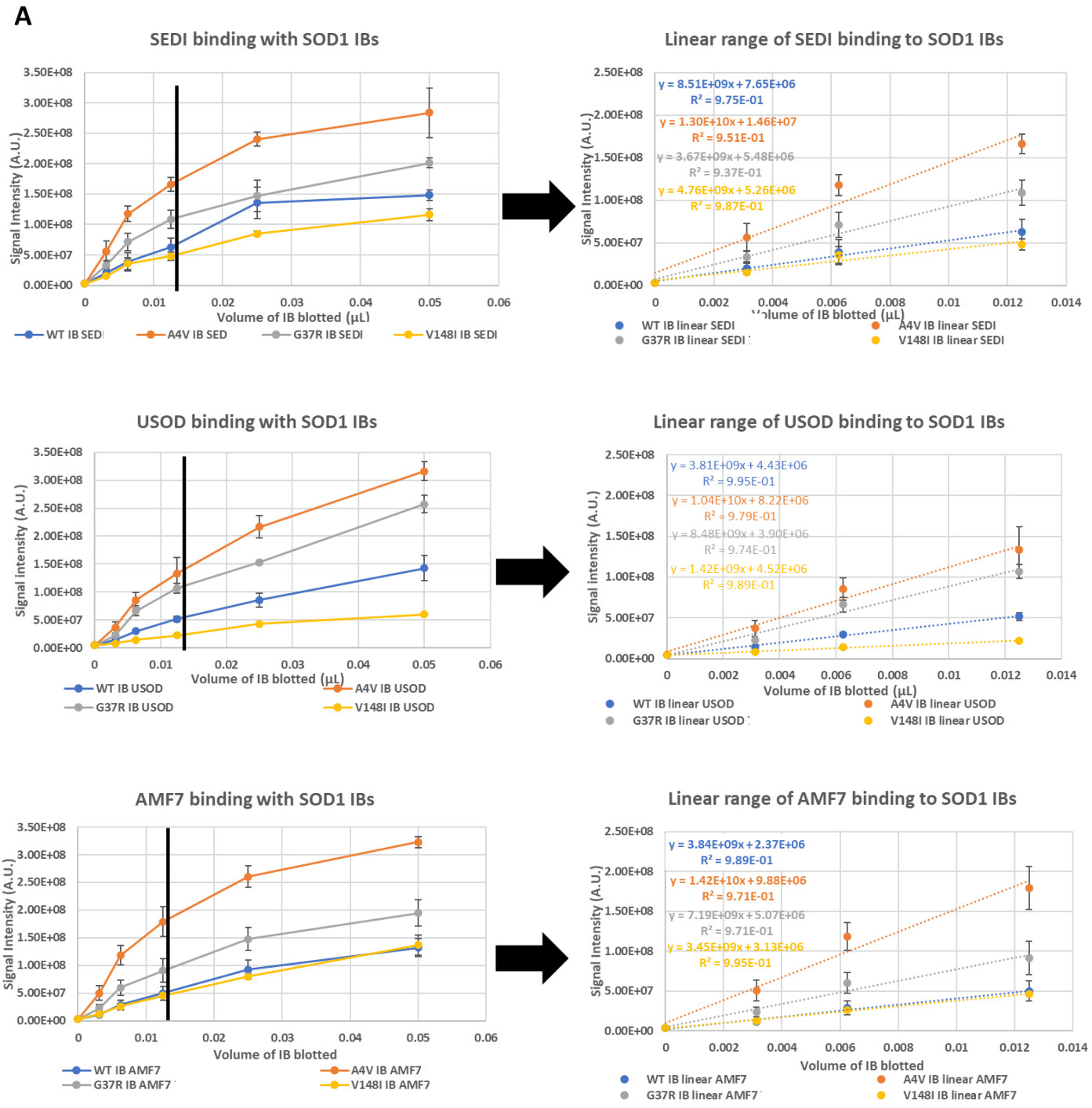

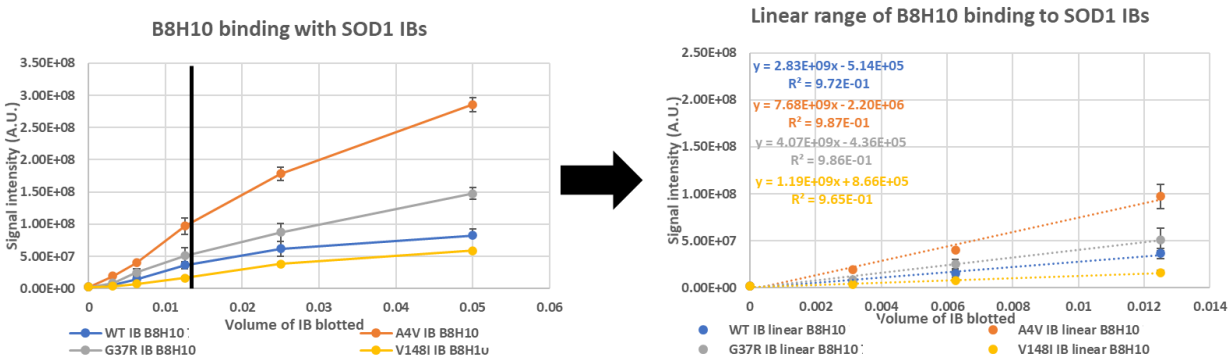

SOD1 mutants	WT	A4V	G37R	V148I
Average protein amount (mg/ml)	0.401	1.344	1.169	0.577
% deviation	5.36	2.21	3.90	5.80

Figure 3.3: Linear range of dot blot signal for IBs of 4 SOD1 mutants with all four conformation-specific antibodies. (A) IB samples were blotted in 5 different concentrations with 2-fold serial dilutions of samples. Average signals for each concentration point was calculated from the triplicate experiments and plotted against the amount of IBs. Similarly, the error bars calculated for each point from the triplicate represent the variation in dot blot signal at each concentration of IB. Good linearity was observed for fits of the average of the 3 blank well signals (0 volume point) with the lowest 3 sample volumes. (B) Amount of SOD1 for each mutant as measured by SDS-PAGE. The concentration of SOD1 IB shown in the table refers to the concentration of undiluted original IB sample which is appropriately diluted in TEN buffer to obtain the highest volume of IB used (0.05µL), and this was then serially diluted 2-fold to obtain rest four amounts. % deviation given above the bars are calculated as 100 x (standard deviation of signals/average signal).

The replicate experiments were carried out with different aliquots of the IB samples from the same growth to investigate the variability in antibody binding. Interestingly, it was observed that the same mutant IB could provide a consistent signal with one antibody while the variable signal with another antibody. An illustration provided in Figure 3.4A shows WT IB binding consistently to SEDI but showing a higher degree of variation for AMF7 (Figure 3.4B). Similarly, the same antibody could provide a consistent signal for one mutant IB whereas variable signal for another mutant IB (data not shown). This indicates that variability in signal for each mutant IB with all four antibodies is important to consider and replicates are necessary to account for this variability. However, linear fits were obtained for all individual replicate experiments of both SEDI and AMF7 with WT IB (Figure 3.4 – right plots) further supporting the idea that signal in this concentration range is consistently linear and slopes of these linear fits could be used to characterise the antibody binding for each mutant.

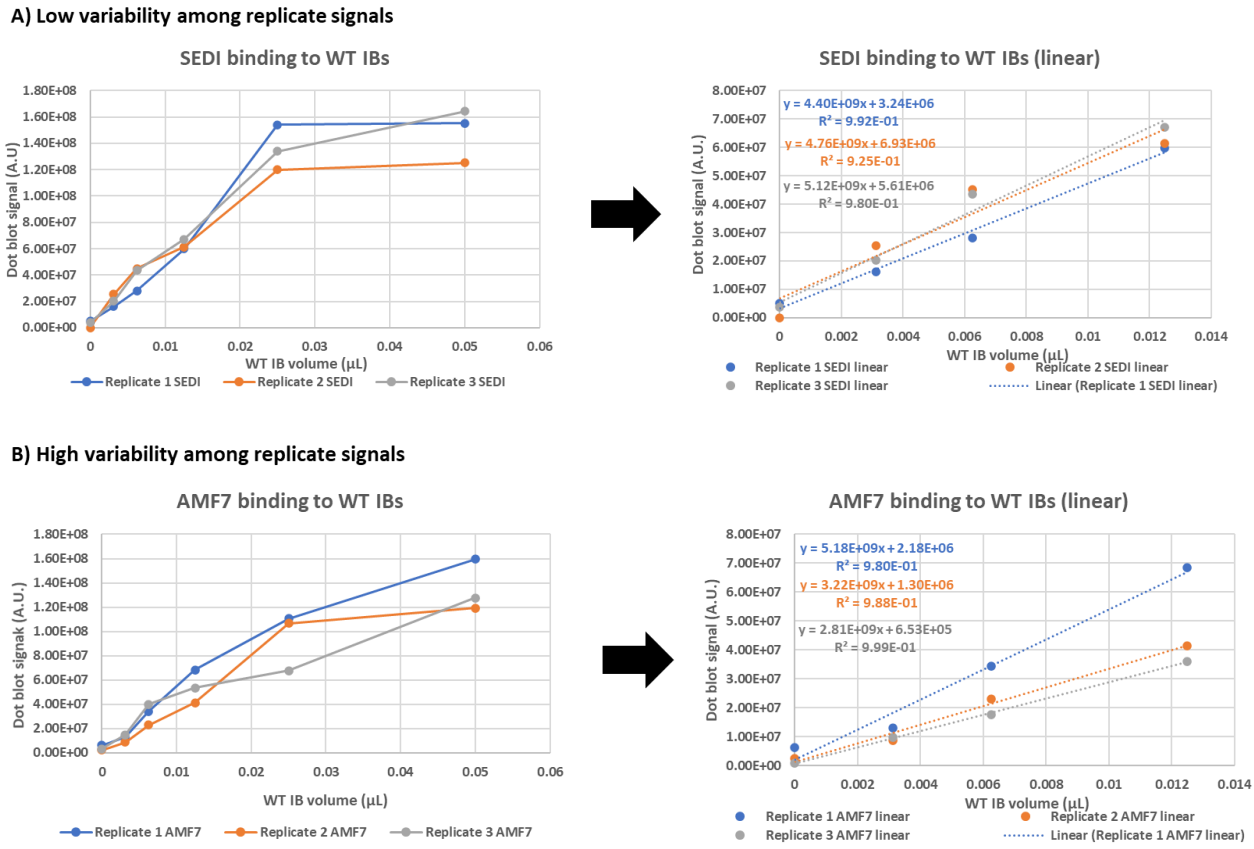

Figure 3.4: Variability in replicate dot blot signal. Different extent of variation in replicate signals could be observed depending on the mutant and the antibody. A) WT IB shows consistent signal with SEDI in its replicate experiments and the slopes from the linear fit are close to each other. B) WT IB shows more variation in signal with AMF7 and the slopes of the linear fit have more variation.

3.2 Optimisation of dot blot signal normalisation

3.2.1 Denatured control for signal normalisation

The normalisation of the signals from the immunoblotting experiment has been widely explored[134,135] as it is crucial for quantitative measurements and comparisons between different samples. Often, Western blot signals for a protein of interest are normalised using housekeeping proteins and/or actin which are known to be ubiquitously expressed in the cell. There are also recent advances like stain-free imaging technique, where the bands on SDS-PAGE are imaged before they are transferred onto a blotting membrane, and the signals from the blots are normalised accordingly. However, with the current dot blot approach, such techniques could not be used for normalisation as various commercially available anti-SOD1 antibodies have some degree of preferential binding to certain conformations of SOD1. Also, quantifying protein on the blot with low resolution staining dyes like ponceau stain is not ideal for normalising dot blot signal quantitatively. Hence, the remaining options were to normalise the dot blot signal with a form of SOD1 sample that can bind uniformly to all conformation-specific antibodies irrespective of the mutant and its maturation state or by quantifying the amount of SOD1 spotted onto the membranes.

As described in Section 3.1.1, the denatured form of SOD1 was a potential candidate for normalisation if it could potentially expose the antibody binding epitope regions of SOD1 to an equal extent upon denaturation and thereby, bind uniformly to all conformation-specific antibodies. Hence, an experiment was carried out where purified apoI113T was denatured using three different agents (SDS, Urea and guanidine hydrochloride (GnHCl)). Five different amounts of denatured samples with 3-fold serial dilutions were spotted onto NC membrane along with native apo I113T, as shown in Figure 3.5A. SDS and urea denatured samples provided a better

signal than GnHCl denatured samples. However, the native form of the purified protein has more signal than any of the denatured samples, and this pattern was consistent for several other dot blot experiments with native and denatured purified SOD1 proteins (data not shown). To check whether this was also the case with IBs, 9 different SOD1 mutant IBs were spotted onto NC membrane in native, and SDS denatured form. Like purified SOD1, IB samples also showed less signal for denatured samples (Figure 3.5B). Possible explanations for such reduced signal could be due to inefficient binding of primary antibodies to denatured samples and/or lower retention capacity of the NC membrane for denatured samples leading to its leakage after being loaded.

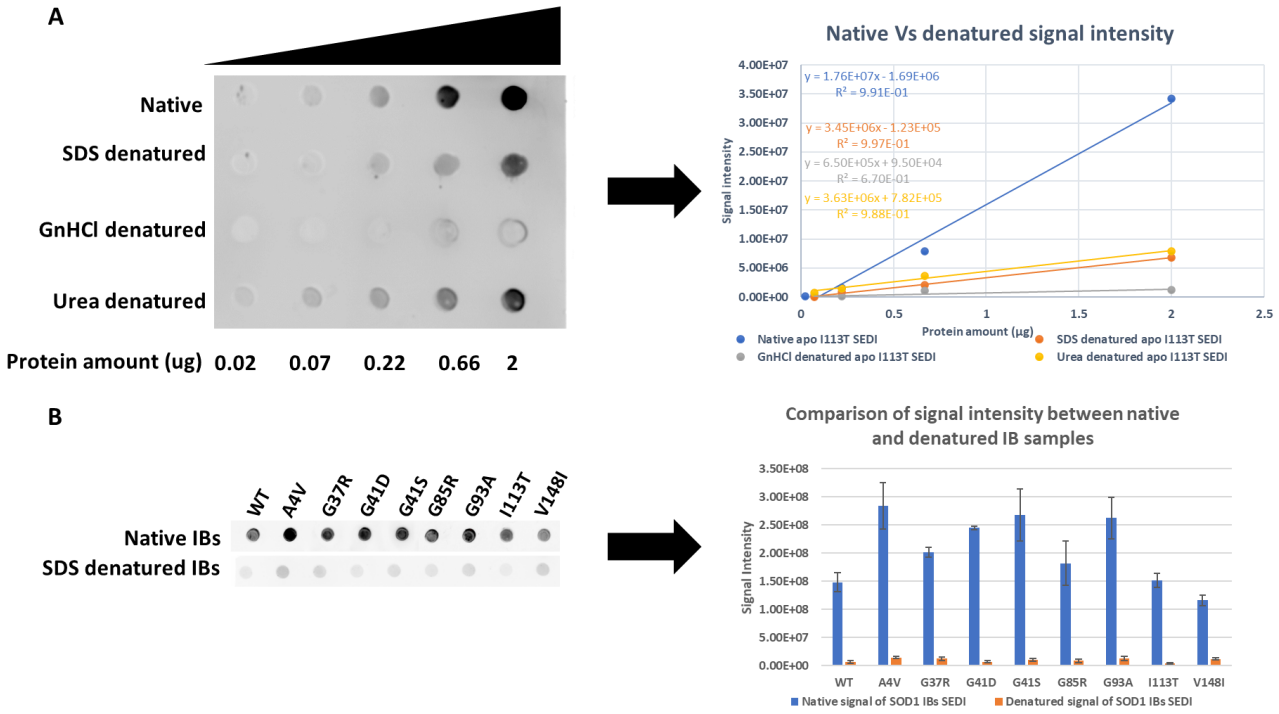

Figure 3.5: Comparison of dot blot signals for native and denatured purified protein and IBs. (A) Purified apoI113T was denatured using different agents, and all the denatured samples were blotted along with native apoI113T. (B) 9 SOD1 mutant IBs were blotted in native, and SDS denatured form, and this experiment was performed in triplicate. Error bars represent the standard deviations for the triplicate signals. The plots show the denatured samples all give lower signal than their native counterparts.

3.2.2 Double membrane experiment to check retention capacity of blotting membranes

There could be two possibilities for the reduced signal observed with denatured samples. One possible explanation could be less efficient binding of the primary antibodies to the denatured samples compared to the native samples. The second possible explanation could be that the denatured samples were leaking through the NC membrane and hence, giving a lower signal. In such a case, it could have potentially been used as the normalisation control if all denatured samples were leaking to an equal extent. Hence, to verify this, a double membrane experiment was carried out. In this experiment, two blotting membranes were used instead of one in the dot blot apparatus with one membrane kept on the top of the other. The upper membrane had a pore size of 0.45 µm, whereas the lower membrane had a pore size of 0.2µm. Three different amounts of IB samples of WT and V148I serially diluted 5-fold 2 times and loaded onto the membrane in both native and denatured form. The results showed that the blotting membrane could retain most of the native inclusion body sample but denatured IBs were passing through the upper membrane (Figure 3.6A). Also, the proportion of denatured sample passing though for the three different amounts of IB loaded was also different, indicating that SDS-denatured IB samples could not be used for our quantitative purpose. The double membrane experiment was repeated with NC membranes with a lower pore size (0.1µm) to see if this could yield better retention, but the denatured samples still passed through unevenly (Figure 3.6B). This suggested that normalisation using SDS denatured samples could not be pursued successfully.

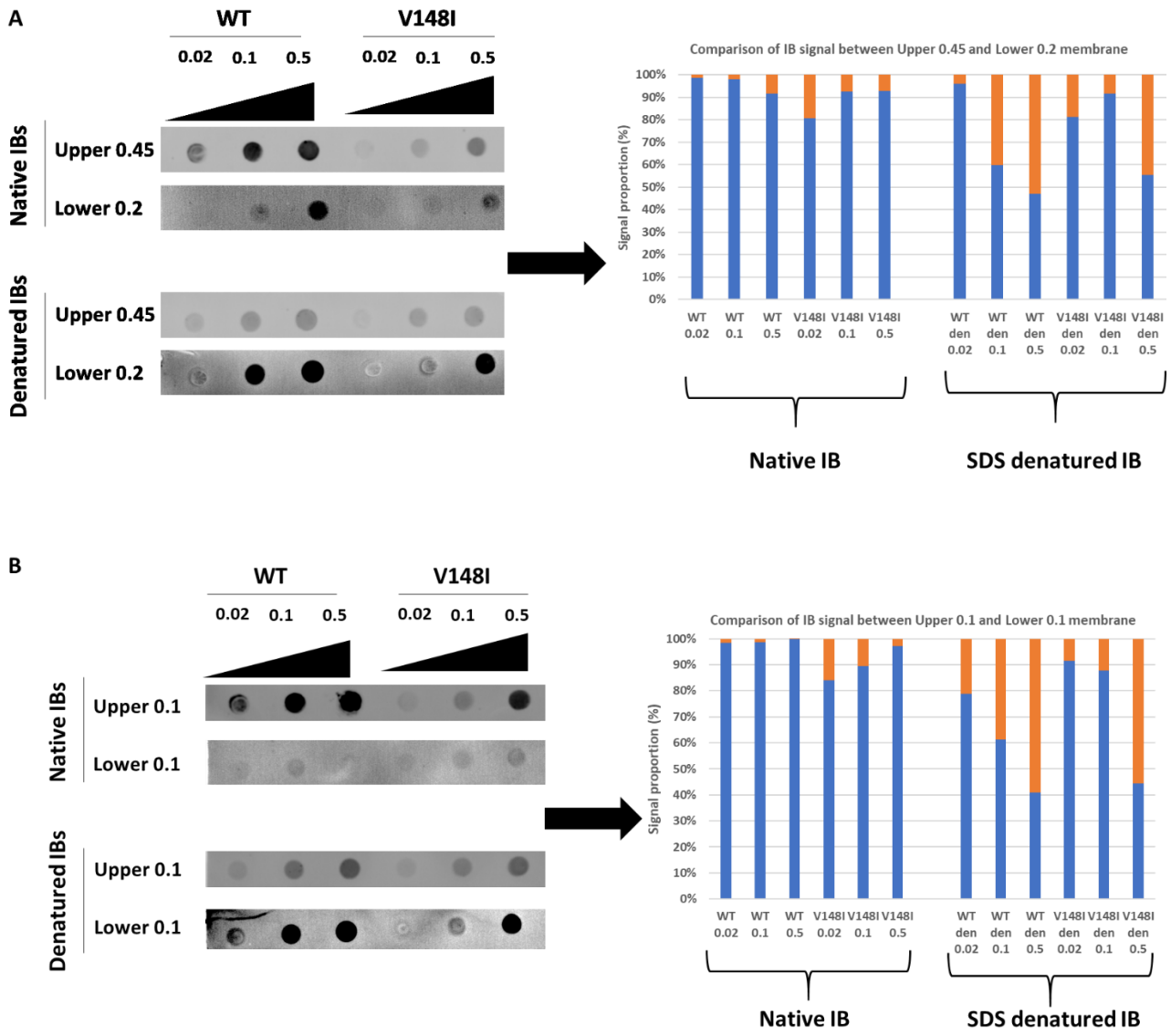

Figure 3.6: Double membrane experiment to measure dot blot sample leakage. (A) The dot blot was performed using upper 0.45 and lower 0.2 µm membranes and (B) upper 0.1 and lower 0.1 µm membranes. Blue and orange indicate the proportion of total signal on the upper and lower membranes, respectively. The results show NC membrane retains native IB samples, but denatured samples leak through irrespective of membrane pore size.

3.2.3 Optimisation of gel densitometry for protein quantification

Since the denatured controls could not be used for signal normalisation, we next examined quantifying the amount of SOD1 in the IBs loaded onto the membrane. Methods like Bradford assay or protein absorbance at 280 nm can not be used in this case as IBs are not pure samples and contain a variety of other cellular proteins. However, one option to quantify SOD1 from the IB samples is using SDS-PAGE densitometry. This technique comes with several challenges, including variability in the amount of the sample loaded and band intensity quantitation. Hence, it was crucial that all the samples for SDS-PAGE were prepared carefully; accordingly, we developed a consistent protocol for sample preparation, loading, gel staining and destaining as well as proper imaging.

In order to properly quantify band intensities from SDS-PAGE, it was crucial that we find a range in which band densitometry signals vary linearly with the amount of SOD1 protein and load all our IBs with an amount so that the SOD1 band intensity falls within that linear range. In order to find this linear range, purified apo pWT was loaded in a varying amount from 0.05 µg to 10 µg. Densitometry of each band was performed as described in the Methods (Section 2.4), with the background-subtracted using the rolling ball technique. With this method, the band intensities stayed linear over 0.625 µg to 5 µg range. Larger amounts of protein showed signal saturation, and lower amounts gave bands too faint for reliable densitometry. However, this 8-fold range was suitable for IB quantification.

Further, to assess the variability in protein quantification, an experiment was carried out where 3 SDS-PAGE gels were run with 7 SOD1 mutants (A4V, G37R, G41D, G41S, G85R, G93A and G93D). Each mutant was loaded once in one gel, and the other two gels were loaded with twice the amount of IB that was loaded in the first gel. Each gel also contained four

different amounts of purified apo pWT (0.625µg, 1.25µg, 2.5µg and 5µg) as the protein standard (Figure 3.7A). After SDS-PAGE was finished, all gels were stained overnight and destained on the next day. Post destaining, the gels were imaged in the ChemiDoc MP imager, and the SOD1 band intensities were calculated using BioRad Image Lab software. SOD1 amounts were quantified for each mutant IBs using the standard plots from purified apo pWT obtained from each gel (Figure 3.7B). The experiment was repeated four times (corresponding to each conformation-specific antibody blot) using different aliquots of the mutant IBs prepared from one growth to account for the variability in quantification.

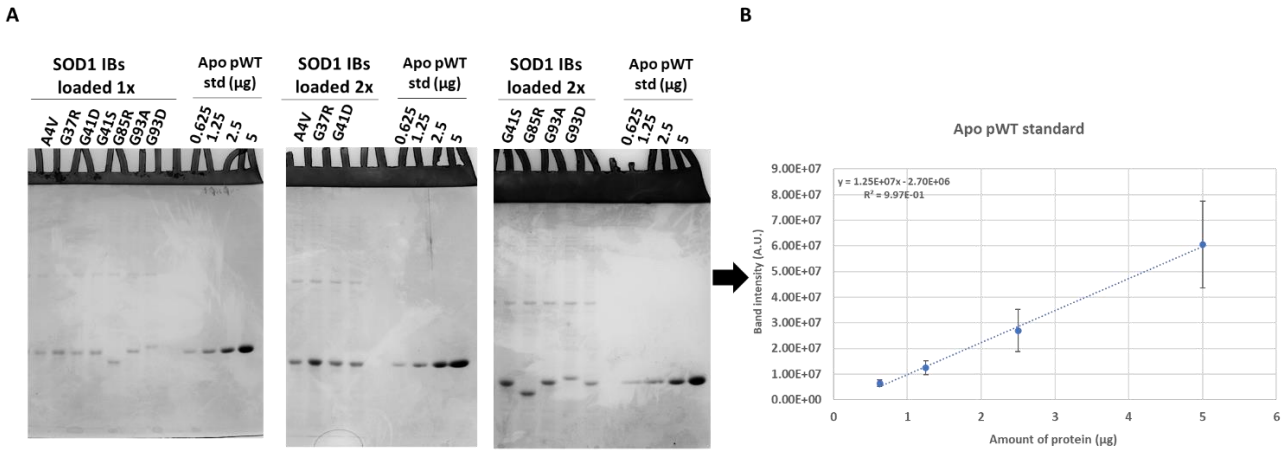

Figure 3.7: Quantitation of SOD1 in IBs by SDS-PAGE. A) 7 different SOD1 mutant IBs were loaded (in 1x and 2x amount) onto 3 SDS-PAGE with purified apo pWT SOD1 as the protein standard. IB samples were loaded with appropriate dilutions so that the SOD1 band intensities stay within the linear range of the protein standard. B) For each SDS-PAGE, band intensities of apo pWT standard were plotted against their respective protein amounts. This was used to quantify the SOD1 bands only of that SDS-PAGE. The plot represents the average band intensities of protein standard obtained from 4 sets of gels (12 SDS-PAGE in total). This is shown here only for illustration purpose of the linearity in the signal. Error bars in the plot represent the error associated with band intensities of different amounts of apo pWT standard.

The results indicated that SOD1 bands could be reliably quantified using this method. Table 3.1 gives the average SOD1 concentrations of the 7 mutants. The values represent concentrations of SOD1 in undiluted IB samples obtained through the protein amount calculated from SDS-PAGE. The variation in the quantified protein amount is represented by % error which is calculated as 100*(standard deviation of protein amounts/average protein amount). SOD1 amounts quantified for most of the mutants showed less than 10% variability except for A4V and G93D, which have a lesser amount of SOD1 in their IBs. However, for these mutants, the % error stayed under 20%. This indicated that higher variability in the densitometry could be expected for mutants expressing less IBs. Quantification using SDS-PAGE thus was the most robust and reliable method. Hence, it was used further in normalising the signals for the quantitative dot blot experiment of 11 SOD1 IBs with four conformation-specific antibodies, as further described next.

SOD1 mutants	**A4V**	**G37R**	**G41D**	**G41S**	**G85R**	**G93A**	**G93D**
Average protein amount (mg/ml)	0.658	1.056	0.711	0.845	0.831	0.836	0.587
% error	14.7	6.6	4.8	2.9	9.6	9.2	20.7

Table 3.2: SOD1 amount quantified using SDS-PAGE. Average values of SOD1 concentrations in 7 mutant IBs calculated using 4 sets of SDS-PAGE (3 gels in each set) are mentioned with their % error to show the extent of variability in protein quantification.

3.3 Quantitative dot blot for WT and 10 mutant SOD1 IBs with four conformation-specific antibodies

After both the dot blot protocol and the normalisation methods were optimised, the quantitative dot blot analysis was performed with 11 SOD1 mutant inclusion bodies and four conformation-specific antibodies. Briefly, all 11 mutant SOD1 IBs were spotted onto NC membrane for five different concentrations prepared by 2-fold serial dilution. The highest concentration of IB samples was also denatured with SDS and spotted onto the membrane. This control was to assess whether the antibodies bind comparably to the same (denatured) conformation for all the mutants. Three spots on the membrane were loaded with only TEN buffer, and signals from these spots were used as blank (0 points, Figure 3.3). SDS-PAGE samples were prepared using the same IB aliquots as were used for the dot blots. All 11 mutants were run in duplicate using a total of three gels, with each of the duplicates loaded on a different gel. All gels also contained the four different amounts of apo pWT as standard, and the amount of SOD1 in the IB sample bands on each gel were quantified using their respective protein standard curve. A higher amount of SOD1 IB samples were loaded for mutants that expressed considerably less IB (such as I113T). Figure 3.8 provides an illustration of the complete experimental setup. Four experiments were performed in this manner, each with a different conformation-specific antibody (SEDI, USOD, AMF7 and B8H10).

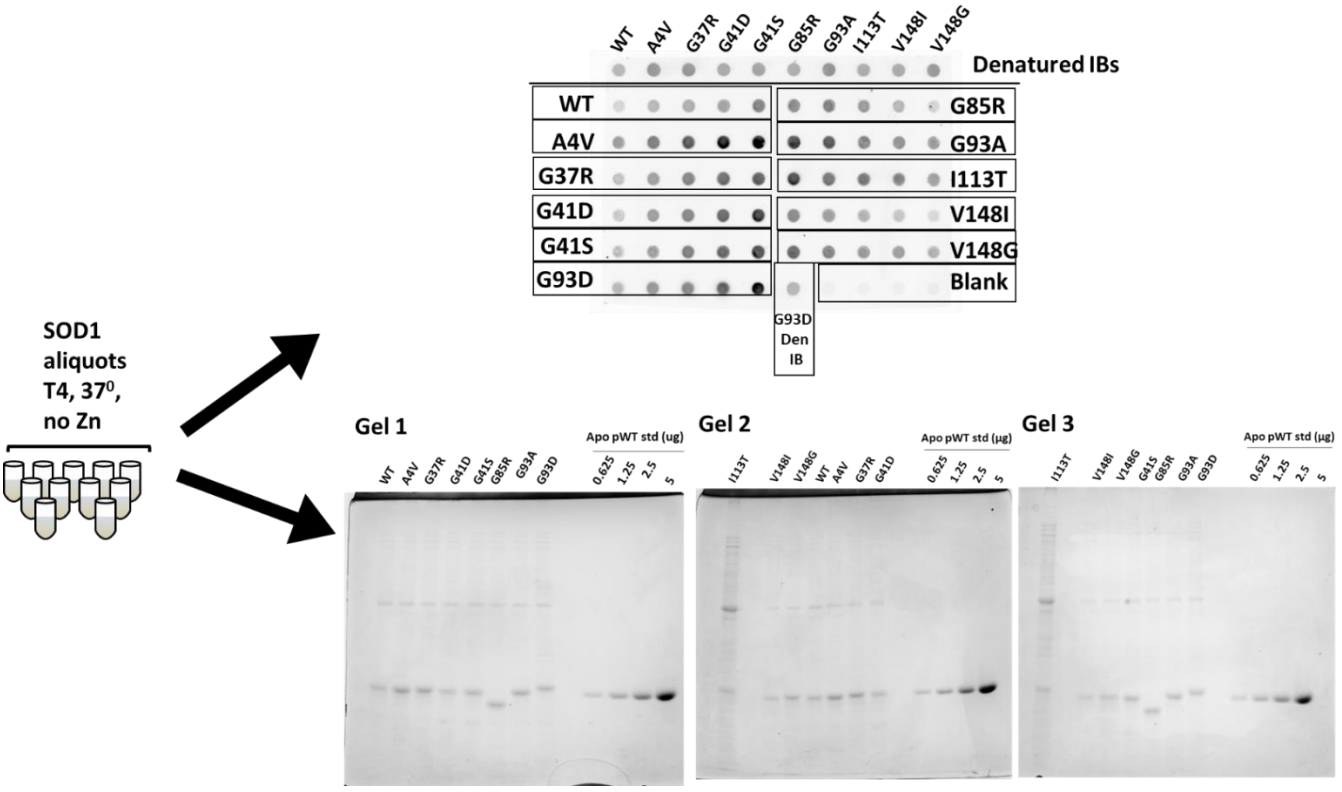

Figure 3.8: The experimental set up for quantitative dot blot. SOD1 aliquots for WT and 10 mutants are spotted on the NC membrane for 5 2-fold serial dilutions of the IB samples and incubated with AMF7 primary antibody. The samples are loaded on SDS-PAGE with apo pWT standard to quantify SOD1 amount in inclusion bodies and normalise dot blot signal.

3.3.1 Comparison of dot blot signal between biological replicates

In order to reliably compare differences in antibody binding for the 11 SOD1 mutants IBs, it was crucial that the experiments were performed in both technical and biological replicates. Technical replicates here refer to replicate experiments performed on aliquots of IBs from the same growth, and biological replicates refer to experiments performed on IBs obtained from two different growths. Both technical and biological replicate dot blot experiments were carried out for all four conformation-specific antibodies. Briefly, dot blot experiments for each

antibody were repeated in triplicate with different aliquots from the same growth (3 technical replicates) of the 11 SOD1 mutants. Data for biological replicates were obtained by growing these mutants again, and the dot blots were performed twice with the aliquots from this growth. Both these sets of replicates are denoted as biological replicates. The quantitative comparison was carried out by calculating the slopes from each dot blot experiment (shown in Figure3.3A). The slopes represent signal per μL of protein and were normalised by dividing with the SOD1 amounts quantified from the gel which is denoted as normalised slopes. Hence, the normalised slopes are calculated as the slope of linear fit/SOD1 concentration calculated from SDS-PAGE and represent antibody binding signal per μg of each SOD1 mutant.

In addition, for normalizing the comparison between different growths, A4V and V148I samples from the first growth were used as controls along with samples from the second growth. Normalised slopes of the these A4V and V148I samples from the first set of blots and the second set of blots were averaged for each set, and the ratio between the 2 averages was used to normalise the slopes obtained from the second set of replicate dot blot experiments. This allows variations in overall intensity of the blots to be taken into account. Thus, the slopes of the 2nd replicate sets were normalised first with their protein amounts and secondly with A4V and V148I normalised slope ratios. Accordingly, these slopes are denoted as double normalised slopes in further sections. A comprehensive flow chart explaining the experimental details and comparison of slopes from both sets of replicates is shown in Figure 3.9.

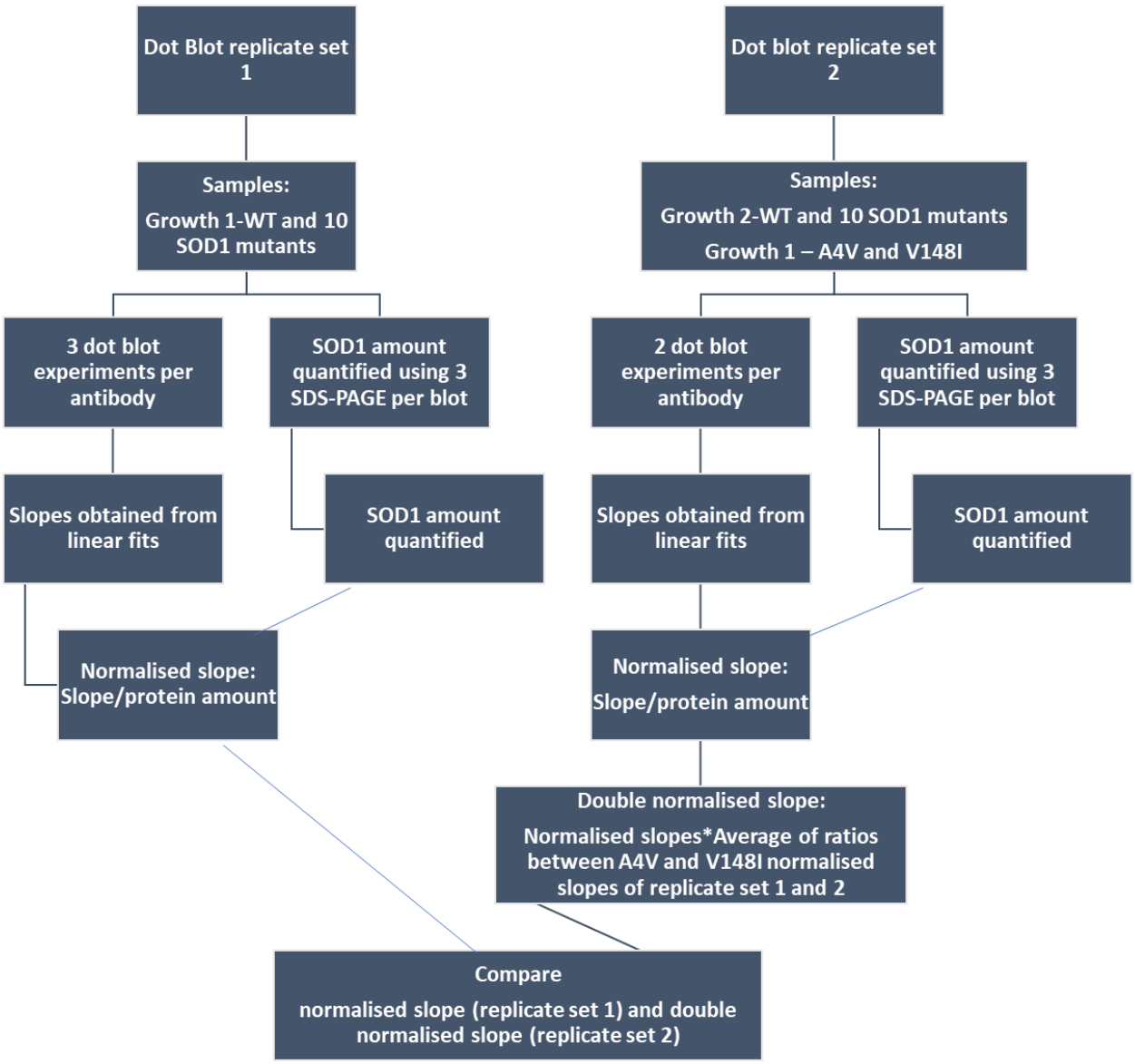

Figure 3.9: Flow chart illustrating signal comparison procedure between biological replicates. The samples used for each set of replicates is described in the second row. Signal was normalised with the protein amount and double normalised for 2nd set of replicates and compared together.

The normalised slopes from the first set of replicates and double normalised slopes from the second set of replicates for all four conformation-specific antibodies are compared and shown in Figure 3.10A. The plot shows there is good agreement between the two sets of replicates, i.e. the absolute values are close to each other, or their experimental uncertainties are

overlapping with each other for each antibody. This confirms that the quantitative dot blot protocol has worked for the selected 11 SOD1 mutants in terms of investigating their binding affinity with all four antibodies. Comparison for I113T mutant is not included as the normalised slope values for I113T were much higher than any of the other mutants. Comparison plots for I113T are later in the discussion section. Note that SEDI and USOD showed markedly reduced binding to V148G/I and G41S/D, respectively, for the denatured IB as well as native IB samples. This is reasonable because SEDI and USOD were raised against peptides that included V148 and G41, respectively. Consequently, V148G/I mutants binding to SEDI and G41S/D binding to USOD can not be compared with other mutants. In order to make the most reliable comparisons of antibody binding between mutants, the results from the biological replicates were averaged (Figure 3.10B).

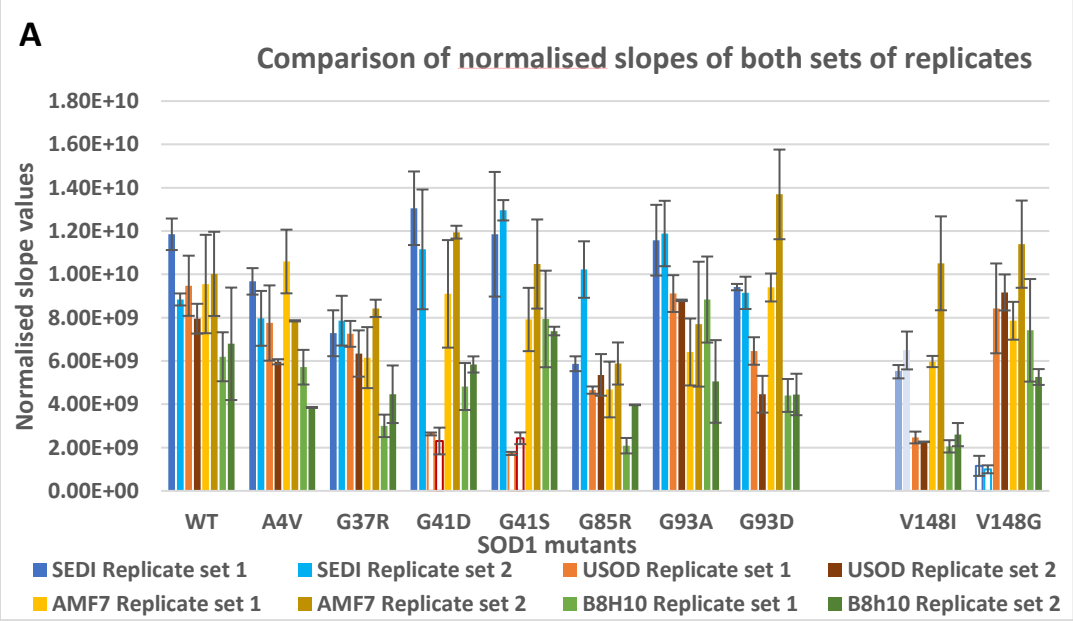

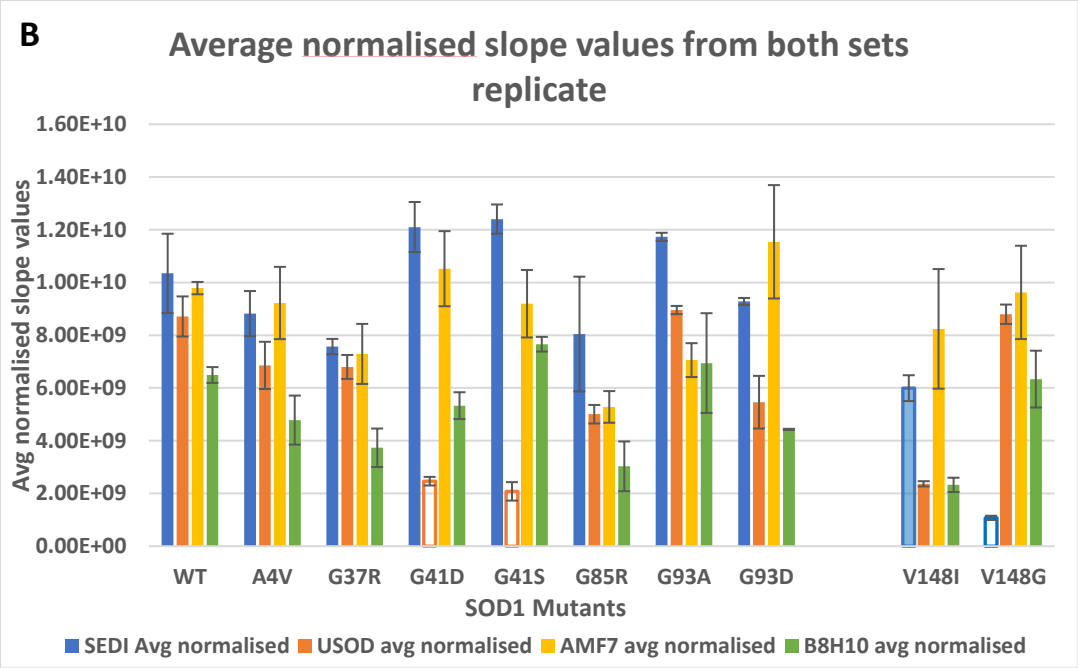

Figure 3.10: Comparison of binding of conformation specific antibodies to mutant SOD1 IBs. (A) Comparison of normalised antibody binding slopes for 2 independent mutant SOD1 IBs growths (biological replicates). Each of the 4 antibody results is shown in a different colour. Error bars represent standard deviations for multiple aliquots from a given grown (technical replicates), 3 for the first growth and 2 for the second growth for four antibodies. (B) Average normalised slope for the 2 biological replicates. Bars for G41S/D in case of USOD and V148G in case of SEDI are coloured white as the mutations occur in the known binding epitope for the antibody, resulting in markedly decreased binding evident in denatured IB controls (Figure 3.13).

3.3.2 Binding pattern of SOD1 mutants with respect to WT SOD1 IB

Many previous studies have shown that immature forms of SOD1 have significant propensity to misfold and aggregate in a variety of ways. The conformation-specific analysis conducted here is consistent with that observation and adds valuable information for comparison with these previous studies. To visualise how all SOD1 mutants bind to these antibodies in comparison to WT IBs, normalised slopes of each mutant were divided with the normalised slope of WT IBs, and the results for the biological replicates were then averaged (Figure 3.11). The error bar on each plot represents the variability in the ratios obtained from both sets of replicates. Values that are close to 1 indicate that those mutants bind to the antibody to a very similar extent as WT IB. The figure shows there are some significant and some minor differences in antibody binding pattern for different SOD1 mutant IBs when compared with WT IB. A detailed interpretation of these results is presented in the discussion 4.2.

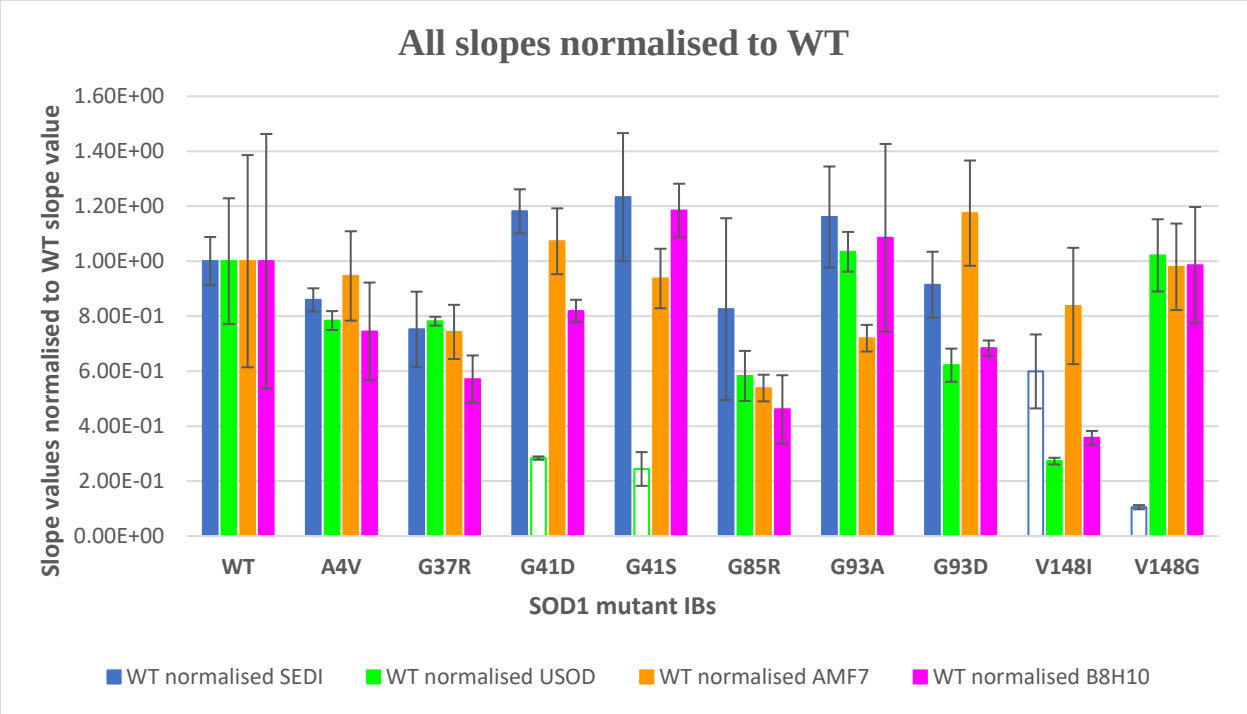

Figure 3.11: Comparison of IB antibody binding for SOD1 mutants relative to WT. Normalised slopes of each mutant was divided with the normalised slope of WT for replicate set 1 and set 2. Both ratios were averaged and plotted here to obtain their relative binding for all four antibodies. Error bar for all mutants except WT represent the variation in both ratios calculated where as error bar in WT represents average value of standard deviations of normalised slopes obtained from both sets of replicates normalised again to WT slope values.

3.3.3 Conformation-specific antibodies binding to I113T

One mutant that has not been shown so far in comparative analysis is I113T. It is an interesting mutant which has been reported to exhibit variable ALS disease duration[136]. During the growth and quantitative analysis, it was seen that I113T expressed much lower amounts of IB. Hence, 10x of the quantity of IB sample had to be loaded on the SDS-PAGE to quantify the I113T-SOD1 band (Figure 3.12A) accurately. Interestingly, the I113T samples showed the highest binding by far for all the conformation-specific antibodies. When the normalised slopes

of I113T were compared with that of WT, it showed ~ 3-7 times more signal for SEDI, USOD and B8H10 (Figure 3.12B). For AMF7, this ratio was >10, probably higher at least in part due to the characteristics of the AMF7 antibody, which generally shows more signal than other antibodies. This observation of much higher binding to I113T was, however, not expected as there is nothing specific about I113T that could explain such high binding. It could be argued that the unusually low expression level for I113T in both the supernatant and pellet fractions is not explained by I113T thermodynamic stability, which is comparable to that of other mutants[137]. However, it may be indicative of increased proteolytic degradation of the protein. Inclusion bodies are known to contain different forms of a given protein, including proteolytic fragments[138]. This could lead to its digestion through proteases which would result in smaller fragments of SOD1 and become more susceptible to bind to antibodies. However, during the analysis, no protease cleavage site was found in I113T sequence. Hence, a high-resolution mass spectrometry analysis would be of interest to understand this result better.

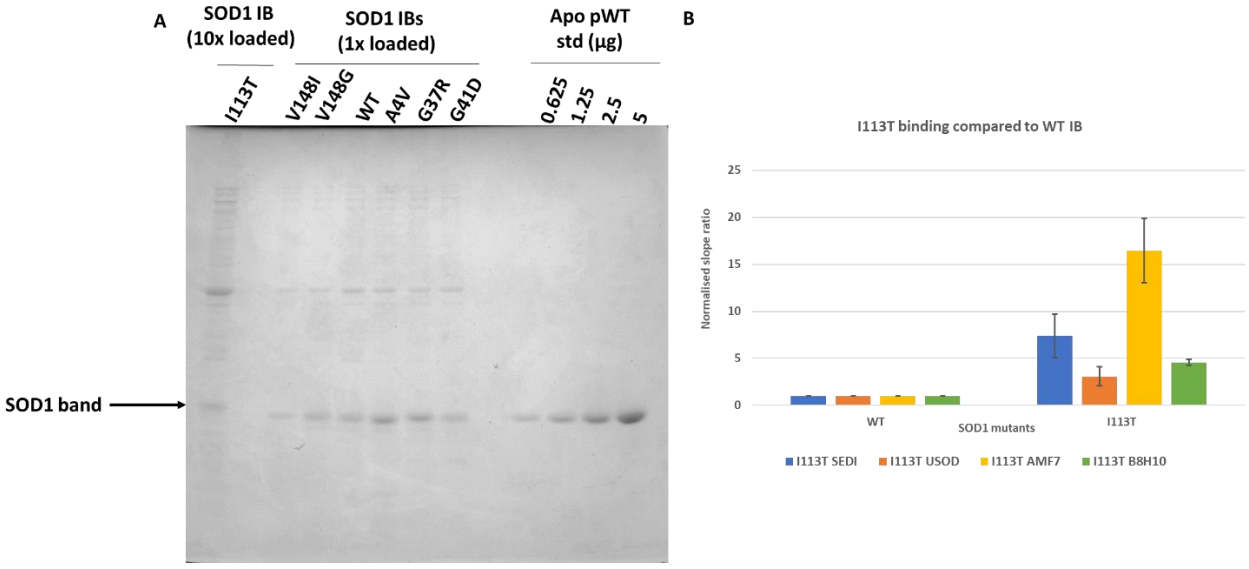

Figure 3.12: **Low protein expression and high antibody binding by I113T**. (A) SDS-PAGE showing SOD1 level in I113T IBs where 10x amount of I113T IB is loaded with 1x amount of other SOD1 mutant IBs along with purified protein standard.

3.3.4 Mutations in the epitope regions affect antibody binding to variable extents

Out of 11 selected set of mutants, G41D and G41S are mutations in the USOD epitope region whereas V148I and V148G are mutations in SEDI epitope. With the dot blot experiment, it was seen that the antibodies bind less or not at all to the aggregates if there is a mutation in their epitope region. This is based on the observation that these antibodies did not produce any signal for these antibodies both in their native aggregate form as well as SDS-denatured form (Figure 3.13). This indicates that the antibodies are not able to bind to the denatured form of the protein as well. Interestingly, V148I does show some signal for SEDI when denatured, whereas V148G does not; this is consistent with V to I being a much more conservative mutation than V to G. Thus, nature of the mutations in the epitope regions is crucial for these conformation-specific antibodies to bind to the denatured form of the protein. However, we also see the low

binding of SEDI to native IB structure of V148I, and it can not be conclusively determined whether it is representing true features of the mutant IB structure or the mutation is hindering the binding of SEDI in native its aggregate.

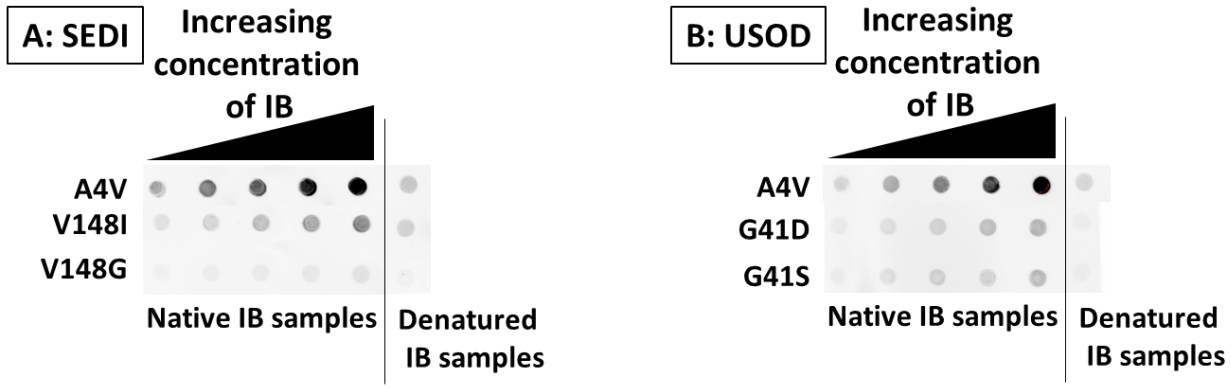

Figure 3.13: **Comparison of antibody binding to native and denatured IBs**. A) Native and heat and chemically denatured IBs of V148I and V148G binding with SEDI. B) Native and denatured IBs of G41S and G41D binding with USOD. A4V is included as a mutation outside the antibody epitopes. Native IBs were loaded in 5 different concentrations with 2-fold increment, and one denatured sample was loaded to check if there is any signal with the antibody. A4V native and denatured IBs are shown as a control for comparative purposes.

3.4 Investigation of inclusion body properties

3.4.1 Checking homogeneity of SOD1 inclusion bodies

SOD1 IBs contain high amounts of SOD1 but also contain other cellular proteins. One of the most prominent cellular proteins is OmpF which is an outer membrane protein in *E. coli* that allows proteins to be exported to the outer membrane space[139]. Previous studies by John Almey, a former MSc student in the Meiering lab, had shown that when SOD1 IBs are grown in rich media and washed with mild detergent like Triton-X 100, the OmpF was not removed from the

SOD1. This result may be accounted for by SOD1 co-aggregating with OmpF, or the two proteins may separately be sedimented into the IB-containing cell pellet. This suggests the possible formation of heterogeneous aggregates of SOD1 where other proteins like OmpF might also be involved. Also, several studies have reported the potential interaction of chaperone proteins with SOD1 inclusion bodies[140]. Note that in general, specificity in protein aggregation has been noted[141]. Hence, it is of interest to investigate whether SOD1 aggregates in the inclusion bodies prepared in minimal media for the current study contain any other proteins making specific interactions with SOD1.

To investigate this, inclusion bodies were washed with four different detergents (Triton-X 100, Tween 20, NP 40 and n-Octylglucoside) as per the protocol described in Method (Section 2.6). The experiment was carried out with A4V IB samples, and it was found that n-Octylglucoside (n-OG) detergent was effective in removing OmpF as well as some other contaminant proteins from A4V IB sample (Figure 3.14A). This detergent was further used to wash five other mutant IBs (WT, G41D, G41S, V148I and V148G) and in all cases, n-Octylglucoside was successful in removing the prominent OmpF band (Figure 3.14B). This suggests that the contaminant proteins in SOD1 IB preparations are likely not making strong or specific interactions with SOD1. Since the major protein component of the IBs is SOD1, the binding pattern demonstrated by various conformation-specific antibodies is likely reporting on the variation in the aggregate structure, which are composed mainly of SOD1 proteins.

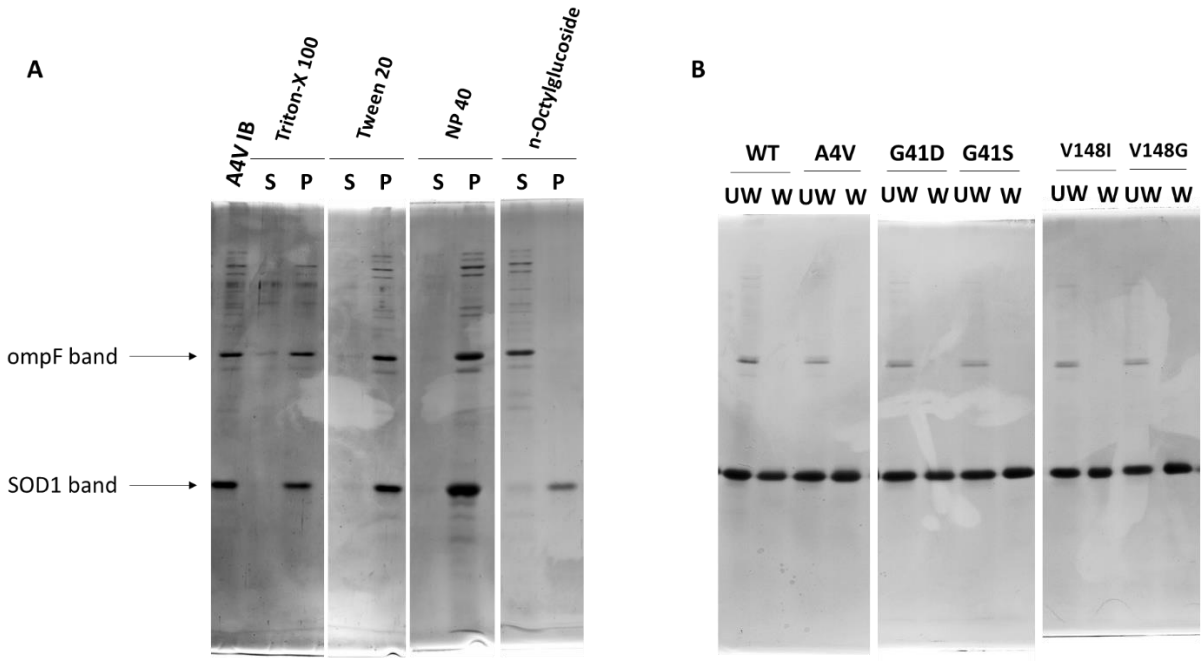

Figure 3.14: Effects of detergent washes on SOD1 IB impurities. (A) A4V IB was washed with four different mild detergents. N-Octylglucoside successfully removed OmpF and other protein bands from the IB sample. S and P represent the Supernatant and Pellet fractions respectively. (B) Other mutant IBs also showed a similar pattern where protein bands, including OmpF, are washed to the supernatant fraction once washed with n-OG. UW and W represent the IBs not washed with detergent and washed with detergent respectively.

3.4.2 Investigating the oxidation status of SOD1 in IBs and soluble cell fractions

The most immature form of SOD1 has Cys57 and Cys 146 in their reduced state, which then becomes oxidised during the process of maturation. Several studies have found that the aggregates in ALS models primarily contain the most immature form of SOD1 where the free cysteine residues are in reduced form. Thus, it was intriguing to check the oxidation status of SOD1 in the inclusion bodies prepared in minimal media. To do so, cell pellets harvested after 4-hour growth post-induction and the IB samples obtained after the freeze-thaw cycle were

labelled using 0.5M iodoacetamide as described in the Method (Section 2.7). The cells were grown at 37^0C or at 25^0C to examine the effect of temperature on oxidation state. The inclusion body samples obtained as the pellet fraction, as well as the soluble cell fraction, were run on non-reducing gels and images of those gels are shown in Figure 3.15. Iodoacetamide binds irreversibly with the thiol group of cysteine preventing it from forming a disulfide or other covalent linkage. Thus, the IA labelling of the free cysteines allows us to check the oxidation state when the cell pellets are harvested. Cysteine residues in SOD1 that are already oxidised, for example in intramolecular or intermolecular disulfide bonds, will not react with IA. Thus, different forms of SOD1 can be distinguished by their different apparent molecular weights in SDS-PAGE where the reduced monomers migrate slower than oxidized monomers, and intermolecular linkages can give rise to bands for dimeric and higher-order SOD1 species. As a standard sample, a reduced IB sample was run along with all IA samples so that the distance of migration for reduced SOD1 could be assessed. All IB samples showed a significant band only for reduced monomer, indicating that SOD1 aggregates present in the inclusion body samples could primarily be in the reduced state. Only V148I supernatant fraction has a prominent oxidised band both at 37 and 25^0C. V148I SOD1 is the most stable variant studied, being slightly more stable than WT[142]; this relatively high stability may promote the formation of the intramolecular disulfide bond by increasing the population of the folded monomer. However, WT soluble fraction has also been shown to contain oxidised SOD1 species based on the observation from previous students in our lab. Here, it appears only to contain reduced band potentially because the sample is run along with reduced WT IB standard which contains β-me (reducing agent) and β-me is known to leak to its neighbouring lanes and thereby, reduce the oxidised species One of the former master's students, Hilary Simon, labelled WT IB and

supernatant fractions from different time points of the growth post IPTG induction (2hrs, 4hrs, 6hrs and 24hrs) with IA to check time-dependent variation in oxidation state. The results showed that the oxidised SOD1 band became dominant over time (especially in the supernatant fraction) (Figure 3.15C). It is noteworthy that A4V, G41D/S grown at 37°C contain little SOD1 in their supernatant fractions. However, this experiment was conducted only once, and hence replicate, and further experiments should be performed to obtain more conclusive information about the oxidation states of inclusion bodies under different growth condition.

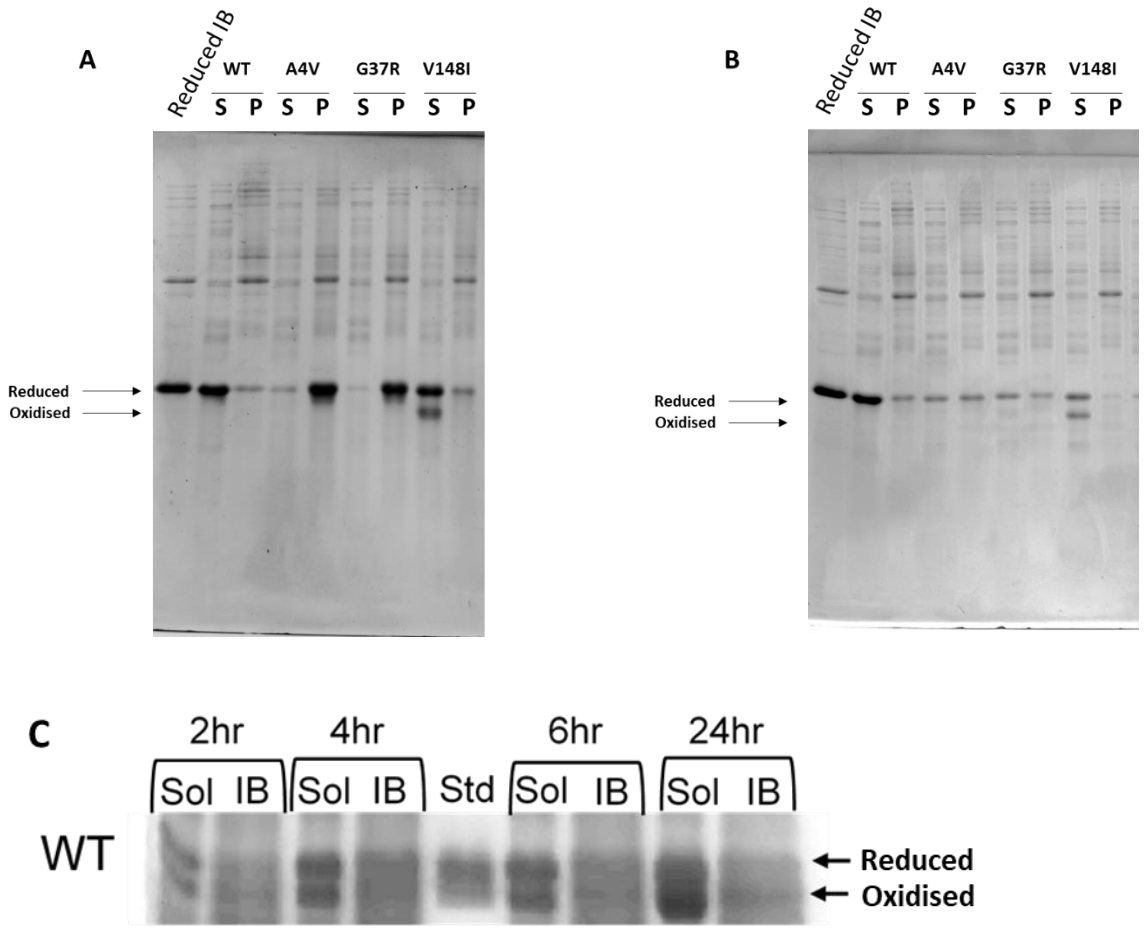

Figure 3.15: IA labelling to check the oxidation status of SOD1. IB and supernatant fractions of 4 SOD1 mutants labelled with IA and analyzed by non-reducing 12.5% SDS-PAGE. A) IA labelled SOD1 samples grown at 37^0C. B) IA labelled SOD1 samples grown at 25^0C. IB samples obtained from both growth conditions are predominantly reduced. Only the V148I supernatant fraction showed prominent oxidised SOD1 band. S and P represent the Supernatant and Pellet fractions, respectively. C) IA labelled SOD1 samples from the different time point of growth at 37^0C. Supernatant fractions show a marked increase in oxidised SOD1 population over time. Sol represents soluble fraction whereas IB represents pellet fraction.

4 Discussion

4.1 Optimisation of the quantitative dot blot

Our results show that developing a quantitative approach to characterise conformation-specific antibodies to SOD1 IBs requires several steps of optimisation. Previous studies have used chemiluminescence for signal detection in their dot blot experiments to characterise the binding of various anti-SOD1 antibodies to SOD1 samples[127, 105]. Here, we reported that secondary fluorescence antibodies work better for developing a quantitative immunoblotting assay because of its consistent signal intensity over time as well as better reproducibility. However, it was crucial to choose a secondary antibody that could give a fairly high and consistent linear signal over a wide range of protein amounts and low signal to noise ratio. Starbright 700 secondary antibody was able to satisfy these properties when imaged in a Chemidoc MP imager. This could probably be due to its unique wavelengths of excitation and emission (Table 3.1). The antibody has its excitation in visible spectrum area while emission near IR region, which is known to provide the best signal to noise ratio[143]. Importantly, it was also noted that incubating the blots with the primary antibody in an open container yielded more consistent results and reduced background signal suggesting that uniform distribution of antibody is crucial for reliable signal detection.

Once, the protocol was optimised, two key aspects of developing quantitative dot blot were explored: 1) finding the linear range of detection for SOD1 IBs, 2) normalisation of dot blot signal through protein quantification. Several concentration-dependent dot blot assays were carried out to address the first issue (Figure 3.3), and we saw a linear trend for the lowest 3 concentration points while the signal generally saturates for the last two highest concentration points. This could be due to an excessive amount of proteins present in the higher concentration

points, which might lead to inefficient binding with the NC membrane and subsequent dissociation during the washing steps. The second explanation could be that the structure of the aggregates might only allow a certain number of primary and secondary antibodies to bind, and this might vary among mutants. For each dot blot, it was also important to keep several blank wells (3 in our case), the average intensity of which was used as the 0-concentration point. However, there could still be some degree of variation in dot blot signal among replicates as shown in Figure 3.4 suggesting that technical as well as biological replicates are necessary to account for this variation and the interpretation of the data should be made accordingly. The results also showed that SDS-denatured samples could not be used for signal normalisation as they leak through the NC membrane unevenly. Quantification using SDS-PAGE proved to be a robust technique for signal normalisation. It is important to note that the band intensities to be quantified should always stay within the linear range. Protein standard should always be used with each SDS-PAGE and SOD1 bands should be quantified only from that standard as background signal/band intensities on SDS-PAGE are highly dependent on the extent of staining and destaining. Finally, double normalisation proved to be an effective technique to compare results from biological replicates. IBs from different growth of the same mutant may contain a variable amount of SOD1 (we saw this for WT, A4V replicate growths). Even with such variability, we see a comparable extent of binding of all mutant IBs to all four conformation-specific antibodies. Hence, these data could be reliably used for quantitatively characterising the binding profile of different SOD1 aggregates to antibodies.

4.2 Various properties of the 11 SOD1 mutants chosen for the dot blot assay

11 SOD1 mutant inclusion bodies were grown in minimal media without the addition of any metal to investigate aggregates formed by immature SOD1 conformations. One of the key unresolved mysteries in SOD1-mediated ALS pathology is the wide variation in disease duration for different SOD1 mutants. For example, A4V mutation in the dimer interface of SOD1 shows an average disease duration of about one year, whereas G37R mutation in the loop III region has an average disease duration of over ten years[144] (Table 4.1). There have been many studies to identify quantifiable biophysical properties of SOD1 such as protein stability, aggregation propensity[142], folding kinetics[145] etc. that could explain these differences. Still, no clear correlation has been found yet. Previous studies by Johnathan Almey and Dalia Naser in the Meiering lab have shown that different SOD1 mutants have different aggregation propensities in rich and minimal media[146]. However, predicting these aggregation propensities using several aggregation predictor software has been met with limited success[146,144]. This is probably influenced by the effects of mutations in SOD1 propagating throughout the structure[147]. Hence, mutation-induced misfolding in SOD1 could disrupt the structures of regions away from the site of mutation unpredictably and, thereby, lead to the formation of a variety of higher-order oligomers and aggregates with different conformations. The growing evidence on prion-like conformational strains of various SOD1 misfolded species further argues for the possibility of different aggregate structures forming due to different "strains" of SOD1 mutants[90].

The 11 mutants chosen for the current study are dispersed throughout the structure of the protein, as shown in Figure 1.3. These mutants are also known to span in their range of average disease durations in ALS, making them attractive candidates for studying aggregate structures. Information on the regions of these mutations, their disease durations, melting temperatures and

aggregation propensities in different growth conditions are summarized in Table 4.1. Some of these mutations are in the β-strands (A4V, G41S/D, G85R, V148I/G), whereas others are in various loop regions (G37R, G93A/D, I113T). Some are in the dimer interface regions as well (A4V, I113T, V148I/G). Thus, investigating the inclusion body structures of these mutants has the potential to provide valuable information on the roles of loop vs strand, dimer interface vs non-dimer interface mutations on aggregate structures. Most of the mutants under study show high aggregation propensity when they are overexpressed for 4hrs at 37^0C in the minimal media. However, it is interesting to note that different mutations in the same residue can lead to different aggregation propensities, such as V148I aggregating much less than V148G (Table 4.1). Aggregation propensities were calculated by running the soluble fractions and insoluble IB fractions together on 12% SDS-PAGE. Densitometry of SOD1 bands was obtained with proper background subtraction (using rolling ball background subtraction method). % insoluble was calculated using the equation shown below.

$$\% \text{ insoluble} = \frac{\text{SOD1 band intensity in IB}}{\text{SOD1 band intensity in IB + SOD1 band intensity in soluble fraction}} * 100$$

SOD1 mutant	Region of mutation	Avg. disease duration (years)	Holo T_m (^{0}C)	Apo oxidised T_m (^{0}C)	Reduced apo T_m (^{0}C)	% insoluble (4hr post-induction)	
						37^{0}C, no Zn	25 ^{0}C no Zn
WT	not applicable		92.7	59.1	47.6	27	22
A4V	β-1 (dimer interface)	1.2	86.7	50.7	36.3	98	86
G37R	Loop III	17		50.1	33.5	98	71
G41D	β-4	14.1	86	45.2		96	81
G41S	β-4	1	84.4			97	78
G85R	β-5	6	77.5	54.7	40.7	98	64
G93A	Loop V	3.1	87.7	47.9		97	73
G93D	Loop V	8.8	85.1	45.6		96	80
I113T	Loop VI (Dimer Interface)	4.3	88.2	47.1		43	45
V148I	β-8 (dimer interface)	1.7	92.7	60.5	51	73	31
V148G	β-8 (dimer interface)	2.1	86.9	49.3	34	96	83

Table 4.1: Properties of SOD1 mutants. Location of 11 mutations in SOD1 structure, their disease duration, melting temperatures of holo, oxidised apo and reduced apo form as well as % insolubility after 4 hours post-induction without in 37 or 25^{0}C in minimal media.

4.3 Structural characterization of SOD1 IBs using conformation-specific antibodies

To investigate the structures of SOD1 mutant IBs, four different conformation-specific antibodies were used that are known to recognise epitopes dispersed through the structure of the protein. These four antibodies are called SEDI, USOD, AMF7 and B8H10, which are known to bind to exposed dimer interface, β-4 strand, electrostatic loop and exon-3 encoded Zn-binding loop, respectively. The binding profile of the inclusion bodies to each of these conformation-specific antibodies was quantified using the dot blot protocol. The degree of binding was represented in terms of normalised slopes. In order to compare the binding profile of each mutant to WT, their normalised slopes were divided with that of WT, as shown in Figure 3.11. For illustrative purpose, these normalised slope ratios were mapped onto the SOD1 structure, as shown in Figure 4.1. For visualisation, the colours are shown in one of the subunits of SOD1 dimer. The intensity of each of these colours represents the degree of antibody binding compared to WT. Hence, darker shades of the colours would mean high degree exposure of epitopes whereas lighter shaded would imply that the epitopes are more buried. The intensities of the colours are also proportional to the absolute values of normalised slope ratios to make the colour scheme quantitatively accurate.

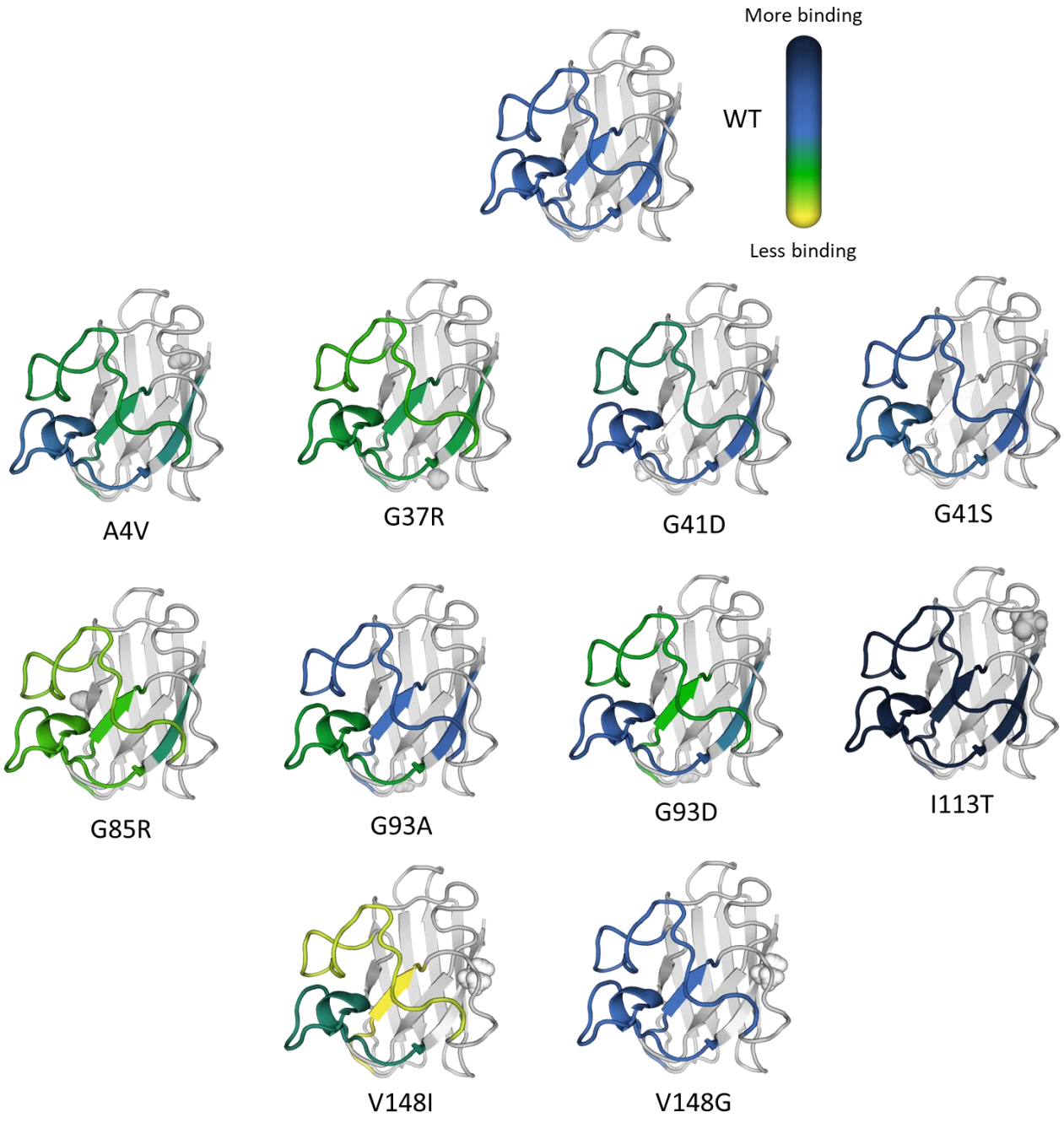

Figure 4.1: Relative binding affinity of 10 SOD1 mutants to four conformation-specific antibodies mapped onto SOD1 monomer structure. The four epitopes corresponding to the binding regions of each antibody is colored in blue in WT structure. Relative binding of each antibody is mapped onto its respective epitope for all 11 mutants. The intensity of the colour is proportional to their binding profile with respect to WT IB, as shown in the top panel of the figure.

4.3.1 SOD1 mutant IBs binding to SEDI and USOD

The normalised ratios indicate that while some of the mutants show equal or more exposure of antibody epitopes compared to WT, some of them significantly show protected patterns indicating that the epitopes are buried in the aggregate structure. SEDI antibody that was raised against the C-terminal dimer interface epitope binds similarly to all SOD1 mutant IBs, with somewhat decreased binding for A4V and G37R. While A4V is a dimer interface mutant, G37R does not reside near the dimer interface but nevertheless, rather surprisingly, shows similar increased protection (Figure 4.1). Similar to A4V, V148I, another mutation in the dimer interface, may also show increased protection compared to WT; since the V148I mutation is in the antibody epitope region, though, conclusions on its aggregate structure due to low binding should be viewed with caution. Interestingly, G41S, G41D and G93A mutants show similar or higher binding to SEDI, indicating that aggregates of these mutants have the comparable degree of dimer interface exposure and misfolding as WT. SEDI antibody was designed by Rakhit *et al.* [148] against amino acid residues 145-151) that lie in the C-terminal dimer interface region. It is a patch of hydrophobic residues that generally stays buried in the native dimeric structure. Hence, the binding with this antibody occurs only when native dimer is disrupted or misfolded, thereby exposing those hydrophobic residues. Using this antibody, Rakhit *et al.* were able to show the presence of such monomeric misfolded species in the aggregates found in spinal cord motor neurons of G37R, G85R, G93A transgenic mice as well as A4V ALS patient samples.

A further study used both SEDI and USOD antibodies to investigate soluble and insoluble fractions of spinal cord samples from ALS patients[149] and found misfolded SOD1 species in both fractions. USOD antibody was raised against amino acid residues 41-48 (residues GLHGFHVH), which form the β-4 strand (residues 41-48). These residues are generally buried

in in mature holo SOD1, under the active site loops, and include two histidine residues that are involved in coordinating with active site copper ion. Hence, binding by this antibody indicates at least disruption of the active site region and was suggested by Kerman *et al.* to report on full unfolding of the monomer, which results in maximal exposure of this epitope.

Our results show some interesting binding pattern of inclusion bodies to USOD. V148I IBs show the least binding to USOD, suggesting the active site and β-barrel structure are not disrupted for this mutant, consistent with its relatively high monomer stability (Table 4.1). G85R and G93D show ~60% of binding whereas A4V and G37R show ~80% of binding to USOD compared to WT. This indicates that A4V and G37R exhibit a similar extent of protection for SEDI and USOD epitopes, whereas G85R and G93D have their dimer interface more exposed than β-4 strand compared to WT aggregates. This is clear evidence of different conformations of SOD1 aggregates and illustrates varying degrees of disruptions in different regions of the structure by these mutants. Two other mutants G93A and V148G show the similar extent of binding to USOD as that of WT. This provides another interesting aspect of the difference in aggregate structures due to different mutations on the same residue of SOD1.

4.3.2 SOD1 mutant IBs binding to AMF7 and B8H10

In contrast to SEDI and USOD, AMF7 and B8H10 were raised against loop regions of SOD1 structure. B8H10 recognises an epitope within the metal-binding loop (loop IV, amino acid 57–80), the exposure of which is associated with a deficiency in metal co-factor binding[120,118,150]. The rabbit monoclonal AMF7-63 is a higher affinity version of the mouse monoclonal DSE2 and was raised against residues in the electrostatic loop (loop VII, amino acid 125–142), the exposure of which is associated with increased conformational flexibility in this region[122,127]. Both loops have been reported to be highly dynamic components of SOD1

structure[151]. AMF7 and B8H10 antibodies were used in a study by Sarah et al. (2016)[122] to show the presence of different conformations of SOD1 aggregates in transgenic mice mouse models. These conformations were seen to localise in different regions of spinal cord mitochondria and later found to interact with several common as well as distinct intracellular proteins[123]. Our results show that most of the mutants bind strongly to AMF7, indicating that a similar extent of destabilisation of the electrostatic loop might be a common pathway for aggregation. The three exceptions that show a protected pattern for AMF7 are G37R, G93A and G85R. While G37R and G93A inclusion bodies show ~70% binding compared to WT, G85R shows ~50% binding. This observation may be consistent with previous studies from Sekhar *et al.* [152] who found that one of the excited conformations of reduced apo WT-SOD1 in which a short helix formed in the electrostatic loop was completely absent in G85R. Moreover, mutagenesis analysis using UCSF Chimera software indicates that the longer side chain of Arginine residue might protrude into the space of Zn-binding and electrostatic loop potentially making both these epitopes inaccessible for antibody binding (Figure 4.2A). This idea is supported by the observation that the native G85R IB binds poorly to AMF7 and B8H10 whereas the denatured form of the aggregate bind to these antibodies to a similar extent as that of high binding mutants (G41S.G41D). The comparison of normalised binding signal for native and denatured G85R IBs with that of G41S/D is shown in Figure 4.2 C.

Unlike AMF7, B8H10 shows wide variation in its extent of binding to various SOD1 aggregates. Apart from G85R, V148I binds poorly to B8H10, which is surprising as the mutation does not lie anywhere near the epitope region. However, mutagenesis analysis shows that the addition of a methyl group due to Isoleucine residue at 148th position might sterically hinder and disrupt the loop region that precedes the B8H10 epitope as shown in Figure 4.2B. Two of the

other mutants G37R, G93D show ~60-65% binding compared to WT while the rest of the mutants show more than 75% binding to B8H10. It is to be noted that while most of the SOD1 mutants exhibit a relatively high exposure of AMF7 epitope in their aggregate structures, B8H10 epitope is more variably exposed by these mutants suggesting that the electrostatic loop and the zinc-binding loop might have different propensities to get disrupted during aggregate formation.

A

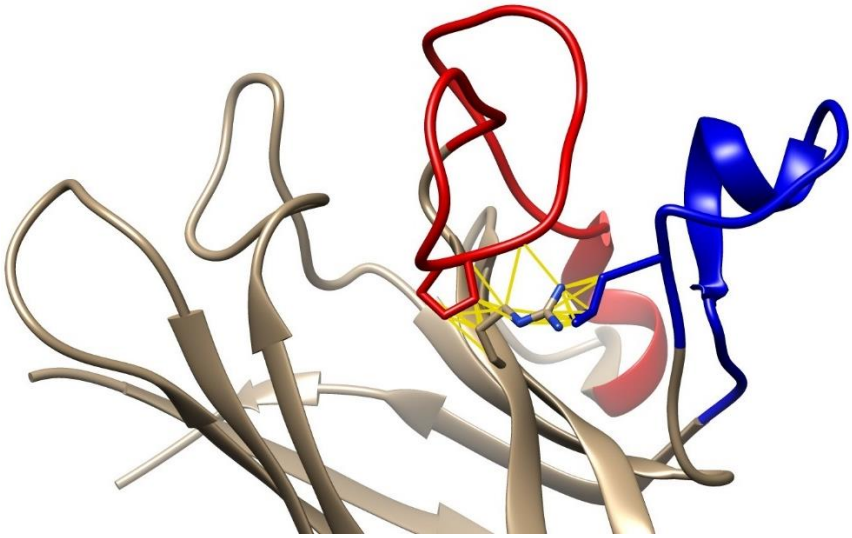

B

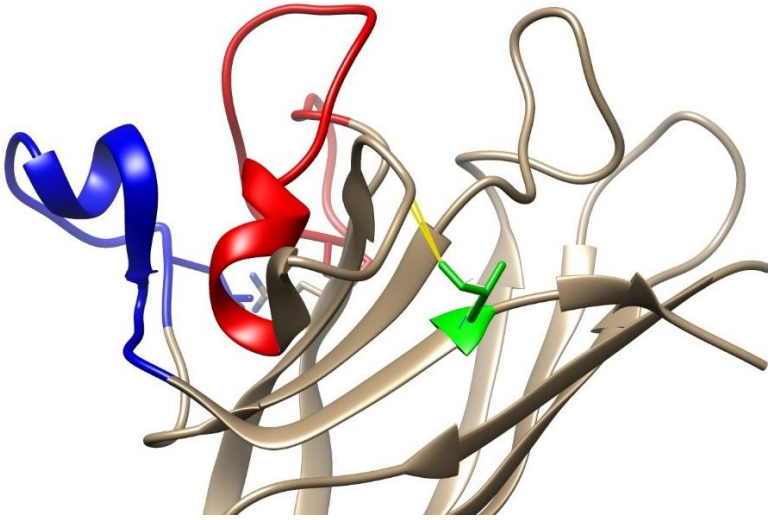

C

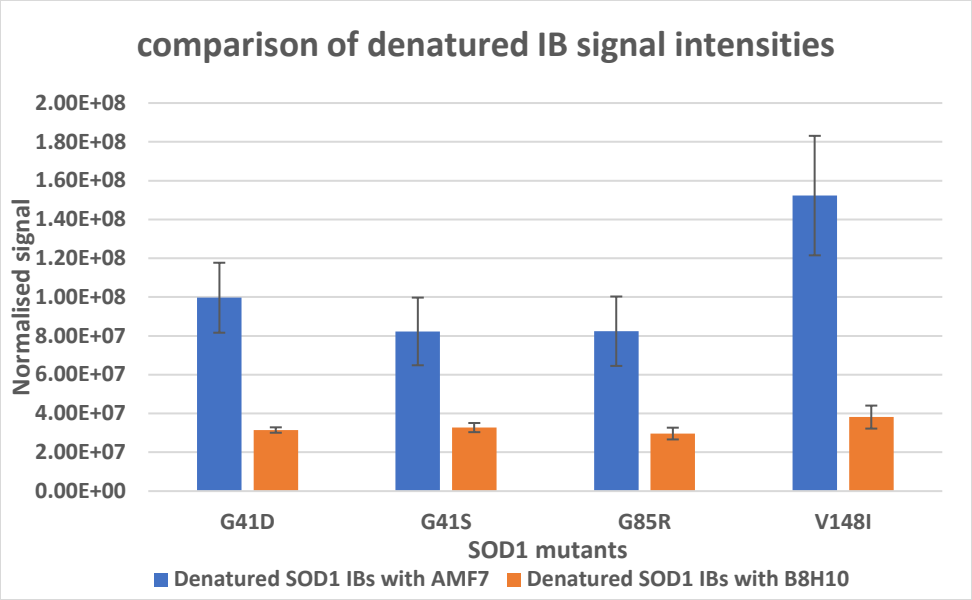

Figure 4.2: **Loop disorder by G85R and V148I.** A) Potential clashes of G85R mutation with electrostatic loop/ AMF7 epitope (Blue) and Zn binding loop/B8H10 epitope (red). B) Potential clashes of V148I mutation with the loop region preceding B8H10 epitope. The mutated residue is shown in green colour. However, it is to be noted that the image is showing one of the rotamers of the mutation out of all possible orientations for visualisation purpose. C) Plot representing denatured signals from 4 SOD1 mutants (G41D, G41S, G85R and V148I) with AMF7 (blue) and B8H10 (orange). G41S/D are high binding mutants for AMF7 and B8H10, whereas G85R is low binding for both and V148I is low binding for B8H10 in native IB structure. All images have been generated using Chimera (version 1.14) with PDB ID: 1HL5.

4.3.3 Comparison of aggregate structures formed by different mutations of the same residue

In our current analysis, there are three pairs of mutants (G41S/D, G93A/D, V148I/G) with different mutations in the same position of SOD1. These mutant pairs are of possible interest as they as associated with different disease duration (Table 4.1). For example, G41D shows less severity with disease duration of more than 10 years, while G41S shows extreme disease severity with average disease duration of ~1 year. However, antibody binding pattern for G41S and G41D were remarkably similar to each other with a slight difference in B8H10 binding. G41S shows a higher binding for B8H10, suggesting that the Zn-binding loop in this mutant might be more destabilised than G41D. Hence, additional experiments on Zn bound species of these mutant aggregates might be required to assess the difference. However, an overall comparable binding pattern between G41S/D might suggest the involvement of other factors in variable disease duration. Unlike these two mutants, G93D showed an overall less binding towards SEDI, USOD and B8H10 compared to G93A and AMF7 bound more to G93D. This suggests charge-dependent packing of SOD1 in aggregate structures. Interestingly, V148I showed overall less binding to all antibodies compared to V148G, which could potentially be explained with its higher stability in reduced apo state. Also, mutation of valine to isoleucine should not significantly affect the conformation of the dimer interface region (where the mutation is present) as compared to the mutation to a glycine residue. Together these data indicate that various other factors that are dependent as well as independent of the aggregate structure might play a crucial role in these mutant mediated disease pathologies.

4.4 Properties of SOD1 aggregates in inclusion bodies

In order to validate the binding profile seen with quantitative dot blot technique, it is also important to obtain complementary information about the composition of IBs formed by SOD1 mutants. A recent study by Semmler *et al*.[123] found that different conformations of SOD1 aggregates interact with several cellular proteins. The presence of various other proteins was also seen in the IB samples used in this study through SDS-PAGE analysis. Apart from SOD1, one of the other prominent proteins present in these samples is OmpF. Previous work by John Almey[146] in the Meiering lab reported that this OmpF band could not be removed from the IB samples when washed with Triton X-100 detergent. Hence, it was suspected that other proteins might be involved in the aggregate structures of SOD1, which is not ideal for the quantitative analysis. However, that work was carried out with IB grown in rich media, whereas the current study is carried out with IB samples grown in minimal media. Hence, the detergent study was performed again with these IB samples. Four different non-ionic detergents were chosen for washing inclusion bodies, as shown in Figure 4.5A. Out of these four detergents, n-Octylglucoside was able to remove OmpF as well as several other proteins from IB sample through washing. This was probably due to the high CMC value of this detergent compared to the other three (Figure 4.5B). CMC value represents the concentration beyond which the detergents form micelles spontaneously in the solution. n-OG has a high CMC value and hence, works as an effective solubilisation agent[153]. Such unique property of n-OG might be ideal for optimum interaction and solubilization of various proteins (like OmpF) from the pellet fraction upon washing. The other three detergents might be predominantly forming micelles due to their low CMC values leading to their poor ability to solubilize proteins from the pellet fractions to the supernatant fractions after washing (Figure 3.14A). However, a systematic concentration-dependent experiment is

required to verify if there are different concentration ranges where each detergent could remove other proteins from the inclusion body sample. However, it is to be noted that washing the IB samples using these mild detergents might potentially affect its structure. Some of the preliminary experiments have shown that conformation-specific anti-SOD1 antibodies bind differently to detergent washed samples compared to native IBs (data not shown). However, whether the change in binding is resulting from presence of detergent or actual change in SOD1 conformation in IBs upon washing is required to be further investigated.

A

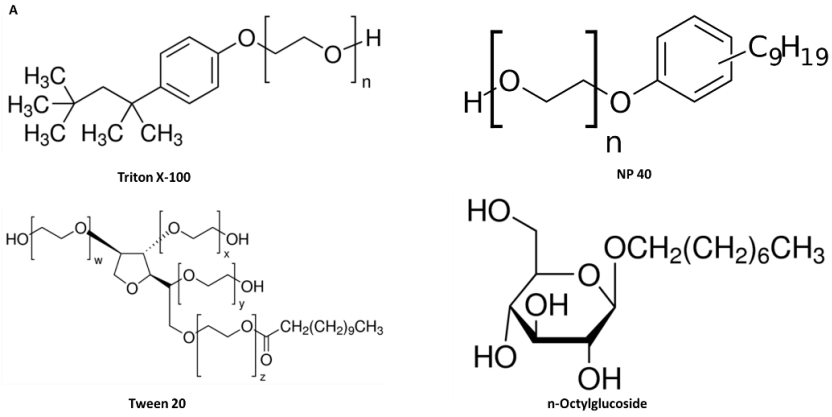

Detergents	CMC in mM @ 25^{0}C
Triton X-100	0.2-0.9
NP-40	0.05-0.3
Tween 20	0.06
n-Octylglucoside	14.5

Figure 4.3: **Structural and chemical properties of non-ionic detergents.** A) Structures of 4 non-ionic detergents used for inclusion body washing. B) Critical micelle concentration of each detergent.

Another experiment was performed to check the oxidation status of SOD1 in these inclusion bodies by labelling the samples with iodoacetamide (IA). Labelling was carried out after cell harvesting as well as IB preparation process to ensure minimising the oxidation of cysteines during the sample preparation steps. Running these sample on a non-denaturing SDS-PAGE revealed that SOD1 in IBs might predominantly exist in the reduced state when grown in minimal media for 4hrs post IPTG induction both at 37^{0}C and 25^{0}C. However, IA labelling

should be performed in triplicate experiments with samples from multiple growths to verify and establish this observation. It would also be interesting to implement this technique on IBs grown under different conditions such as temperature, presence of Zn and/or Cu to account for the roles of these factors in SOD1 oxidation.

4.5 Mechanism of protein aggregation in IB formation

With over 30% of the biopharmaceuticals produced by industries using the *E. coli* recombinant protein expression systems[154], the formation of IBs which contain the majority of the overexpressed protein is often considered a prime obstacle in the field of biotechnology[154]. Although as IBs are a relatively pure form of the recombinant protein, this can also facilitate purification if the protein can be easily refolded[108]. In addition, there have been growing reports about the potential use of IBs in various areas such as bioprocess engineering, material science and medical applications[155,156]. Indeed, the ease of isolation, resistance to proteolytic degradation, mechanical stability, presence of high amounts of overexpressed proteins as well as biological activity[112,155,157] have made IBs an increasingly attractive system to explore both for research and industrial purposes. Despite such high value, the use of IBs is still limited in part due to minimal understanding of the molecular mechanisms of protein aggregation during IB formation.

Our results indicate that IBs vary markedly in terms of their expression level and structure, depending on mutation as well as growth conditions. Table 4.1 shows that when SOD1 variants are grown in minimal media for 4 hours at 37^0C, most of the mutants show high aggregation levels (above 90%), except for WT and V148I which aggregate less. Interestingly, both of these variants are more stable than the others, yet they still vary in their antibody binding pattern. Also, the aggregation level of each SOD1 variants reduce when they are grown at 25^0C as opposed to

37^0C for 4hrs post induction. A previous study by Trainor *et al.*[158] has shown that changes in local stability due to different mutations could result in variable aggregation propensities. Together, these observations indicate that the extent of protein aggregation is highly dependent on the stability of the protein as well as various environmental factors such as growth condition, expression system.

Inclusion bodies could be composed of various conformations of the overexpressed protein as well as other cellular components such as membrane protein, phospholipids, and nucleic acids[159]. Current knowledge of protein conformation in IBs is predominantly at low structural resolution. While some reports argue for the presence of various conformations ranging from unfolded to partially or natively folded to higher-order aggregates[111], other reports claim that IBs could primarily be composed of native-like conformations which convert into amyloid structures over time due to accumulation of unfolded or misfolded structures[160]. The quantitative analysis here using the new dot blot protocol has shown that different SOD1 mutants form different IB structures. It would be of much interest in future to apply this technique further to investigate the change in aggregate structure over time. Also, it can be expanded to study the effect of environmental conditions by growing IBs in different growth media, temperature, presence or absence of cofactors for a variety of protein with different structures.

Along with the structural aspect, it is of interest to investigate the composition of inclusion bodies. A study by Gardner *et al.*[161] has shown that cysteine residues in proinsulin IBs stay reduced. A similar observation was made for SOD1 IBs in IA labelling experiment where IBs of most SOD1 variants showed the presence of predominantly reduced species (Figure 3.15 A, B). This could be attributed to the reduced cytoplasmic environment of *E coli*. Hence, a comprehensive analysis of the factors that regulate IB structures, and composition as well as the

presence of post-translational modifications would significantly enhance our understanding of these intriguing protein aggregates and potentially open up ways to use IBs for a wide range of functions.

5 Conclusions and Future work

The quantitative dot blot assay indicates that SOD1 may exhibit different mutation dependent mechanisms of aggregation, which may be consistent with prion-like strain behaviour. The experiments provide a sense of the extent of misfolding and exposure of four epitope regions of SOD1 in various mutant aggregates. Data from these experiments nicely complement high-resolution quenched amide exchange NMR experiment that are currently being conducted in the Meiering lab to obtain residue-specific information. Together, both these experiments will provide an unprecedented detailed view of differences in aggregate structures of SOD1 mutants.

In future various other techniques of IB preparation should be explored. For example, inclusion bodies should also be extracted from E coli using other methods such as emulsification, sonication to check the effect of sample processing on aggregate structure. Western blots on the IB samples should also be carried out to check if there are other proteins that antibodies could potentially bind. This might also reveal any degradation product of SOD1 in IB samples. Additionally, mass spectrometry could be carried out with I113T IB to check for any degradation which might explain its high degree of binding to conformation-specific antibodies. Finally, the developed quantitative dot blot assay could be further applied to characterise aggregate structures of other forms of SOD1 aggregates. The compatibility of this assay with inclusion bodies suggests its potential application in biotechnology industries which are increasingly exploring properties of IB for wide-ranging applications in industry and medicine.

6 References

1. Daggett V, Fersht A. The present view of the mechanism of protein folding. *Nat Rev Mol Cell Biol*. 2003;4(6):497-502. doi:10.1038/nrm1126

2. Díaz-Villanueva JF, Díaz-Molina R, García-González V. Protein folding and mechanisms of proteostasis. *Int J Mol Sci*. 2015;16(8):17193-17230. doi:10.3390/ijms160817193

3. Englander SW, Mayne L. The nature of protein folding pathways. *Proc Natl Acad Sci U S A*. 2014;111(45):15873-15880. doi:10.1073/pnas.1411798111

4. Levinthal C. ARE THERE PATHWAYS FOR PROTEIN FOLDING ? *Extr du J Chim Phys*. 1968;65(1):45. Accessed April 16, 2020. doi: https://doi.org/10.1051/jcp/1968650044

5. Anfinsen CB. Principles that govern the folding of protein chains. *Science (80-)*. 1973;181(4096):223-230. doi:10.1126/science.181.4096.223

6. Dobson CM. Protein folding and misfolding. *Nature*. 2003;426(6968):884-890. doi:10.1038/nature02261

7. Hartl FU, Hayer-Hartl M. Protein folding. Molecular chaperones in the cytosol: From nascent chain to folded protein. *Science (80-)*. 2002;295(5561):1852-1858. doi:10.1126/science.1068408

8. Ellis RJ, Minton AP. Protein aggregation in crowded environments. *Biol Chem*. 2006;387(5):485-497. doi:10.1515/BC.2006.064

9. Hartl FU, Hayer-Hartl M. Converging concepts of protein folding in vitro and in vivo. *Nat Struct Mol Biol*. 2009;16(6):574-581. doi:10.1038/nsmb.1591

10. Cheng C, Wu J, Liu G, Shi S, Chen T. Effects of Non-native Interactions on Frustrated Proteins Folding under Confinement. *J Phys Chem B*. 2018;122(31):7654-7667. doi:10.1021/acs.jpcb.8b04147

11. Chiti F, Dobson CM. Protein Misfolding, Amyloid Formation, and Human Disease: A Summary of Progress Over the Last Decade. *Annu Rev Biochem*. 2017;86(1):27-68. doi:10.1146/annurev-biochem-061516-045115

12. Balchin D, Hayer-Hartl M, Hartl FU. In vivo aspects of protein folding and quality control. *Science (80-)*. 2016;353(6294). doi:10.1126/science.aac4354

13. Labbadia J, Morimoto RI. The Biology of Proteostasis in Aging and Disease. *Annu Rev Biochem*. 2015;84(1):435-464. doi:10.1146/annurev-biochem-060614-033955

14. Miller SBM, Mogk A, Bukau B. Spatially organized aggregation of misfolded proteins as cellular stress defense strategy. *J Mol Biol*. 2015;427(7):1564-1574. doi:10.1016/j.jmb.2015.02.006

15. Hartl FU, Bracher A, Hayer-Hartl M. Molecular chaperones in protein folding and proteostasis. *Nature*. 2011;475(7356):324-332. doi:10.1038/nature10317

16. Wolff S, Weissman JS, Dillin A. Differential scales of protein quality control. *Cell*. 2014;157(1):52-64. doi:10.1016/j.cell.2014.03.007

17. Brehme M, Voisine C, Rolland T, Wachi S, Soper JH, Zhu Y, Orton K, Villella A, Garza D, Vidal M, Ge H, Morimoto RI. A chaperome subnetwork safeguards proteostasis in aging and neurodegenerative disease. *Cell Rep*. 2014;9(3):1135-1150. doi:10.1016/j.celrep.2014.09.042

18. Dantuma NP, Bott LC. The ubiquitin-proteasome system in neurodegenerative diseases: Precipitating factor, yet part of the solution. *Front Mol Neurosci*. 2014;7(JULY). doi:10.3389/fnmol.2014.00070

19. Chiti F, Dobson CM. Amyloid formation by globular proteins under native conditions. *Nat Chem Biol*. 2009;5(1):15-22. doi:10.1038/nchembio.131

20. Sethuraman A, Belfort G. Protein structural perturbation and aggregation on homogeneous surfaces. *Biophys J*. 2005;88(2):1322-1333. doi:10.1529/biophysj.104.051797

21. Jiang L, Cao S, Cheung PPH, Zheng X, Leung CWT, Peng Q, Shuai Z, Tang BZ, Yao S, Huang X. Real-time monitoring of hydrophobic aggregation reveals a critical role of cooperativity in hydrophobic effect. *Nat Commun*. 2017;8(1):1-8. doi:10.1038/ncomms15639

22. Wang W, Roberts CJ. Protein aggregation – Mechanisms, detection, and control. *Int J Pharm*. 2018;550(1-2):251-268. doi:10.1016/j.ijpharm.2018.08.043

23. Alam P, Siddiqi K, Chturvedi SK, Khan RH. Protein aggregation: From background to inhibition strategies. *Int J Biol Macromol*. 2017;103:208-219. doi:10.1016/j.ijbiomac.2017.05.048

24. Wang W, Nema S, Teagarden D. Protein aggregation-Pathways and influencing factors. *Int J Pharm*. 2010;390(2):89-99. doi:10.1016/j.ijpharm.2010.02.025

25. Barnett G V., Drenski M, Razinkov V, Reed WF, Roberts CJ. Identifying protein aggregation mechanisms and quantifying aggregation rates from combined monomer depletion and continuous scattering. *Anal Biochem*. 2016;511:80-91. doi:10.1016/j.ab.2016.08.002

26. Tu LH, Raleigh DP. Role of aromatic interactions in amyloid formation by islet amyloid polypeptide. *Biochemistry*. 2013;52(2):333-342. doi:10.1021/bi3014278

27. Galm L, Amrhein S, Hubbuch J. Predictive approach for protein aggregation: Correlation of protein surface characteristics and conformational flexibility to protein aggregation propensity. *Biotechnol Bioeng*. 2017;114(6):1170-1183. doi:10.1002/bit.25949

28. Austerberry JI, Dajani R, Panova S, Roberts D, Golovanov AP, Pluen A, van der Walle CF, Uddin S, Warwicker J, Derrick JP, Curtis R. The effect of charge mutations on the stability and aggregation of a human single chain Fv fragment. *Eur J Pharm Biopharm*. 2017;115:18-30. doi:10.1016/j.ejpb.2017.01.019

29. Wang W. Protein aggregation and its inhibition in biopharmaceutics. *Int J Pharm*. 2005;289(1-2):1-30. doi:10.1016/j.ijpharm.2004.11.014

30. Nemergut M, Žoldák G, Schaefer J V., Kast F, Miškovský P, Plückthun A, Sedlák E. Analysis of IgG kinetic stability by differential scanning calorimetry, probe fluorescence and light scattering. *Protein Sci*. 2017;26(11):2229-2239. doi:10.1002/pro.3278

31. Owczarz M, Arosio P. Sulfate anion delays the self-assembly of human insulin by modifying the aggregation pathway. *Biophys J*. 2014;107(1):197-207. doi:10.1016/j.bpj.2014.05.030

32. Lilyestrom WG, Yadav S, Shire SJ, Scherer TM. Monoclonal antibody self-association, cluster formation, and rheology at high concentrations. *J Phys Chem B.* 2013;117(21):6373-6384. doi:10.1021/jp4008152

33. Breydo L, Uversky VN. Structural, morphological, and functional diversity of amyloid oligomers. *FEBS Lett*. 2015;589(19):2640-2648. doi:10.1016/j.febslet.2015.07.013

34. Šarić A, Michaels TCT, Zaccone A, Knowles TPJ, Frenkel D. Kinetics of spontaneous filament nucleation via oligomers: Insights from theory and simulation. *J Chem Phys*. 2016;145(21). doi:10.1063/1.4965040

35. Hartl FU. Protein Misfolding Diseases. *Annu Rev Biochem*. 2017;86(1):21-26. doi:10.1146/annurev-biochem-061516-044518

36. Ross CA, Poirier MA. Protein aggregation and neurodegenerative disease. *Nat Med*. 2004;10(7):S10. doi:10.1038/nm1066

37. Jones R. Protein aggregation increases with age. *PLoS Biol*. 2010;8(8):7-8. doi:10.1371/journal.pbio.1000449

38. David DC, Ollikainen N, Trinidad JC, Cary MP, Burlingame AL, Kenyon C. Widespread Protein Aggregation as an Inherent Part of Aging in C. elegans. Ahringer J, ed. *PLoS Biol*. 2010;8(8):e1000450. doi:10.1371/journal.pbio.1000450

39. Ow SY, Dunstan DE. A brief overview of amyloids and Alzheimer's disease. *Protein Sci*. 2014;23(10):1315-1331. doi:10.1002/pro.2524

40. Vaquer-Alicea J, Diamond MI. Propagation of Protein Aggregation in Neurodegenerative Diseases. *Annu Rev Biochem*. 2019;88(1):785-810. doi:10.1146/annurev-biochem-061516-045049

41. Blokhuis AM, Groen EJN, Koppers M, Van Den Berg LH, Pasterkamp RJ. Protein aggregation in amyotrophic lateral sclerosis. *Acta Neuropathol*. 2013;125(6):777-794. doi:10.1007/s00401-013-1125-6

42. Ashraf G, Greig N, Khan T, Hassan I, Tabrez S, Shakil S, Sheikh I, Zaidi S, Akram M, Jabir N, Firoz C, Naeem A, Alhazza I, Damanhouri G, Kamal M. Protein Misfolding and Aggregation in Alzheimer's Disease and Type 2 Diabetes Mellitus. *CNS Neurol Disord - Drug Targets*. 2014;13(7):1280-1293. doi:10.2174/1871527313666140917095514

43. Arrasate M, Finkbeiner S. Protein aggregates in Huntington's disease. *Exp Neurol*. 2012;238(1):1-11. doi:10.1016/j.expneurol.2011.12.013

44. Jahn TR, Radford SE. Folding versus aggregation: Polypeptide conformations on competing pathways. *Arch Biochem Biophys*. 2008;469(1):100-117. doi:10.1016/j.abb.2007.05.015

45. Erkkinen MG, Kim MO, Geschwind MD. Clinical neurology and epidemiology of the major neurodegenerative diseases. *Cold Spring Harb Perspect Biol*. 2018;10(4). doi:10.1101/cshperspect.a033118

46. Davis AA, Leyns CEG, Holtzman DM. Intercellular Spread of Protein Aggregates in Neurodegenerative Disease. *Annu Rev Cell Dev Biol*. 2018;34(1):545-568. doi:10.1146/annurev-cellbio-100617-062636

47. Ross CA, Poirier MA. Protein aggregation and neurodegenerative disease. *Nat Med*. 2004;10(7):S10. doi:10.1038/nm1066

48. DiFiglia M, Sapp E, Chase KO, Davies SW, Bates GP, Vonsattel JP, Aronin N. Aggregation of huntingtin in neuronal intranuclear inclusions and dystrophic neurites in brain. *Science (80-)*. 1997;277(5334):1990-1993. doi:10.1126/science.277.5334.1990

49. Sengupta U, Nilson AN, Kayed R. The Role of Amyloid-β Oligomers in Toxicity, Propagation, and Immunotherapy. *EBioMedicine*. 2016;6:42-49. doi:10.1016/j.ebiom.2016.03.035

50. Gill C, Phelan JP, Hatzipetros T, Kidd JD, Tassinari VR, Levine B, Wang MZ, Moreno A, Thompson K, Maier M, Grimm J, Gill A, Vieira FG. SOD1-positive aggregate accumulation in the CNS predicts slower disease progression and increased longevity in a mutant SOD1 mouse model of ALS. *Sci Rep*. 2019;9(1):1-13. doi:10.1038/s41598-019-43164-z

51. Valentine JS, Doucette PA, Zittin Potter S. COPPER-ZINC SUPEROXIDE DISMUTASE AND AMYOTROPHIC LATERAL SCLEROSIS. *Annu Rev Biochem*. 2005;74(1):563-593. doi:10.1146/annurev.biochem.72.121801.161647

52. Zarei S, Carr K, Reiley L, Diaz K, Guerra O, Altamirano PF, Pagani W, Lodin D, Orozco G, Chinea A. A comprehensive review of amyotrophic lateral sclerosis. *Surg Neurol Int*. 2015;6(1). doi:10.4103/2152-7806.169561

53. Broom HR, Rumfeldt JAO, Meiering EM. Many roads lead to Rome? Multiple modes of Cu,Zn superoxide dismutase destabilization, misfolding and aggregation in amyotrophic lateral sclerosis. *Essays Biochem*. 2014;56(1):149-165. doi:10.1042/BSE0560149

54. Hardiman O, Al-Chalabi A, Chio A, Corr EM, Logroscino G, Robberecht W, Shaw PJ, Simmons Z, Van Den Berg LH. Amyotrophic lateral sclerosis. *Nat Rev Dis Prim*. 2017;3. doi:10.1038/nrdp.2017.71

55. Wang Q, Johnson JL, Agar NY., Agar JN. Protein Aggregation and Protein Instability Govern Familial Amyotrophic Lateral Sclerosis Patient Survival. Weissman JS, ed. *PLoS Biol*. 2008;6(7):e170. doi:10.1371/journal.pbio.0060170

56. Kikuchi H, Almer G, Yamashita S, Guégan C, Nagai M, Xu Z, Sosunov AA, McKhann GM, Przedborski S. Spinal cord endoplasmic reticulum stress associated with a microsomal accumulation of mutant superoxide dismutase-1 in an ALS model. *Proc Natl Acad Sci U S A*. 2006;103(15):6025-6030. doi:10.1073/pnas.0509227103

57. Shi P, Gal J, Kwinter DM, Liu X, Zhu H. Mitochondrial dysfunction in amyotrophic lateral sclerosis. *Biochim Biophys Acta - Mol Basis Dis*. 2010;1802(1):45-51. doi:10.1016/j.bbadis.2009.08.012

58. Crapo JD, Oury T, Rabouille C, Slot JW, Chang LY. Copper,zinc superoxide dismutase is primarily a cytosolic protein in human cells. *Proc Natl Acad Sci U S A*. 1992;89(21):10405-10409. doi:10.1073/pnas.89.21.10405

59. Strange RW, Antonyuk S, Hough MA, Doucette PA, Rodriguez JA, Hart PJ, Hayward LJ, Valentine JS, Hasnain SS. The structure of holo and metal-deficient wild-type human Cu, Zn superoxide dismutase and its relevance to familial amyotrophic lateral sclerosis. *J Mol Biol*. 2003;328(4):877-891. doi:10.1016/S0022-2836(03)00355-3

60. Tainer JA, Getzoff ED, Beem KM, Richardson JS, Richardson DC. Determination and analysis of the 2 Å structure of copper, zinc superoxide dismutase. *J Mol Biol*. 1982;160(2):181-217. doi:10.1016/0022-2836(82)90174-7

61. Kayatekin C, Zitzewitz JA, Matthews CR. Zinc Binding Modulates the Entire Folding Free Energy Surface of Human Cu,Zn Superoxide Dismutase. *J Mol Biol*. 2008;384(2):540-555. doi:10.1016/j.jmb.2008.09.045

62. Rakhit R, Chakrabartty A. Structure, folding, and misfolding of Cu,Zn superoxide dismutase in amyotrophic lateral sclerosis. *Biochim Biophys Acta - Mol Basis Dis*. 2006;1762(11-12):1025-1037. doi:10.1016/j.bbadis.2006.05.004

63. Rakhit R, Chakrabartty A. Structure, folding, and misfolding of Cu,Zn superoxide dismutase in amyotrophic lateral sclerosis. Published online 2006. doi:10.1016/j.bbadis.2006.05.004

64. Rosen DR, Siddique T, Patterson D, Figlewicz DA, Sapp P, Hentati A, Donaldson D, Goto J, O'Regan JP, Deng HX, Rahmani Z, Krizus A, McKenna-Yasek D, Cayabyab A, Gaston SM, Berger R, Tanzi RE, Halperin JJ, Herzfeldt B, Den Bergh R Van, Hung WY, Bird T, Deng G, Mulder DW, Smyth C, Laing NG, Soriano E, Pericak-Vance MA, Haines J, Rouleau GA, Gusella JS, Horvitz HR, Brown RH. Mutations in Cu/Zn superoxide dismutase gene are associated with familial amyotrophic lateral sclerosis. *Nature*. 1993;362(6415):59-62. doi:10.1038/362059a0

65. Deng HX, Hentati A, Tainer JA, Iqbal Z, Cayabyab A, Hung WY, Getzoff ED, Hu P, Herzfeldt B, Roos RP, Warner C, Deng G, Soriano E, Smyth C, Parge HE, Ahmed A, Roses AD, Hallewell RA, Pericak-Vance MA, Siddique T. Amyotrophic lateral sclerosis and structural defects in Cu,Zn superoxide dismutase. *Science (80-).* 1993;261(5124):1047-1051. doi:10.1126/science.8351519

66. Banci L, Bertini I, Boca M, Girotto S, Martinelli M, Valentine JS, Vieru M. SOD1 and amyotrophic lateral sclerosis: Mutations and oligomerization. *PLoS One*. 2008;3(2). doi:10.1371/journal.pone.0001677

67. Barber SC, Mead RJ, Shaw PJ. Oxidative stress in ALS: A mechanism of neurodegeneration and a therapeutic target. *Biochim Biophys Acta - Mol Basis Dis*. 2006;1762(11-12):1051-1067. doi:10.1016/j.bbadis.2006.03.008

68. Gurney ME, Pu H, Chiu AY, Dal Canto MC, Polchow CY, Alexander DD, Caliendo J, Hentati A, Kwon YW, Deng HX, Chen W, Zhai P, Sufit RL, Siddique T. Motor neuron degeneration in mice that express a human Cu,Zn superoxide dismutase mutation. *Science (80-).* 1994;264(5166):1772-1775. doi:10.1126/science.8209258

69. Borchelt DR, Lee MK, Slunt HS, Guarnieri M, Xu ZS, Wong PC, Brown RH, Price DL, Sisodia SS, Cleveland DW. Superoxide dismutase 1 with mutations linked to familial amyotrophic lateral sclerosis possesses significant activity. *Proc Natl Acad Sci U S A*. 1994;91(17):8292-8296. doi:10.1073/pnas.91.17.8292

70. Reaume AG, Elliott JL, Hoffman EK, Kowall NW, Ferrante RJ, Siwek DF, Wilcox HM, Flood DG, Beal MF, Brown RH, Scott RW, Snider WD. Motor neurons in Cu/Zn superoxide dismutase-deficient mice develop normally but exhibit enhanced cell death after axonal injury. *Nat Genet*. 1996;13(1):43-47. doi:10.1038/ng0596-43

71. Gurney ME, Pu H, Chiu AY, Dal Canto MC, Polchow CY, Alexander DD, Caliendo J, Hentati A, Kwon YW, Deng HX, Chen W, Zhai P, Sufit RL, Siddique T. Motor neuron degeneration in mice that express a human Cu,Zn superoxide dismutase mutation. *Science (80-)*. 1994;264(5166):1772-1775. doi:10.1126/science.8209258

72. Saxena S, Cabuy E, Caroni P. A role for motoneuron subtype-selective ER stress in disease manifestations of FALS mice. *Nat Neurosci*. 2009;12(5):627-636. doi:10.1038/nn.2297

73. Urushitani M, Ezzi SA, Julien JP. Therapeutic effects of immunization with mutant superoxide dismutase in mice models of amyotrophic lateral sclerosis. *Proc Natl Acad Sci U S A*. 2007;104(7):2495-2500. doi:10.1073/pnas.0606201104

74. Pickles S, Vande Velde C. Misfolded SOD1 and ALS: Zeroing in on mitochondria. *Amyotroph Lateral Scler*. 2012;13(4):333-340. doi:10.3109/17482968.2012.648645

75. Howland DS, Liu J, She Y, Goad B, Maragakis NJ, Kim B, Erickson J, Kulik J, DeVito L, Psaltis G, DeGennaro LJ, Cleveland DW, Rothstein JD. Focal loss of the glutamate transporter EAAT2 in a transgenic rat model of SOD1 mutant-mediated amyotrophic lateral sclerosis (ALS). *Proc Natl Acad Sci U S A*. 2002;99(3):1604-1609. doi:10.1073/pnas.032539299

76. Watanabe M, Dykes-Hoberg M, Cizewski Culotta V, Price DL, Wong PC, Rothstein JD. Histological evidence of protein aggregation in mutant SOD1 transgenic mice and in amyotrophic lateral sclerosis neural tissues. *Neurobiol Dis*. 2001;8(6):933-941. doi:10.1006/nbdi.2001.0443

77. Forsberg K, Graffmo K, Pakkenberg B, Weber M, Nielsen M, Marklund S, Brännström T, Andersen PM. Misfolded SOD1 inclusions in patients with mutations in C9orf72 and other ALS/FTD-associated genes. *J Neurol Neurosurg Psychiatry*. 2019;90(8):861-869. doi:10.1136/jnnp-2018-319386

78. Chattopadhyay M, Valentine JS. Aggregation of copper-zinc superoxide dismutase in familial and sporadic ALS. *Antioxidants Redox Signal*. 2009;11(7):1603-1614. doi:10.1089/ars.2009.2536

79. Karch CM, Prudencio M, Winkler DD, Hart PJ, Borchelt DR. Role of mutant SOD1 disulfide oxidation and aggregation in the pathogenesis of familial ALS. *Proc Natl Acad Sci U S A*. 2009;106(19):7774-7779. doi:10.1073/pnas.0902505106

80. Brotherton TE, Li Y, Glass JD. Cellular toxicity of mutant SOD1 protein is linked to an easily soluble, non-aggregated form in vitro. *Neurobiol Dis*. 2013;49(1):49-56. doi:10.1016/j.nbd.2012.08.010

81. Sen Mojumdar S, Scholl ZN, Dee DR, Rouleau L, Anand U, Garen C, Woodside MT. Partially native intermediates mediate misfolding of SOD1 in single-molecule folding trajectories. *Nat Commun*. 2017;8(1):1-11. doi:10.1038/s41467-017-01996-1

82. Seetharaman S V., Prudencio M, Karch C, Holloway SP, Borchelt DR, Hart PJ. Immature copper-zinc superoxide dismutase and familial amyotrophic lateral sclerosis. *Exp Biol Med*. 2009;234(10):1140-1154. doi:10.3181/0903-MR-104

83. Mejzini R, Flynn LL, Pitout IL, Fletcher S, Wilton SD, Akkari PA. ALS Genetics, Mechanisms, and Therapeutics: Where Are We Now? *Front Neurosci*. 2019;13. doi:10.3389/fnins.2019.01310

84. Banci L, Bertini I, Cantini F, Kozyreva T, Massagni C, Palumaa P, Rubino JT, Zovo K. Human superoxide dismutase 1 (hSOD1) maturation through interaction with human copper chaperone for SOD1 (hCCS). *Proc Natl Acad Sci U S A*. 2012;109(34):13555-13560. doi:10.1073/pnas.1207493109

85. Furukawa Y, Torres AS, O'Halloran T V. Oxygen-induced maturation of SOD1: A key role for disulfide formation by the copper chaperone CCS. *EMBO J*. 2004;23(14):2872-2881. doi:10.1038/sj.emboj.7600276

86. Luchinat E, Barbieri L, Banci L. A molecular chaperone activity of CCS restores the maturation of SOD1 fALS mutants. *Sci Rep*. 2017;7(1). doi:10.1038/s41598-017-17815-y

87. Carroll MC, Girouard JB, Ulloa JL, Subramaniam JR, Wong PC, Valentine JS, Culotta VC. Mechanisms for activating Cu- and Zn-containing superoxide dismutase in the absence of the CCS Cu chaperone. *Proc Natl Acad Sci U S A*. 2004;101(16):5964-5969. doi:10.1073/pnas.0308298101

88. Furukawa Y, Kaneko K, Yamanaka K, O'Halloran T V., Nukina N. Complete loss of post-translational modifications triggers fibrillar aggregation of SOD1 in the familial form of amyotrophic lateral sclerosis. *J Biol Chem*. 2008;283(35):24167-24176. doi:10.1074/jbc.M802083200

89. Furukawa Y, Anzai I, Akiyama S, Imai M, Cruz FJC, Saio T, Nagasawa K, Nomura T, Ishimori K. Conformational disorder of the most immature Cu, Zn-superoxide dismutase leading to amyotrophic lateral sclerosis. *J Biol Chem*. 2016;291(8):4144-4155. doi:10.1074/jbc.M115.683763

90. McAlary L, Plotkin SS, Yerbury JJ, Cashman NR. Prion-Like Propagation of Protein Misfolding and Aggregation in Amyotrophic Lateral Sclerosis. *Front Mol Neurosci*. 2019;12:262. doi:10.3389/fnmol.2019.00262

91. Prusiner SB. Novel proteinaceous infectious particles cause scrapie. *Science (80-).* 1982;216(4542):136-144. doi:10.1126/science.6801762

92. Luo F, Gui X, Zhou H, Gu J, Li Y, Liu X, Zhao M, Li D, Li X, Liu C. Atomic structures of FUS LC domain segments reveal bases for reversible amyloid fibril formation. *Nat Struct Mol Biol*. 2018;25(4):341-346. doi:10.1038/s41594-018-0050-8

93. Prasad A, Bharathi V, Sivalingam V, Girdhar A, Patel BK. Molecular mechanisms of TDP-43 misfolding and pathology in amyotrophic lateral sclerosis. *Front Mol Neurosci*. 2019;12:25. doi:10.3389/fnmol.2019.00025

94. Abdolvahabi A, Shi Y, Chuprin A, Rasouli S, Shaw BF. Stochastic Formation of Fibrillar and Amorphous Superoxide Dismutase Oligomers Linked to Amyotrophic Lateral Sclerosis. *ACS Chem Neurosci*. 2016;7(6):799-810. doi:10.1021/acschemneuro.6b00048

95. Chattopadhyay M, Nwadibia E, Strong CD, Gralla EB, Valentine JS, Whitelegge JP. The disulfide bond, but not zinc or dimerization, controls initiation and seeded growth in amyotrophic lateral sclerosis-linked Cu,Zn superoxide dismutase (SOD1) fibrillation. *J Biol Chem*. 2015;290(51):30624-30636. doi:10.1074/jbc.M115.666503

96. McAlary L, Aquilina JA, Yerbury JJ. Susceptibility of mutant SOD1 to form a destabilized monomer predicts cellular aggregation and toxicity but not in vitro aggregation propensity. *Front Neurosci*. 2016;10(NOV). doi:10.3389/fnins.2016.00499

97. Morales R. Prion strains in mammals: Different conformations leading to disease. *PLoS Pathog*. 2017;13(7). doi:10.1371/journal.ppat.1006323

98. Tanaka M, Collins SR, Toyama BH, Weissman JS. The physical basis of how prion conformations determine strain phenotypes. *Nature*. 2006;442(7102):585-589. doi:10.1038/nature04922

99. Ayers JI, Cashman NR. Prion-like mechanisms in amyotrophic lateral sclerosis. In: *Handbook of Clinical Neurology*. Vol 153. Elsevier B.V.; 2018:337-354. doi:10.1016/B978-0-444-63945-5.00018-0

100. Chattopadhyay M, Durazo A, Se HS, Strong CD, Gralla EB, Whitelegge JP, Valentine JS. Initiation and elongation in fibrillation of ALS-linked superoxide dismutase. *Proc Natl Acad Sci U S A*. 2008;105(48):18663-18668. doi:10.1073/pnas.0807058105

101. Münch C, O'Brien J, Bertolotti A. Prion-like propagation of mutant superoxide dismutase-1 misfolding in neuronal cells. *Proc Natl Acad Sci U S A*. 2011;108(9):3548-3553. doi:10.1073/pnas.1017275108

102. Grad LI, Guest WC, Yanai A, Pokrishevsky E, O'Neill MA, Gibbs E, Semenchenko V, Yousefi M, Wishart DS, Plotkin SS, Cashman NR. Intermolecular transmission of superoxide dismutase 1 misfolding in living cells. *Proc Natl Acad Sci U S A*. 2011;108(39):16398-16403. doi:10.1073/pnas.1102645108

103. Silverman JM, Christy D, Shyu CC, Moon KM, Fernando S, Gidden Z, Cowan CM, Ban Y, Greg Stacey R, Grad LI, McAlary L, Mackenzie IR, Foster LJ, Cashman NR. CNS-derived extracellular vesicles from superoxide dismutase 1 (SOD1) G93A ALS mice originate from astrocytes and neurons and carry misfolded SOD1. *J Biol Chem*. 2019;294(10):3744-3759. doi:10.1074/jbc.RA118.004825

104. Ayers JI, Diamond J, Sari A, Fromholt S, Galaleldeen A, Ostrow LW, Glass JD, Hart PJ, Borchelt DR. Distinct conformers of transmissible misfolded SOD1 distinguish human SOD1-FALS from other forms of familial and sporadic ALS. *Acta Neuropathol*. 2016;132(6):827-840. doi:10.1007/s00401-016-1623-4

105. Bergh J, Zetterström P, Andersen PM, Brännström T, Graffmo KS, Jonsson PA, Lang L, Danielsson J, Oliveberg M, Marklund SL. Structural and kinetic analysis of protein-aggregate strains in vivo using binary epitope mapping. *Proc Natl Acad Sci U S A*. 2015;112(14):4489-4494. doi:10.1073/pnas.1419228112

106. García-Fruitós E, González-Montalbán N, Morell M, Vera A, Ferraz RM, Arís A, Ventura S, Villaverde A. Aggregation as bacterial inclusion bodies does not imply inactivation of enzymes and fluorescent proteins. *Microb Cell Fact*. 2005;4(1):27. doi:10.1186/1475-2859-4-27

107. Vera A, González-Montalbán N, Arís A, Villaverde A. The conformational quality of insoluble recombinant proteins is enhanced at low growth temperatures. *Biotechnol Bioeng*. 2007;96(6):1101-1106. doi:10.1002/bit.21218

108. Singhvi P, Saneja A, Srichandan S, Panda AK. Bacterial Inclusion Bodies: A Treasure Trove of Bioactive Proteins. *Trends Biotechnol*. 2020;38(5):474-486. doi:10.1016/j.tibtech.2019.12.011

109. Nahalka J, Nidetzky B. Fusion to a pull-down domain: A novel approach of producing Trigonopsis variabilis D-amino acid oxidase as insoluble enzyme aggregates. *Biotechnol Bioeng*. 2007;97(3):454-461. doi:10.1002/bit.21244

110. Sánchez JM, López-Laguna H, Álamo P, Serna N, Sánchez-Chardi A, Nolan V, Cano-Garrido O, Casanova I, Unzueta U, Vazquez E, Mangues R, Villaverde A. Artificial Inclusion Bodies for Clinical Development. *Adv Sci*. 2020;7(3):1902420. doi:10.1002/advs.201902420

111. de Groot NS, Sabate R, Ventura S. Amyloids in bacterial inclusion bodies. *Trends Biochem Sci*. 2009;34(8):408-416. doi:10.1016/j.tibs.2009.03.009

112. Ramón A, Señorale-Pose M, Marín M. Inclusion bodies: Not that bad... *Front Microbiol*. 2014;5(FEB). doi:10.3389/fmicb.2014.00056

113. Invernizzi G, Aprile FA, Natalello A, Ghisleni A, Penco A, Relini A, Doglia SM, Tortora P, Regonesi ME. The Relationship between Aggregation and Toxicity of Polyglutamine-Containing Ataxin-3 in the Intracellular Environment of Escherichia coli. Baskakov I V., ed. *PLoS One*. 2012;7(12):e51890. doi:10.1371/journal.pone.0051890

114. Sabaté R, Espargaró A, Saupe SJ, Ventura S. Characterization of the amyloid bacterial inclusion bodies of the HET-s fungal prion. *Microb Cell Fact*. 2009;8(1):56. doi:10.1186/1475-2859-8-56

115. Broering TJ, Wang H, Boatright NK, Wang Y, Baptista K, Shayan G, Garrity KA, Kayatekin C, Bosco DA, Matthews CR, Ambrosino DM, Xu Z, Babcock GJ. Identification of Human Monoclonal Antibodies Specific for Human SOD1 Recognizing Distinct Epitopes and Forms of SOD1. *PLoS One*. 2013;8(4). doi:10.1371/journal.pone.0061210

116. Kerman A, Liu HN, Croul S, Bilbao J, Rogaeva E, Zinman L, Robertson J, Chakrabartty A. Amyotrophic lateral sclerosis is a non-amyloid disease in which extensive misfolding of SOD1 is unique to the familial form. *Acta Neuropathol*. 2010;119(3):335-344. doi:10.1007/s00401-010-0646-5

117. Yu YJ, Watts RJ. Developing Therapeutic Antibodies for Neurodegenerative Disease. *Neurotherapeutics*. 2013;10(3):459-472. doi:10.1007/s13311-013-0187-4

118. Gros-Louis F, Soucy G, Larivière R, Julien JP. Intracerebroventricular infusion of monoclonal antibody or its derived Fab fragment against misfolded forms of SOD1 mutant delays mortality in a mouse model of ALS. *J Neurochem*. 2010;113(5):1188-1199. doi:10.1111/j.1471-4159.2010.06683.x

119. Benkler C, O'Neil AL, Slepian S, Qian F, Weinreb PH, Rubin LL. Aggregated SOD1 causes selective death of cultured human motor neurons. *Sci Rep*. 2018;8(1). doi:10.1038/s41598-018-34759-z

120. Patel P, Kriz J, Gravel M, Soucy G, Bareil C, Gravel C, Julien JP. Adeno-associated virus-mediated delivery of a recombinant single-chain antibody against misfolded superoxide dismutase for treatment of amyotrophic lateral sclerosis. *Mol Ther*. 2014;22(3):498-510. doi:10.1038/mt.2013.239

121. Dong Q xiu, Zhu J, Liu S ying, Yu X lin, Liu R tian. An oligomer-specific antibody improved motor function and attenuated neuropathology in the SOD1-G93A transgenic mouse model of ALS. *Int Immunopharmacol*. 2018;65:413-421. doi:10.1016/j.intimp.2018.10.032

122. Pickles S, Semmler S, Broom HR, Destroismaisons L, Legroux L, Arbour N, Meiering E, Cashman NR, Vande Velde C. ALS-linked misfolded SOD1 species have divergent impacts on mitochondria. *Acta Neuropathol Commun*. 2016;4(1):43. doi:10.1186/s40478-016-0313-8

123. Semmler S, Gagné M, Garg P, Pickles SR, Baudouin C, Hamon-Keromen E, Destroismaisons L, Khalfallah Y, Chaineau M, Caron E, Bayne AN, Trempe JF, Cashman NR, Star AT, Haqqani AS, Durcan TM, Meiering EM, Robertson J, Grandvaux N, Plotkin SS, McBride HM, Velde C Vande, DeMartino GN. TNF receptor-associated factor 6 interacts with ALS-linked misfolded superoxide dismutase 1 and promotes aggregation. *J Biol Chem*. 2020;295(12):3808-3825. doi:10.1074/jbc.RA119.011215

124. Ekhtiari Bidhendi E, Bergh J, Zetterström P, Forsberg K, Pakkenberg B, Andersen PM, Marklund SL, Brännström T. Mutant superoxide dismutase aggregates from human spinal cord transmit amyotrophic lateral sclerosis. *Acta Neuropathol*. 2018;136(6):939-953. doi:10.1007/s00401-018-1915-y

125. Zhong Y, Wang J, Henderson MJ, Yang P, Hagen BM, Siddique T, Vogel BE, Deng HX, Fang S. Nuclear export of misfolded SOD1 mediated by a normally buried NES-like sequence reduces proteotoxicity in the nucleus. *Elife*. 2017;6. doi:10.7554/eLife.23759

126. Paré B, Lehmann M, Beaudin M, Nordström U, Saikali S, Julien JP, Gilthorpe JD, Marklund SL, Cashman NR, Andersen PM, Forsberg K, Dupré N, Gould P, Brännström T, Gros-Louis F. Misfolded SOD1 pathology in sporadic Amyotrophic Lateral Sclerosis. *Sci Rep*. 2018;8(1):1-13. doi:10.1038/s41598-018-31773-z

127. Atlasi RS, Malik R, Corrales CI, Tzeplaeff L, Whitelegge JP, Cashman NR, Bitan G. Investigation of Anti-SOD1 Antibodies Yields New Structural Insight into SOD1 Misfolding and Surprising Behavior of the Antibodies Themselves. *ACS Chem Biol*. 2018;13(9):2794-2807. doi:10.1021/acschembio.8b00729

128. Lepock JR, Frey HE, Hallewell RA. Contribution of Conformational Stability and Reversibility of Unfolding to the Increased Thermostability of Human and Bovine Superoxide Dismutase Mutated at Free Cysteines. *J Biol Chem*. 1990;265:21612-21618.

129. Stathopulos PB, Rumfeldt JAO, Scholz GA, Irani RA, Frey HE, Hallewell RA, Lepock JR, Meiering EM. Cu/Zn superoxide dismutase mutants associated with amyotrophic lateral sclerosis show enhanced formation of aggregates in vitro. *Proc Natl Acad Sci U S A*. 2003;100(12):7021-7026. doi:10.1073/pnas.1237797100

130. Rumfeldt JAO, Stathopulos PB, Chakrabarrty A, Lepock JR, Meiering EM. Mechanism and thermodynamics of guanidinium chloride-induced denaturation of ALS-associated mutant Cu,Zn superoxide dismutases. *J Mol Biol*. 2006;355(1):106-123. doi:10.1016/j.jmb.2005.10.042

131. Stathopulos PB, Rumfeldt JAO, Karbassi F, Siddall CA, Lepock JR, Meiering EM. Calorimetric analysis of thermodynamic stability and aggregation for Apo and Holo amyotrophic lateral sclerosis-associated Gly-93 mutants of superoxide dismutase. *J Biol Chem*. 2006;281(10):6184-6193. doi:10.1074/jbc.M509496200

132. Bio-Rad Technical Support Department. Image Lab. *Image Lab^{TM} Softw User Guid*. Published online 2017:115-119. http://www.bio-rad.com/webroot/web/pdf/lsr/literature/10000076953.pdf

133. Bio-Rad Laboratories I. ChemiDoc and ChemiDoc MP Imaging Systems with Image Lab Touch SoftwareNo Title. https://www.bio-rad.com/webroot/web/pdf/lsr/literature/10000062126.pdf

134. Pillai-Kastoori L, Schutz-Geschwender AR, Harford JA. A systematic approach to quantitative Western blot analysis. *Anal Biochem*. 2020;593:113608. doi:10.1016/j.ab.2020.113608

135. Tian G, Tang F, Yang C, Zhang W, Bergquist J, Wang B, Mi J, Zhang J. Quantitative dot blot analysis (QDB), a versatile high throughput immunoblot method. *Oncotarget*. 2017;8(35):58553-58562. doi:10.18632/oncotarget.17236

136. Lopate G, Baloh RH, Al-Lozi MT, Miller TM, Fernandes Filho JA, Ni O, Leston A, Florence J, Schierbecker J, Allred P. Familial ALS with extreme phenotypic variability due to the I113T SOD1 mutation. *Amyotroph Lateral Scler*. 2010;11(1-2):232-236. doi:10.3109/17482960902898069

137. Doyle CM, Rumfeldt JA, Broom HR, Sekhar A, Kay LE, Meiering EM. Concurrent Increases and Decreases in Local Stability and Conformational Heterogeneity in Cu, Zn Superoxide Dismutase Variants Revealed by Temperature-Dependence of Amide Chemical Shifts. *Biochemistry*. 2016;55(9):1346-1361. doi:10.1021/acs.biochem.5b01133

138. Ventura S, Villaverde A. Protein quality in bacterial inclusion bodies. *Trends Biotechnol*. 2006;24(4):179-185. doi:10.1016/j.tibtech.2006.02.007

139. Leinweber B, Barofsky E, Barofsky DF, Ermilov V, Nylin K, Beckman JS. Aggregation of als mutant superoxide dismutase expressed in Escherichia coli. *Free Radic Biol Med*. 2004;36(7):911-918. doi:10.1016/j.freeradbiomed.2003.12.021

140. Kabashi E, Durham HD. Failure of protein quality control in amyotrophic lateral sclerosis. *Biochim Biophys Acta - Mol Basis Dis*. 2006;1762(11-12):1038-1050. doi:10.1016/j.bbadis.2006.06.006

141. Rajan RS, Illing ME, Bence NF, Kopito RR. Specificity in intracellular protein aggregation and inclusion body formation. *Proc Natl Acad Sci U S A*. 2001;98(23):13060-13065. doi:10.1073/pnas.181479798

142. Vassall KA, Stubbs HR, Primmer HA, Tong MS, Sullivan SM, Sobering R, Srinivasan S, Briere LAK, Dunn SD, Colón W, Meiering EM. Decreased stability and increased formation of soluble aggregates by immature superoxide dismutase do not account for disease severity in ALS. *Proc Natl Acad Sci U S A*. 2011;108(6):2210-2215. doi:10.1073/pnas.0913021108

143. Calvert VS, Tang Y, Boveia V, Wulfkuhle J, Schutz-Geschwender A, Olive DM, Liotta LA, Petricoin EF. Development of multiplexed protein profiling and detection using near infrared detection of reverse-phase protein microarrays. *Clin Proteomics*. 2004;1(1):81-89. doi:10.1385/cp:1:1:081

144. Wang Q, Johnson JL, Agar NYR, Agar JN. Protein aggregation and protein instability govern familial amyotrophic lateral sclerosis patient survival. *PLoS Biol*. 2008;6(7):1508-1526. doi:10.1371/journal.pbio.0060170

145. Khare SD, Wilcox KC, Gong P, Dokholyan N V. Sequence and structural determinants of Cu, Zn superoxide dismutase aggregation. *Proteins Struct Funct Genet*. 2005;61(3):617-632. doi:10.1002/prot.20629

146. Almey J. Inclusion Body formation of Familial Amyotrophic Lateral Sclerosis Associated Cu, Zn-Superoxide Dismutase Mutants in Escherichia coli. Published online 2015.

147. Broom HR, Rumfeldt JAO, Vassall KA, Meiering EM. Destabilization of the dimer interface is a common consequence of diverse ALS-associated mutations in metal free SOD1. *Protein Sci*. 2015;24(12):2081-2089. doi:10.1002/pro.2803

148. Rakhit R, Robertson J, Velde C Vande, Horne P, Ruth DM, Griffin J, Cleveland DW, Cashman NR, Chakrabartty A. An immunological epitope selective for pathological monomer-misfolded SOD1 in ALS. *Nat Med*. 2007;13(6):754-759. doi:10.1038/nm1559

149. Kerman A, Liu HN, Croul S, Bilbao J, Rogaeva E, Zinman L, Robertson J, Chakrabartty A. Amyotrophic lateral sclerosis is a non-amyloid disease in which extensive misfolding of SOD1 is unique to the familial form. *Acta Neuropathol*. 2010;119(3):335-344. doi:10.1007/s00401-010-0646-5

150. Roberts BR, Lim NKH, McAllum EJ, Donnelly PS, Hare DJ, Doble PA, Turner BJ, Price KA, Lim SC, Paterson BM, Hickey JL, Rhoads TW, Williams JR, Kanninen KM, Hung LW, Liddell JR, Grubman A, Monty JF, Llanos RM, Kramer DR, Mercer JFB, Bush AI, Masters CL, Duce JA, Li QX, Beckman JS, Barnham KJ, White AR, Crouch PJ. Oral treatment with CuII(atsm) increases mutant SOD1 in vivo but protects motor neurons and improves the phenotype of a transgenic mouse model of amyotrophic lateral sclerosis. *J Neurosci*. 2014;34(23):8021-8031. doi:10.1523/JNEUROSCI.4196-13.2014

151. Sekhar A, Rumfeldt JAO, Broom HR, Doyle CM, Bouvignies G, Meiering EM, Kay LE. Thermal fluctuations of immature SOD1 lead to separate folding and misfolding pathways. *Elife*. 2015;4(JUNE). doi:10.7554/eLife.07296

152. Sekhar A, Rumfeldt JAO, Broom HR, Doyle CM, Sobering RE, Meiering EM, Kay LE. Probing the free energy landscapes of ALS disease mutants of SOD1 by NMR spectroscopy. *Proc Natl Acad Sci U S A*. 2016;113(45):E6939-E6945. doi:10.1073/pnas.1611418113

153. Morandat S, El Kirat K. Solubilization of supported lipid membranes by octyl glucoside observed by time-lapse atomic force microscopy. *Colloids Surfaces B Biointerfaces*. 2007;55(2):179-184. doi:10.1016/j.colsurfb.2006.11.039

154. Walsh G. Biopharmaceutical benchmarks 2018. *Nat Biotechnol*. 2018;36(12):1136-1145. doi:10.1038/nbt.4305

155. Marco A de, Ferrer-Miralles N, Garcia-Fruitós E, Mitraki A, Peternel S, Rinas U, Trujillo-Roldán MA, Valdez-Cruz NA, Vázquez E, Villaverde A. Bacterial Inclusion Bodies Are Industrially Exploitable Amyloids - PubMed. *FEMS Microbiol Rev*. 2019;43(1):53-72. Accessed May 28, 2020. https://academic.oup.com/femsre/article/43/1/53/5144214

156. Rinas U, Garcia-Fruitós E, Corchero JL, Vázquez E, Seras-Franzoso J, Villaverde A. Bacterial Inclusion Bodies: Discovering Their Better Half. *Trends Biochem Sci*. 2017;42(9):726-737. doi:10.1016/j.tibs.2017.01.005

157. García-Fruitós E, Vázquez E, Díez-Gil C, Corchero JL, Seras-Franzoso J, Ratera I, Veciana J, Villaverde A. Bacterial inclusion bodies: Making gold from waste. *Trends Biotechnol*. 2012;30(2):65-70. doi:10.1016/j.tibtech.2011.09.003

158. Trainor K, Gingras Z, Shillingford C, Malakian H, Gosselin M, Lipovšek D, Meiering EM. Ensemble Modeling and Intracellular Aggregation of an Engineered Immunoglobulin-Like Domain. *J Mol Biol*. 2016;428(6):1365-1374. doi:10.1016/j.jmb.2016.02.016

159. Ventura S, Villaverde A. Protein quality in bacterial inclusion bodies. *Trends Biotechnol*. 2006;24(4):179-185. doi:10.1016/j.tibtech.2006.02.007

160. Elia F, Cantini F, Chiti F, Dobson CM, Bemporad F. Direct Conversion of an Enzyme from Native-like to Amyloid-like Aggregates within Inclusion Bodies. *Biophys J*. 2017;112(12):2540-2551. doi:10.1016/j.bpj.2017.05.011

161. Gardner QA, Hassan N, Hafeez S, Arif M, Akhtar M. Exploring the nature of inclusion bodies by MALDI mass spectrometry using recombinant proinsulin as a model protein. *Int J Biol Macromol*. 2019;139:647-653. doi:10.1016/j.ijbiomac.2019.07.131